Synthesis and Properties of Corannulene Derivatives: Journey to Materials Chemistry and Chemical Biology

Dissertation

zur

Erlangung der naturwissenschaftlichen Doktorwürde
(Dr. sc. nat.)

vorgelegt der

Mathematisch-naturwissenschaftlichen Fakultät

der

Universität Zürich

von

Tomoharu Hayama

aus Japan

Promotionskomitee:

Prof. Dr. Jay S. Siegel (Vorsitz)

Prof. Dr. Nathan W. Luedtke

Prof. Dr. Kim K. Baldridge

PD Dr. Nathaniel S. Finney

Zürich, 2008

Die vorliegende arbeit wurde von

der Mathematisch-naturwissenschaftlichen Fakultät

der Universität Zürich im Januar 2008

als Dissertation angenommen

Promotionskomitee:

Prof. Dr. Jay S. Siegel

Vorsitz

Prof. Dr. Nathan W. Luedtke

Prof. Dr. Kim K. Baldridge

PD Dr. Nathaniel S. Finney

Universität Zürich 2008

Table of Contents

List of Figures v

Acknowledgements x

Curriculum Vitae xi

Abstract of the Dissertation xiii

Zusammenfassung xv

1. Corannulene and Fullerene 1

1.1. Introduction 2

1.1.1. Historical Overview and Synthesis 2

1.1.2. Structure 3

1.1.3. Electrochemistry 5

1.1.4. Reactivity 8

1.1.5. Application 10

1.2. References 12

2. Synthetic Method 15

2.1. Introduction 16

2.1.1. Pioneering Synthesis of Corannulene (B1) 16

2.1.2. Gas-Phase Synthesis of B1 with Flash Vacuum Pyrolysis 17

2.1.3. Development of Efficient Solution-Phase Synthesis of B1 19

2.1.4. Substituted Corannulene Synthesized from Halocorannulenes 23

2.2. Present Work 30

2.2.1. Synthesis of *sym*-Pentaarylcorannulenes 30

2.2.2. Crystal Structures 34

2.2.3. Experimental Section 36

2.3. Appendix 49

2.3.1. Crystallographic Data of B93 49

2.3.2. Crystallographic Data of B94 50

2.4. References 52

3. Bowl-to-Bowl Inversion 55

3.1. Introduction 56

3.1.1. Correlation between Structure and Inversion Energy 56

3.1.2. Influence of *endo* Groups of *sym*-Pentamanisylcorannulene (C26) 63

3.2. Present Work 64

3.2.1. Solvent Effect on Inversion Energies 64

3.2.2. Experimental Section 76

3.3. References 85

4. Passage to Nanotube 87

4.1. Introduction 88

4.1.1. Carbon Nanotubes (CNTs) 88

4.1.2. From Buckybowl to Buckytube 89

4.1.3. Exploitation of Acetylene Chemistry 90

4.2. Present Work 91

4.2.1. Synthesis of Decapentynylcorannulene (D12) 92

4.2.2. Biscumulenyl[10]annulene (D13) 95

4.2.3. Experimental Section 101

4.3. Appendix 105

4.3.1. Crystallographic Data of D12 105

4.3.2. Crystallographic Data of D13 106

4.4. References 108

5. Synthetic Receptor 111

5.1. Introduction 112

5.1.1. Cholera Toxin and Heat-Labile Enterotoxin 112

5.1.2. Symmetrical Pentavalent Recognition 115

5.2. Present Work 117

5.2.1. Experimental Design 117

5.2.2. Synthesis 121

5.2.3. Affinity Measurement 132

5.2.4. Experimental Section 135

5.3. References 149

List of Figures

Figure A1. Corannulene (A1) and buckminsterfullerene (A2) 2

Figure A2. Structure of A1 and A2 3

Figure A3. Definition of POAV angle 4

Figure A4. Energy diagram of the bowl-to-bowl inversion process 5

Figure A5. Estimation of the inversion barrier of A1 5

Figure A6. Reduction of A2 in acetonitrile/toluene 6

Figure A7. Li-corannulene complex 7

Figure B1. Selected bromides for the coupling reaction 31

Figure B2. NHC ligand and its palladium complex 33

Figure B3. Crystal structure of B93 35

Figure B4. Crystal structure of B94 35

Figure C1. Bowl inversion of C1 56

Figure C2. Correlation between structures and $\Delta G^{\ddagger}_{inv}$ 56

Figure C3. Structure-energy correlation of $\Delta G^{\ddagger}_{inv}$ versus bowl depth 60

Figure C4. Energy diagram of the bowl-to-bowl inversion process of C1 60

Figure C5. Reaction profiles of the corannulene derivatives perturbation 61

Figure C6. Correlation of Φ_{POAV} and bowl-to-bowl inversion barrier 62

Figure C7. VdW attractive forces among the *endo* methyl groups 63

Figure C8. Selected corannulene derivatives for solvent effect study 64

Figure C9. Relationship between $\Delta G^{\ddagger}_{inv}$ and the solvent volume in C26 67

Figure C10. Relationship between $\Delta G^{\ddagger}_{inv}$ and $\Delta S_{vap}(T_{bp})$ in C26 70

Figure C11. Solvent cage fixes the movement of C26 in ground state 70

Figure C12. Relationship between $\Delta G^{\ddagger}_{inv}$ and dielectric constant in C29 72

Figure C13. Relationship between $\Delta H^{\ddagger}_{inv}$ and dielectric constant in C29 72

Figure C14. Relationship between $\Delta S^{\ddagger}_{inv}$ and dielectric constant in C29 73

Figure C15. Ordered solvent cage and smaller vibrational movement of C29 74

Figure C16. An additional term, $\Delta S^{\ddagger}_{x}$ should be large and negative 75

Figure C17. Conformations of ethylbenzen and anisole 75

Figure C18. Eyring plot of C26 80

Figure C19. Eyring plot of C29 81

Figure C20. Eyring plot of C19 82

Figure D1. Corannulene (D1) and carbon-nanotube isomer $C_{40}H_{10}$ (D2) 89

Figure D2. From buckybowl to buckytube ($C_{10n}H_{10}$, n = 1, 2, 3, and 4) 89

Figure D3. Energy gain (ΔG) from the dissociation energies (D) of C-C bonds 90

Figure D4. Tetraethynylethenes (D5-6) and hexaethynylbenzenes (D7-8) 91

Figure D5. Decaethynylcorannulene (D9) as a per-ethynylated PAH 91

Figure D6. Skeleton and space filling models of D12 94

Figure D7. Skeleton and space filling models of D13 96

Figure D8. Two resonance forms of the [10]annulene fragment of D13 96

Figure D9. [10]annulene derivatives, D17 and D18 99

Figure D10. Relative energies of D18 and its diradical 99

Figure D11. Diradical intermediate (D19) 99

Figure E1. Crystal structure of LT with the sites for molecular recognition 113

Figure E2. Monovalent ligands to CT and LT 114

Figure E3. B-pentamer, pentavalent inhibitor, and their complex 115

Figure E4. Acylated pentacyclen and 4,7,10-trioxa-1,13-tridecanediamine 115

Figure E5. Core units using large cyclic peptides 117

Figure E6. Adjustable recognition circle 118

Figure E7. Distance between the binding sites of CT B pentamer 118

Figure E8. Proposed structure of the corannulene-based synthetic receptor 119

Figure E9. Fixation of the "Fingers" by larger "Core" with shorter "Linker" 119

Figure E10. Calculation of "Linker" length 120

Figure E11. Peaks of final product E12 and side products E51-52 on MALDI 131

Figure E12. UV and fluorescent spectra of E12 in H_2O/DMSO = 80/20 v/v% 132

Figure E13. Binding effect of GM1 and sugar on the fluorescent spectra of CT 133

List of Tables

Table B1. Synthesis of corannulene derivatives under various conditions 22

Table B2. Synthesis of monosubstituted corannulenes 24

Table B3. Synthesis of 2,3-disubstitutedcorannulenes 27

Table B4. Synthesis of pentasubstitutedcorannulenes 28

Table C1. Bowl depths and $\Delta G^{\ddagger}_{inv}$ for various corannulene derivatives 57

Table C2. Inversion energies of C27 and C28 64

Table C3. $\Delta G^{\ddagger}_{inv}$ in different kinds of solvents 65

Table C4. Some physical properties of solvents 66

Table C5. Activation parameters of C19 67

Table C6. Activation parameters of C26 68

Table C7. Enthalpy and entropy of vaporization 69

Table C8. Polarity parameters of solvents 71

Table C9. Activation parameters of C29 73

Table D1. Geometry of D1, D2, D9, and D12 94

Table D2. Geometrical parameters of the [10]annulene fragment of D13 97

Table E1. IC_{50} of pentavalent ligands against the LT B pentamer 116

List of Schemes

Scheme A1. Typical addition reaction of A2 8

Scheme A2. Electrophilic aromatic substitution of A1 8

Scheme A3. Unique chlorination with iodine monochloride 9

Scheme A4. Reaction of A1 with dichlorocarbene 9

Scheme B1. First synthesis of B1 by Lawton 16

Scheme B2. Failed attempts to improve the synthesis of B1 17

Scheme B3. Preparation of fluoranthenes 17

Scheme B4. First synthesis of B1 with FVP 18

Scheme B5. Different route to B1 with FVP 18

Scheme B6. First solution-phase synthesis of corannulene derivative 19

Scheme B7. Solution-phase synthesis of B1 20

Scheme B8. Base catalyzed synthesis of B1 by Sygula and Rabideau 20

Scheme B9. Mild reaction conditions using nickel powder 21

Scheme B10. Synthesis of 1,2,5,6-tetrasubstitutedcorannulenes 25

Scheme B11. Synthesis of 2,3-dichlorocorannulene (B56) 26

Scheme B12. Chlorinations of B1 27

Scheme B13. Synthesis of decasubstitutedcorannulenes 29

Scheme B14. Effect of steric hindrance for coupling reaction 30

Scheme B15. Synthesis of bromides 32

Scheme B16. Synthesis of *sym*-pentaarylcorannulenes 34

Scheme C1. Synthesis of C19 65

Scheme D1. Retrosynthetic analysis of D2 derivatives 92

Scheme D2. Synthesis of decachlorocorannulene (D10) 92

Scheme D3. Synthesis of decapentynylcorannulene (D12) 93

Scheme D4. Conversion into the nanotube derivative (D14) 95

Scheme D5. Conceptual enediyne cyclization of D9 to [10]annulene (D16) 98

Scheme E1. Corannulene-based synthetic receptor from E11 117

Scheme E2. Retrosynthetic analysis of the synthetic receptor 121

Scheme E3. Synthesis of sugar component 121

Scheme E4. Synthesis of bromophenol (E26) 122

Scheme E5. Synthesis of arylbromide (E31) 123

Scheme E6. Selective protection with TIPS group 123

Scheme E7. Coupling reaction with E31 125

Scheme E8. Synthesis of arylbromide (E40) 126

Scheme E9. Successful Suzuki coupling with boronic ester (E42) 127

Scheme E10. Coupling reaction with E11 followed by removal of TIPS group 127

Scheme E11. Unsuccessful Suzuki coupling with boronic ester (E46) 128

Scheme E12. General reaction scheme of the CuAAC 128

Scheme E13. CuAAC of U40 with deprotected sugar E20 129

Scheme E14. Synthesis of target compound (E12) with using the CuAAC 130

Scheme E15. Adjustment of the "Linker" length from intermediate E17 134

Acknowledgements

Prof. Dr. Jay S. Siegel
Prof. Dr. Kim K. Baldridge
Prof. Dr. John A. Robinson
PD Dr. Anthony Linden
PD Dr. Nathaniel S. Finney

UNIZH NMR Service
UNIZH MS Service

Prof. Dr. Yao-Ting Wu (National Cheng-Kung University)
Prof. Dr. Hans-Beat Bürgi (University of Bern)
Prof. Dr. Anna Bernardi (University of Milan)

Dr. Jui-Chang Tseng
Anna Butterfield
Davide Bandera
Michael Löpfe

All Siegel and Baldridge group members past and present

Paul Sharer Institut

Tomoharu Hayama

Organic Chemistry Institut, University of Zurich
Winterthurerstrasse 190, CH-8057 Zurich, Switzerland
tomoharu@oci.unizh.ch

EDUCATION

May 2005-:	Ph.D. Studies in Organic Chemistry, University of Zurich, Switzerland
Apr 2005:	M.S. Organic Chemistry, University of Zurich, Switzerland
Apr 2003:	B.S. Pharmaceutical Sciences, Kyoto University, Japan

PROFESSIONAL EXPERIENCE

Sept 2003-:	Research Assistant, University of Zurich with Professor Jay S. Siegel

HONORS AND AWARDS

2002:	Pharmacist License, Japan

PUBLICATIONS AND PRESENTATIONS

"Solvent Effect in the Bowl-Inversion Energy of *sym*-Pentaarylsubstituted-corannulenes"; T. Hayama, K. K. Baldridge, A. Linden, J. S. Siegel; *Manuscript in preparation*.

"Synthesis, Structure, and Isomerization of Decapentynylcorannulene: Enediyne Cyclization/Interconversion of $C_{40}R_{10}$ Isomers"; T. Hayama, Y.-T. Wu, K. K. Baldridge, A. Linden, J. S. Siegel; *J. Am. Chem. Soc.* **129**, 12612-12613 (2007).

"Steric Isotope Effects Gauged by the Bowl-Inversion Barrier in Selectively Deuterated Pentaarylcorannulenes"; T. Hayama, Y.-T. Wu, K. K. Baldridge, A. Linden, J. S. Siegel; *J. Am. Chem. Soc. Accepted*.

"Synthesis of Fluoranthenes and Indenocorannulenes: Elucidation of Chiral Stereoisomers on the Basis of Static Molecular Bowls"; Y.-T. Wu, T. Hayama, K. K. Baldridge, A. Linden, J. S. Siegel; *J. Am. Chem. Soc.* **128**, 6870-6884 (2006).

"Mechanistic Aspects of Thiyl Radical-Promoted Acyl Radical Cyclization of Formylenoate-Cyclization versus Oxidation"; K. Yoshikai, T. Hayama, K. Nishimura, K. Yamada, K. Tomioka; *Chem. Pharm. Bull.* **53**, 586-588 (2005).

"Thiol-Catalyzed Acyl Radical Cyclization of Alkenals"; K. Yoshikai, T. Hayama, K. Nishimura, K. Yamada, K. Tomioka; *J. Org. Chem.* **70**. 681-683 (2005).

"Asymmetric Michael-Aldol Tandem Cyclization of ω-oxo-α,β-Unsaturated Esters with 10-Mercaptoisoborneol Methyl Ether"; K. Nishimura, H. Tsubouchi, M. Ono, T. Hayama, Y, Nagaoka, K. Tomioka; *Tetrahedron Lett*. **44**, 2323-2326 (2003).

"Synthesis and Structure of Decapentynylcorannulene: Passage to Solution Phase Carbon-Based Nanotube Synthesis"; T. Hayama, Y.-T. Wu, A. T. Linden, K. K. Baldridge, J. S. Siegel; poster presented at the *12th International Symposium on Novel Aromatic Compounds*; Awaji Island, Japan. July 22, 2007.

"Efficient Synthesis of *sym*-Pentaarylcorannulenes"; T. Hayama, A. T. Linden, J. S. Siegel; poster presented at the *2nd Dorothy Crowfoot Hodgkin Symposium*; Zurich, Switzerland; April 27, 2007.

"Steric Isotope Effect in Corannulene Bowl-Inversion: VdW (CD_3//CD_3) > VdW (CH_3//CH_3)"; T. Hayama, Y.-T. Wu, K. K. Baldridge, A. T. Linden, J. S. Siegel; poster presented at the *1st International Conference on Cutting-Edge Organic Chemistry in Asia*; Okinawa, Japan. October 16, 2006.

"Synthesis and Dynamics of *sym*-Pentamannisylcorannulene"; T. Hayama, Y.-T. Wu, K. K. Baldridge, A. T. Linden, J. S. Siegel; poster presented at the *1st Dorothy Crowfoot Hodgkin Symposium*; Zurich, Switzerland; May 5, 2006.

ABSTRACT OF THE DISSERTATION

Synthesis and Properties of Corannulene Derivatives:

Journey to Materials Chemistry and Chemical Biology

by

Tomoharu Hayama

Doctor of Philosophy in Chemistry

University of Zurich, 2008

Professor Jay S. Siegel, Chair

Corannulene, also called as [5]-circulene, is a $C_{20}H_{10}$ fragment of buckminsterfullerene, C_{60}. The most interesting property of corannulene is probably its bowl structure and bowl-to-bowl inversion. The unique curvature has many possiblities for applications in different fields. Today, large-scale synthesis of corannulene is possible and thus, the time has come to exploit its physical properties. This dissertation is divided into four areas: 1) efficient synthesis of *sym*-pentaarylsubstituedcorannulene derivatives, 2) solvent effect on the bowl inversion, 3) development of the method for solution-phase nanotube synthesis, and 4) designing a corannulene-based synthetic receptor.

sym-Pentaarylsubstituedcorannulenes are quite attractive compounds because of their five-fold symmetry and curvature. The efficient synthesis has been accomplished from *sym*-pentachlorocorannulene with the coupling reaction using *N*-heterocyclic carbene ligands in a moderately good yield in spite of its five low-reactive chlorides.

The inversion energies of some *sym*-pentaarylsubstituedcorannulenes have been investigated in different types of solvent. The variable temperature ^{1}H-NMR spectra were measured, and line shape analysis or coalescence approximation were used to evaluate the rate parameters. This experiment suggested *endo*-group interactions of those compounds and shows influences of solvent polarity or volume on the inversion energies. In addition, the bowl depths will also be compared and discussed using the crystallographic structural data.

The high-energy per-ethynylated polynuclear compound decapentynyl-corannulene has been prepared via aryl-alkyne coupling chemistry of decachlorocorannulene. During the reaction, an astonishing compound, biscumulenyl[10]annulene was also produced by the corannulene ring-open mechanism through the diradical from the enediyne cyclization. The relative structure and energetics of those compounds and its carbon nanotube isomer $C_{40}H_{10}$ are discussed with some computational data. This study suggests the potential route of the first solution-phase single-walled carbon-based nanotubes.

Cholera toxin from *Vibrio cholerae* and heat-labile enterotoxin from enterotoxigenic *Escherichia coli* have similar structures and both belong to the AB_5 bacterial toxins. The synthetic recepor for those toxins has been synthesized from *sym*-pentachlorocorannulene, which has the same five-hold symmetry. The structure has a "Finger-Linker-Core" motif and could exploit the pentavalent recognition for toxins. In addition, the synthetic strategy enables the modification of the "Linker" length and the introduction of many functional groups.

ZUSAMMENFASSUNG

Synthese und Eigenschaften von Corannulen Derivaten:

Ausflug zu Materialwissenschaften und chemischer Biology

von

Tomoharu Hayama

Dr. sc. nat.

Universität Zürich, 2008

Jay S. Siegel, Vorsitz

Corannulen, auch als [5]-Circulen bekannt, ist ein $C_{20}H_{10}$ Fragment des Buckminsterfullerens, C_{60}. Die interessanteste Eigenschaft von Corannulen stellt seine Schüsselform sowie die Schüsel-Schüssel-Inversion dar. Diese charakteristische Wölbung erlaubt Anwendungen von Corannulenen in verschiedenen Gebieten. Die Tatsache, dass heute Corannulen auch in grosser Menge hergestellt werden kann, erlaubt die Untersuchung seiner physikalischen Eigenschaften. Diese Dissertation ist in vier Bereiche geteilt: 1) Effiziente Synthese *sym*-pentaarylsubstituierter Corannulenderivate, 2) Studie des Lösungsmitteleffekts auf die Schüssel-Inversion, 3) Entwicklung einer Methode für die Nanotubesynthese in Lösung sowie 4) das Design eines corannulenbasierten, synthetischen Rezeptors.

sym-Pentaarylsubstituierte Corannulene sind aufgrund ihrer fünffachen Symmetrie sowie ihrer Wölbung interessante Verbindungen. Eine effiziente Synthese *sym*-pentaarylierter Corannulene wurde ausgehend vom *sym*-Pentachlorcorannulene erreicht, durch Kopplungsreaktionen mit Hilfe *N*-heterozyklischer Carbenliganden in, unter Berücksichtigung der fünf nur wenig reaktiven Chlorsubstituenten, vernünftigen Ausbeuten.

Die Inversionsbarriere einiger *sym*-pentaarylsubstituierter Corannulene wurde in verschiedenen Lösungsmitteln untersucht. In gemessenen temperaturabhängigen ^{1}H-NMR Spektren wurden die Geschwindigkeitsparameter mittels Linienformanalyse oder Koaleszenzapproximation bestimmt. Diese Experimente ergaben, dass *endo*-Gruppeninteraktionen bei solchen Verbindungen auftreten. Weiter wurde der Lösungsmittelpolaritätseinfluss sowie der Einfluss der Lösungsmittelmenge auf die Inversionsbarriere bestimmt. Zusätzlich wurden Schüsseltiefen verglichen auf Grundlage kristallographischer Daten.

Die hochenergetische per-ethinilierte polynucleare Verbindung Decapentincorannulen mittels Aryl-Alkinkopplung aus Decachlorcorannulen hergestellt. Während der Reaktion entstand eine erstaunliche Verbindung, das Biscumulenyl[10]annulen, durch einen Corannulenringöffnungsmechanismus über das Diradikal der En-diinzyklisierung. Die relativen Strukturen und Energien dieser Verbindungen sowie des Kohlenstoff Nanotube Isomeren $C_{40}H_{10}$ werden besprochen auf Grundlage theoretischer Daten. Diese Studie schlägt eine mögliche Route zur ersten Synthese einwändiger auf Kohlenstoff basierenden Nanotubes in Lösung vor.

Choleratoxin von *Vibrio cholerae* sowie das thermolabile Enterotoxin der enterotoxischen *Escherichia coli* haben ähnliche Strukturen und gehören beide zu den AB_5 Bakterientoxinen. Ein synthetischer Rezeptor für diese Toxine wurde hergestellt ausgehend vom *sym*-Pentachlorcorannulen, das eine fünffache Symmetrie aufweist. Die Struktur besitzt eine „Finger-Linker-Core“ Architektur und könnte die fünffache Erkennung des Toxins nachahmen. Zusätzliche synthetische Strategien, die Modifikationen in der Linkerlänge erlauben, sowie die Einführung zahlreicher funktioneller Gruppen werden besprochen.

Chapter 1. Corannulene and Fullerene

1.1. Introduction

This chapter provides a comparison of corannulene (**A1**) with a fullerene, specifically buckminsterfullerene (**A2**, C_{60}), as a representative of non-planar polycyclic aromatic hydrocarbons (PAHs) (Figure A1). **A1** equals one-third of **A2**; the comparison of their structural or physical properties will give us some insight for the study of **A1**. In addition, the recognition of the importance of **A2** and analysis of their similarities and differences will also answer the question, "Why is **A1** important?"

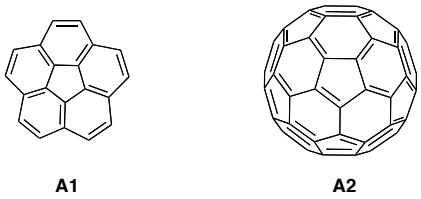

Figure A1. Corannulene (A1) and buckminsterfullerene (A2).

1.1.1. Historical Overview and Synthesis

A1, first synthesized by Lawton and Barth in 1966, has been known for a long time as the first bowl-shaped π-conjugated system.[1] Although the existence of **A2** was suggested by Osawa based on the structure of **A1** in 1970,[2] its discovery was made by Kroto, Smalley, and Curl in 1985.[3] First, they found an unusually stable ion C_{60}^{+} among the gas-phase carbon ions produced by laser vaporization of graphite and hypothesized that the stability resulted from its truncated icosahedron structure. The structure was dubbed "buckminsterfullerene" after the famous architect who popularized the truncated icosahedron broadly. Various kinds of gas-phase experiments and theoretical works supported this idea and when Krätschmer and Huffman discovered a method for making macroscopic quantities of **A2** and higher fullerenes by resistive heating of graphite in 1990, the soccer-ball structure was finally confirmed.[4] Since the discovery of **A2**, a number of reports have been publishied concerning new carbon allotropes having a variety of three-dimensional structures, especially carbon nanotubes because of their many applications in nanotechnology.[5] At the same time, an interest in bowl-shaped aromatic hydrocarbons was directed to **A1** again, when short and practical synthetic methods were reported by Scott, Rabideau, and Siegel.[6]

Today, although a chemical synthesis with flash vacuum pyrolysis (FVP) was reported,[7,8] the synthesis of **A2** is mainly done by two physical methods; the vaporization of graphite by resistive heating under carefully defined condition[4,9,10] or the combustion of simple hydrocarbons in fuel-rich flames.[11] These technologies are utilized on an industrial scale to produce **A2** on a metric ton scale. Such an abundant supply of **A2** in one step from cheap starting materials makes it possible to investigate many applications of **A2**. On the other hand, in the case of **A1**, the moderate scale of synthesis was done in solution-phase.[6] The synthesis of **A1** is done using normal solution-phase techniques and relatively limited amounts (multi-gram scale) of **A1** can be produced. The synthetic difficulty of **A1** compared to **A2** seems to be one of the reasons to prevent the industrial application of **A1**.

1.1.2. Structure

A1 is sometimes called a buckybowl because of its bowl structure, and relationship to the spherical structure **A2**, which is called buckyball. The closed structure of **A2** makes the curvature deeper than that of **A1**. X-ray crystallographic analysis of **A1** shows a bowl depth of 0.875 Å from the plane containing the rim carbon atoms to the plane of the hub carbon atoms (Figure A2).[12] The same distance in **A2** is 1.50 Å.[13] Whereas **A1** has four different C-C bond lengths (1.45 Å (flank), 1.38 Å (rim), 1.38 Å (spoke), and 1.42 Å (hub)), **A2** has only two types of C-C bond length (1.38 Å (adjacent hexagons) and 1.45 Å (pentagon/hexagon)).

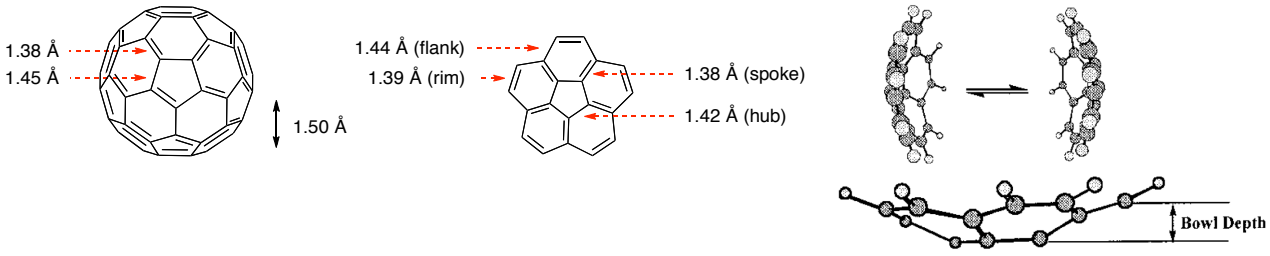

Figure A2. Structures of A1 and A2.

The π-orbital axis vector (POAV) pyramidalization angle is an index of the curvature of individual carbon atoms as proposed by Haddon.[14] An imaginary vector is defined such that its location is equidistant between the three σ-bonds of an sp_2 hybridized carbon atom so that the maximum angle is achieved (Figure A3). If the angle between the vector and the C-C axis is $\theta_{\sigma\pi}$, then POAV angle is defined as $\phi_{POAV} = \theta_{\sigma\pi} - 90$. In general, an sp_2-hybridized carbon atom prefers to form a planar σ-framework with its neighbors, leaving its p-orbital perpendicular to the σ-bonds. However, in the case of curved structures like **A1** or **A2**, the sp_2-hybridized carbon atom is pyramidalized. In the case of **A2**, all the carbons are the same and $\phi_{POAV} = 11.6°$.[14] On the other hand, the POAV angles of **A1** are 8.7° (hub), 5.5° (spoke), and 1.1° (rim), respectively.[12] Since the POAV angle is a good measure of the curvature-induced local weakening of π-conjugation, the reactivity of **A2** is expected to be higher than **A1**.[15]

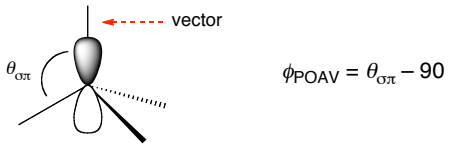

Figure A3. Definition of POAV angle.

Although **A2** is a static spherical structure, **A1** is a dynamic structure. The bowl-to-bowl inversion process of **A1** was first suggested by Lawton and Barth in 1971 (Figure A2, Figure A4).[16] They defined the inversion as the bowl form (ground state) converting to flat form (transition state) as shown in Figure A4. The static C_{5V} symmetry prevents direct measurement of the inversion barrier by normal variable temperature NMR techniques. Thus, several derivatives containing stereochemical probes, which have little effect on the inversion barrier, were used and 11.5 kcal/mol was estimated for the inversion energy of **A1** (Figure A5).[17] The bowl-to-bowl inversion of **A1** will be discussed in the third chapter.

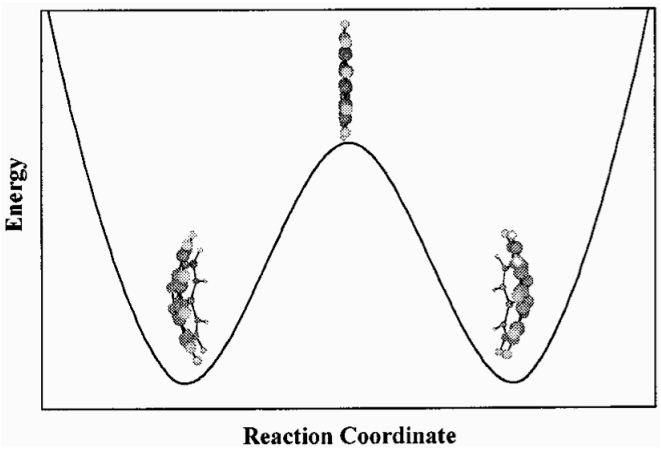

Figure A4. Energy diagram of the bowl-to-bowl inversion process.

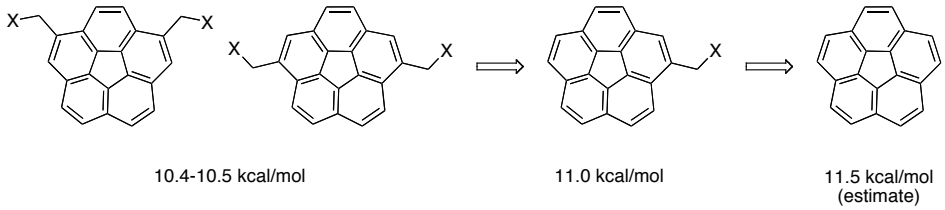

Figure A5. Estimation of the inversion barrier of A1.

1.1.3. Electrochemistry[18]

Immediately after the discovery of **A2**, theoretical predictions indicated that the lowest unoccupied molecular orbital (LUMO) of **A2** was energetically low-lying and triply degenerate, and therefore capable of accepting at least six electrons on reduction.[19] Consequently, electroanalytical techniques such as cyclic voltammetry (CV) quickly became the methods of choice to investigate the rich electronic properties of the fullerenes in solution.[20]

The descovery of **A2** anion was done in several steps with the detection of C_{60}^{2-},[21] C_{60}^{3-},[22] C_{60}^{4-},[23] C_{60}^{5-},[24] and C_{60}^{6-}.[25] Cyclic voltammetric data showed six reversible electron reductions (Figure A6).[25] The voltammetric experiments were carried out under vacuum, using the mixed solvent system acetonitrile/toluene (1/5), and at low temperature of –10 °C the potentials observed were –0.98, –1.37, –1.87, –2.35, –2.85, and –3.26 V. Reduction of a mixture of **A2** and C_{70} using lithium metal in THF-d_8 with the aid of an ultrasonic bath generated a red-brown solution.[26] On the other hand, it was predicted theoretically that oxidation of **A2** would be difficult because of its high gas-phase ionization potential (ca. 7.6 eV).[19,27] The first chemically reversible and electrochemically quasireversible oxidation of **A2** was reported by Echegoyen in 1993.[28] Voltammetric studies showed that the 1-electron oxidation of **A2** in 1,1,2,2-tetrachloroethane indeed occurs at a very positive potential, +1.26 V. These results showed the rich redox chemistry of **A2**, with eight accessible oxidation states.

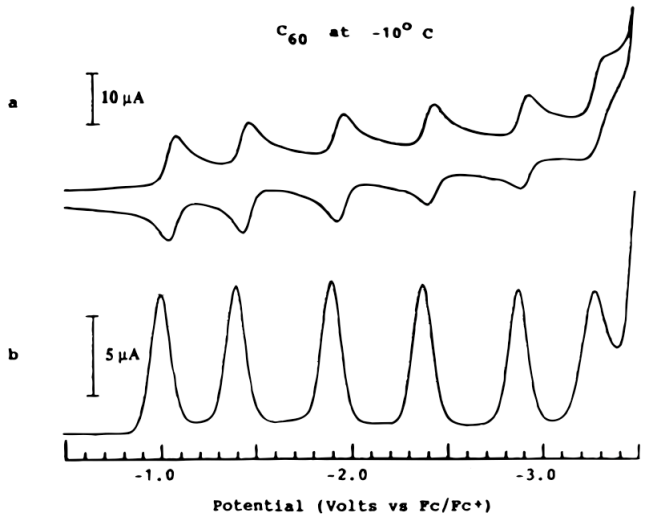

Figure A6. Reduction of A2 in acetonitrile/toluene.

In the case of **A1**, reduction is also possible. It was first reported that reduction of **A1** with excess lithium metal in THF-d_8 leads to a series of three color changes, first to green, second to purple, and then to brownish-red.[29] Such a change of colors results from the different reduction stages of **A1**, $C_{20}H_{10}^{-}$ (green), $C_{20}H_{10}^{2-}$ (purple), $C_{20}H_{10}^{3-}$ (brownish-red), and $C_{20}H_{10}^{4-}$ (brownish-red), confirmed by NMR and EPR. The tetraanion has been characterized as a sandwich dimer with eight lithium counterions (Figure A7).[30] In these sandwich structures, four lithium ions sit between two tetraanionic corannulenes and the four others exist out of sandwiches. The ^{7}Li-NMR spectra recorded at a low temperature (210 K) features two signals of equal intensity (δ_{Li} –4.5 and –11.7 ppm). These chemical shifts represent two different types of Li cations, one sandwiched between the two tetraanion units and one on the outside. At higher temperatures (*e.g.* 260 K), the Li cations all undergo exchange, resulting in a single line at δ = –8.1 ppm. The cation of **A1** was generated by electron impact of vaporized **A1** and the reaction with **A2** was investigated.[31] These redox properties of **A1** show six oxidation states and could lead to rich reactivity similar to that of **A2**.

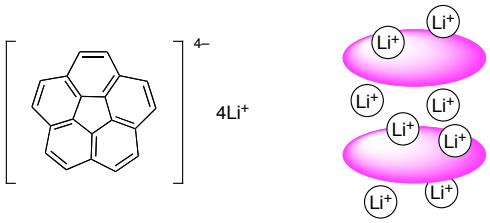

Figure A7. Li-corannulene complex.

1.1.4. Reactivity

The chemical reactivity of **A2** is that of a fairly localized electron deficient polyolefin.[32] Therefore, **A2** reacts readily with nucleophiles and is a reactive 2p component in cycloaddition reactions (Scheme A1).[33] The main type of chemical transformation occurs at the 6,6 ring junction of **A2**. The pyramidalization of the sp_2-hybridized carbon atoms confers an excess of strain to **A2**, which is responsible for the enhanced reactivity of **A2**. A release of strain is in fact associated with the change of hybridization from sp^2 to sp^3 that accompanies most chemical reactions.[34] The regioselectivity of the reaction is governed by the minimization of 5,6 double bonds within the fullerene framework. Double bonds in the five-membered rings are unfavorable because they increase the strain in the cage.[32] Generally, in the reaction of **A2**, the spherical core structure is maintained. However, several open-cage fullerene derivatives have been synthesized.[35] In these syntheses, the reactivity of **A2** as an electrophilic olefin is also utilized in first step of the reactions.

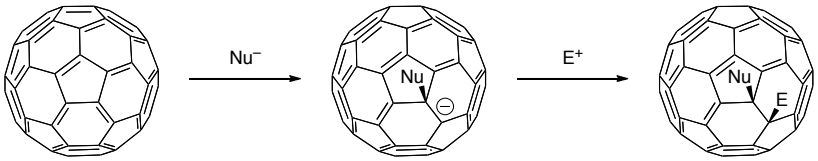

Scheme A1. Typical addition reaction of A2.

On the other hand, a typical reaction of **A1** is electrophilic aromatic substitution like bromination (Scheme A2).[36] However, **A1** also has unique reactivities, which is not shown in normal PAHs. For example, the reaction of **A1** with iodine monochloride gives *sym*-pentachlorocorannulene (**A3**) (Scheme A3).[37] Due to the smaller electronegativity of iodine, **A1** should react with iodine first. Therefore, the production of **A3** suggests that a hub carbon of **A1** reacts with iodine followed by addition of chloride at a rim carbon and rearomatization.

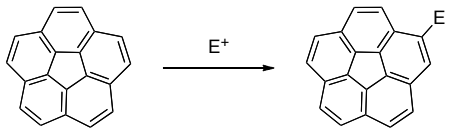

Scheme A2. Electreophilic aromatic substitution of A1.

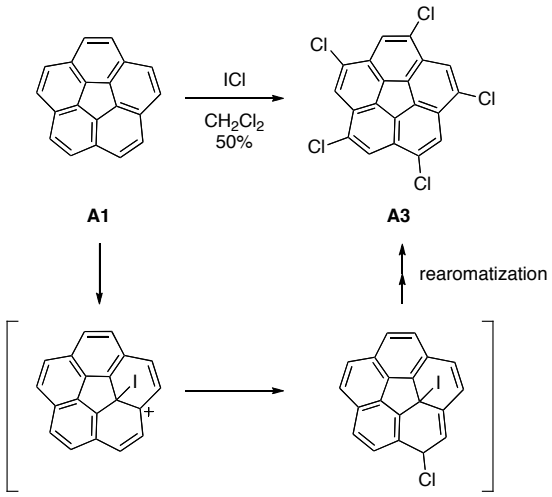

Scheme A3. Unique chlorination with iodine monochloride.

Another interesting example is the reaction with dichlorocarbene (Scheme A4).[38] In this reaction, dichlorocarbene reacts with **A1** first at the 6,6 ring junction to form **A4** followed by addition to yield diadduct **A5**. This selective attack is similar to that seen with **A2**. The stepwise mechanism was suggested by the fact that thermal decomposition of **A4** in the presence of cyclohexene leads to **A1** and 3,3'-dicyclohexenyl. The supposed mechanism is the C-C bond break in the cyclopropane moiety of **A4** following hydrogen abstraction and loss of $HCCl_2$ radical.

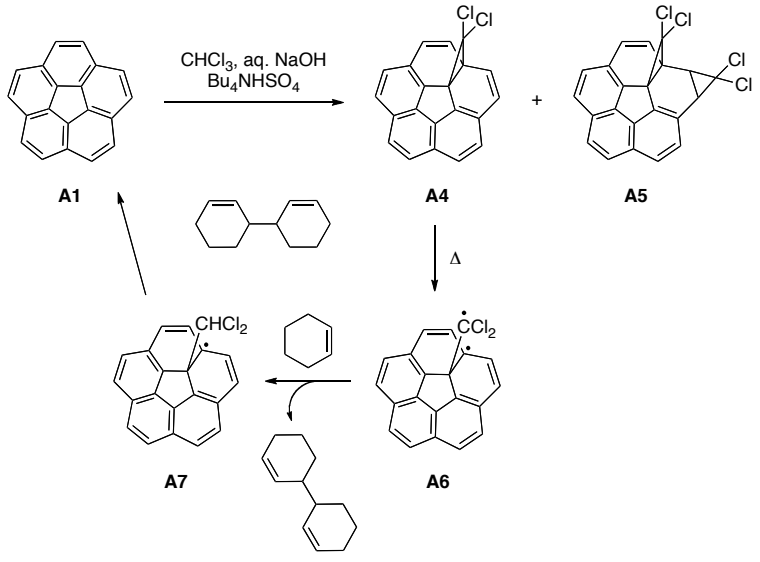

Scheme A4. Reaction of A1 with dichlorocarbene.

The reactivity studies performed on **A1** are limited compared with that of **A2**. However, the unique reactivities observed must result from the electrochemistry and structure of **A1**. The further synthetic methods will be discussed in the second chapter.

1.1.5. Application

The bulk production of **A2** promoted its application in many fields like materials or polymer chemistry and chemical biology. A wide variety of chemically modificated **A2** has been synthesized and utilized in many systems. For example, in the materials or polymer chemistry,[39] **A2** is used for electronic devices,[40] surface chemistry,[41] liquid crystals,[42] etc. On the other hand, the application of **A2** to biological systems was limited because **A2** is soluble in aromatic solvents and carbon disulfide, but virtually insoluble in water and alcohol.[43] However, the properties as an electron deficient olefin enable the modification of the structure with water-soluble functional groups. Those derivatives of **A2** are known to show a variety of pharmacological activities.[44] For example, they can exhibit photoinduced DNA scission properties[45] or are able to inhibit HIV-1 protease.[46] In addition, **A2** is capable of specific interactions with proteins, as shown by the production of fullerene-specific antibodies.[47] Such applications of **A2** are possible due to the unique electrochemistry, spherical structure, or reactivity and probably the most important point is its abundant supply.

The application of **A1** was limited mainly due to the relative synthetic difficulty. When the properties of **A1** are compared with those of **A2**, there are some noticeable similarities and differences. On the point of electrochemical properties, **A1** has accessible six oxidation states, although this is still less than eight seen for **A2**. Therefore, the materials or polymer chemistry of **A1** could also be attractive. On the other hand, the cap-type structure of **A1** may be useful as the base of a synthetic receptor and in this case, the unique dynamic bowl-to-bowl inversion property of **A1** would have some influence on the receptor efficiency. In addition, the buckybowl structure can be converted into not only the closed structure, but also the open-type nanometric scaffolds.

There are also differences in the reactivities and structures. First, **A1** has easily accessible convex and concave faces, which allow one to control the reaction points. Second, because of the open structure, the curvature can be adjusted by varying the rim substituents. Third is the ease of the structural modifications possible, which lead to various symmetries. Although **A1** loses the robust spherical structure of **A2**, the open buckybowl structure seems to have other advantages.

The recent development of efficient synthetic routes to **A1** in solution-phase provides large enough amounts of **A1** to investigate the materials or biological applications, although **A1** is still commercially unavailable and the supply is not sufficient for an industrial application. Therefore, the time has come to exploit its physical properties. In this thesis, the application of **A1** to carbon-based nanotube synthesis and synthetic receptors will be disscussed in chapter 4 and 5, respectively.

1.2. References

[1] Barth, W. E.; Lawton, R. G. *J. Am. Chem. Soc.* **1966**, *88*, 380.

[2] Osawa, E. *Kagaku (Chemistry).* **1970**, *25*, 854.

[3] Kroto, H. W.; Heath, J. R.; O'Brien, S. C.; Curl, R. F.; Smalley, R. E. *Nature* **1985**, *318*, 162.

[4] Krätschmer, W.; Lamb, L. D.; Fostiropoulos, K.; Huffman, D. R. *Nature* **1990**, *347*, 354.

[5] (a) Iijima, S. *Nature* **1991**, *354*, 56. (b) Smith, B. W.; Monthioux, M.; Luzzi, D. E. *Nature* **1998**, *396*, 323.

[6] (a) Wu, Y.-T.; Siegel, J. S. *Chem. Rev.* **2006**, *106*, 4843. (b) Tsefrikas, V. M.; Scott, L. T. *Chem. Rev.* **2006**, *106*, 4868.

[7] Scott, L. T. *Angew. Chem. Int. Ed. Engl.* **2004**, *43*, 4994.

[8] (a) Boorum, M. M.; Vasil'ev, Y. V.; Drewello, T.; Scott, L. T. *Science* **2001**, *294*, 828. (b) Scott, L. T.; Boorum, M. M.; McMahon, B. J.; Hagen, S.; Mack, J.; Blank, J.; Wegner, H.; de Meijere, A. *Science* **2002**, *295*, 1500.

[9] (a) *Fullerenes and Related Structures: Topics in Current Chemistry*; Vol. 199, Hirsch, A. (ed), Springer, Berlin, 1999. (b) Taylor, R. *Lecture Notes on Fullerene Chemistry: A Handbook for Chemists*; Imperial College, London, 1999,

[10] Alekseyev, N. I.; Dyuzhev, G. A. *Carbon* **2003**, *41*, 1343.

[11] (a) Howard, J. B.; McKinnon, J. T.; Makarovsky, Y.; Lafleur, A. L.: Johnson, M. E. *Nature* **1991**, *352*, 139. (b) Goel, A.; Howard, J. B. *Carbon* **2003**, *41*, 1949.

[12] (a) Hanson, J. C.; Nordman, C. E. *Acta. Crystallogr., Sect. B* **1976**, *B32*, 1147. (b) Sevryugina. Y.; Rogachev, A. Y.; Jackson, E. A.; Scott, L. T.; Petrukhina, M. A. *J. Org. Chem.* **2006**, *71*, 6615.

[13] Fedurco, M.; Olmstead, M. M.; Fawcett, W. R. *Inorg. Chem.* **1995**, *34*, 390.

[14] (a) Haddon, R. C.; Scott, L. T. *Pure. Appl. Chem.* **1986**, *58*, 137. (b) Haddon, R. C. *Acc. Chem. Res.* **1988**, *21*, 243. (c) Haddon, R. C. *J. Am. Chem. Soc.* **1990**, *112*, 3385. (d) Haddon, R. C. *Science* **1993**, *261*, 1545.

[15] (a) Chen, Z.; King, B. *Chem. Rev.* **2005**, *105*, 3613. (b) Lu, X.; Chen, Z. *Chem. Rev.* **2005**, *105*, 3643.

[16] Lawton, R. G.; Barth, W. E. *J. Am. Chem. Soc.* **1971**, *93*, 1730.

[17] (a) Scott, L. T.; Hashemi, M. M.; Bratcher, M. S. *J. Am. Chem. Soc.* **1992**, *114*, 1920. (b) Seiders, T. J.; Baldridge, K. K.; Grube, G. H.; Siegel, J. S. *J. Am. Chem. Soc.* **2001**, *123*, 517.

[18] Benshafrut, R.; Shabtai, E.; Ravinovitz, M.; Scott, L. T. *Eur. J. Org. Chem.* **2000**, 1091.

[19] Haddon, R. C.; Brus, L. E.; Raghavachari, K. *Chem. Phys. Lett.* **1986**, *125*, 459.

[20] Echegoyen, L.; Echegoyen, L. E. *Acc. Chem. Res.* **1998**, *31*, 593.

[21] Haufler, R. E.; Conceicao, J.; Chibante, L. P. F.; Chai, Y.; Byrne, N. E.; Flanagan, S.; Haley, M. M.; O'Brien, S. C.; Pan, C.; Xiao, Z.; Billups, W. E.; Ciufolini, M. A.; Hauge, R. H.; Margrave, J. L.; Wilson, L. J.; Curl, R. F.; Smalley, R. E. *J. Phys. Chem.* **1990**, *94*, 8634.

[22] Allemand, P.-M.; Koch, A.; Wudl, F.; Rubin, Y.; Diederich, F.; Alvarez, M. M.; Anz, S. J.; Whetten, R. L. *J. Am. Chem. Soc.* **1991**, *113*, 1050.

[23] Dubois, D.; Kadish, K. M.; Flanagan, S.; Haufler, R. E.; Chibante, L. P. F.; Wilson, L. J. *J. Am. Chem. Soc.* **1991**, *113*, 4364.

[24] Dubois, D.; Kadish, K. M.; Flanagan, S.; Wilson, L. J. *J. Am. Chem. Soc.* **1991**, *113*, 7773.

[25] Xie, Q.; Perez-Cordero, E.; Echegoyen, L. *J. Am. Chem. Soc.* **1992**, *114*, 3978.

[26] Joseph, W.; Surya Prakash, G. K.; Olah, G. A.; Tse, D. S.; Lorents, D. C.; Bae, Y. K.; Malhotra, R. *J. Am. Chem. Soc.* **1991**, *113*, 3205.

[27] (a) Zimmerman, J. A.; Eyler, J. R.; Bach, S. B. H.; McElvany, S. W. *J. Chem. Phys.* **1991**, *94*, 3556. (b) Lichtenberger, D. L.; Nebesny, K. W.; Ray, C. D.; Huffman, L.; Lamb, D. *Chem. Phys. Lett.* **1991**, *176*, 203. (c) Cox, D. M.; Trevor, D. J.; Reichmann, K. C.; Kaldor, A. *J. Am. Chem. Soc.* **1986**, *108*, 2457.

[28] Xie, Q.; Arias, F.; Echegoyen, L. *J. Am. Chem. Soc.* **1993**, *115*, 9818.

[29] Ayalon, A.; Rabinovitz, M.; Cheng, P.; Scott, L. T. *Angew. Chem. Int. Ed. Engl.* **1992**, *31*, 1636.

[30] Ayalon, A.; Sygula, A.; Cheng, P.; Rabinovitz, M.; Rabideau, P. W.; Scott, L. T. *Science* **1994**, *265*, 1065.

[31] Becker, H.; Javahery, G.; Petrie, S.; Cheng, P.; Schwarz, H.; Scott, L. T.; Bohme, D. K. *J. Am. Chem. Soc.* **1993**, *115*, 11636.

[32] Hirsch, A. *J. Phys. Chem. Solids* **1997**, *58*, 1729.

[33] *Fullerenes: Synthesis, Properties and Chemistry of Large Carbon Clusters*, Hammond, G. S.; Kuck, V. J. (eds), ACS Symp. Ser., 481, American Chemical Society, Washington, DC, 1992.

[34] Haddon, R. C. *Science* **1993**, *261*, 1545.

[35] Kitagawa, T.; Murata, Y.; Komatsu, K. *Carbon-Rich Compounds: from Molecules to Materials*; Haley, M. M.; Tykwinski, R. R. (eds), Wiley-VCH, Weinheim, 2006, Chapter 9.

[36] Cheng, P.-C. Ph.D. Dissertation, Boston College: Boston, MA, 1996; p212.

[37] Grube, G. H.; Elliott, E. L.; Steffens, R. J.; Jones, C. S.; Baldridge, K. K.; Siegel, J. S. *Org. Lett.*

2003, *5*, 713.

[38] Preda, D. V.; Scott, L. T. *Tetrahedron Lett*. **2000**, *41*, 9633.

[39] (a) Prato, M. *J*. *Mat*. *Chem*. **1997**, *7*, 1097. (b) Gigacalone, F.; Martín, N. *Chem*. *Rev*. **2006**, *106*, 5136.

[40] Illescas, B. M.; Martín, N. *C*. *R*. *Chimie*. **2006**, *9*, 1038.

[41] (a) Chupa, J. A.; Xu, S.; Fischetti, R. F.; Strongin, R. M.; McCauley, J. P.; Smith, A. B.; Blasie, J. K.; Peticolas, L. J.; Bean, J. C. *J*. *Am*. *Chem*. *Soc*. **1993**, *115*, 4383. (b)Bonifazi, D.; Enger, O.; Diederich, F. *Chem*. *Soc*. *Rev*. **2007**, *36*, 390.

[42] Chuard, T.; Deschenaux, R. *Helv*. *Chim*. *Acta*. **1996**, *79*, 736.

[43] Nakajima-Yamakoshi, Y.; Tagami, T.; Fukuhara, K.; Sueyoshi, S.; Miyata, N. *J*. *Chem*. *Soc*. *Chem*. *Commun*. **1994**, 517.

[44] (a) Jensen, A. W.; Wilson, S. R.; Schuster, D. I. *Bioorg*. *Med*. *Chem*. **1996**, *4*, 767. (b) Satoh, M.; Takayanagi, I. *J*. *Pharmacol*. *Sci*. **2006**, 100, 513.

[45] Tokuyama, H.; Yamago, S.; Nakamura, E. *J*. *Am*. *Chem*. *Soc*. **1993**, *115*, 7918.

[46] Sijbesma, R.; Srdanov, G.; Wudl, F.; Castoro, J. A.; Wilkins, C.; Friedman, S. H.; DeCamp, D. L.; Kenyon, G. L. *J*. *Am*. *Chem*. *Soc*. **1993**, *115*, 6510.

[47] Chen, B.-X.; Wilson, S. R.; Das, M.; Couglin, D. J.; Erlanger, B. F. *Proc*. *Natl*. *Acad*. *Sci*. *USA*. **1998**, *95*, 10809.

Chapter 2. Synthetic Method

2.1. Introduction

The synthetic methods to corannulene (**B1**) and its derivatives are classified into two conditions: solution- and gas-phase. For both conditions, relatively new reviews are available.[1,2] The following chapter will analyze the synthetic methods, paying particular attention to the solution-phase approach developed in our laboratories.

2.1.1. Pioneering Synthesis of Corannulene (B1)

The first synthesis of **B1** was reported in 1966 by Lawton and Barth.[3] Their synthesis starts from acenaphthalene (**B2**) and the key synthetic strategy is the formation of the partially saturated corannulene skeleton to overcome the strain distortions and aromatization at the final step (Scheme B1). Although Lawton's synthesis was many steps (17 steps) and low yielding (< 1%), it became a milestone of a non-planar PAH synthesis and enabled simple physical property measurements of **B1**.[4,5]

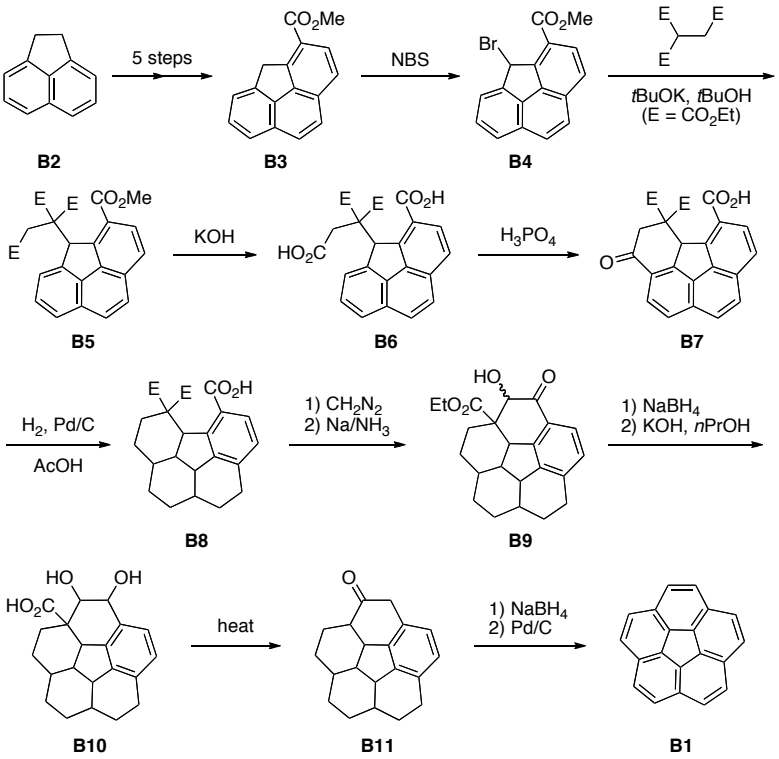

Scheme B1. First synthesis of B1 by Lawton.

Following Lawton's pioneering synthesis, strategies to improve the synthesis of **B1** were tried by 1) Davy and Reiss and 2) Craig and Robbins (Scheme B2). The former group tried the cyclization of a cyclophane (**B12**),[6] the latter group tried a Friedel-Crafts acylation of a fluoranthene derivative (**B13**).[7] Both attempts were not successful, but the latter group left the beneficial strategy for the fluoranthene synthesis as a key precursor of **B1** (Scheme B3).

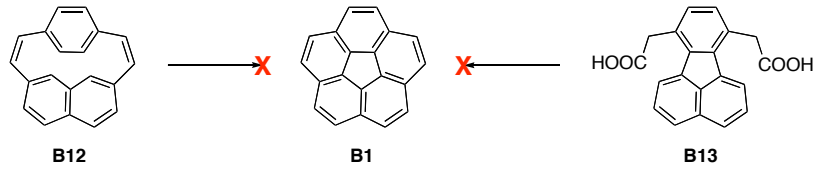

Scheme B2. Failed attempts to improve the synthesis of B1.

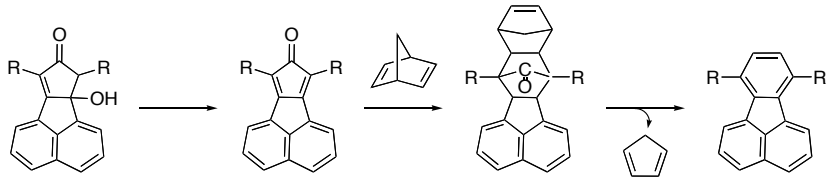

Scheme B3. Preparation of fluoranthenes.

2.1.2. Gas-Phase Synthesis of B1 with Flash Vacuum Pyrolysis

In 1991, many years after the first total synthesis by Lawton, an improved synthesis of **B1** using flash vacuum pyrolysis (FVP) was reported by Scott (Scheme B4).[8] Diyne (**B14**), prepared with Craig and Robbins' method,[7] was chosen as a precursor to **B1** for two reasons. The first reason was Brown's report of the transformation of ethynylnaphthalene to acenaphthalene. This suggested that terminal alkynes isomerize reversibly under FVP conditions by 1,2-shifts of hydrogen atoms and that the resulting vinylidenes can be trapped by insertion into nearby C-H bonds.[9] Based on this reasoning, the intermediate (**B15**) was predicted. Second, he reasoned that the bending of the fluoranthene skeleton because of the high energy from FVP would allow the ring-closing into **B1**, which failed in earlier reports.[7]

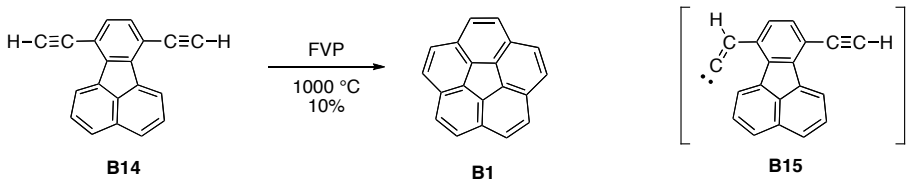

Scheme B4. First synthesis of B1 by FVP.

After his first report, Scott found that tetrabromide (**B16**) gives a better yield because it suffers less thermal polymerization during sublimation (Scheme B5).[10] Contemporarily with the work of Scott, Siegel reported two syntheses using FVP in 1992.[11] First, tetrakis(bromomethyl)-fluoranthene (**B17**) can be directly transformed into **B1**. On the other hand, the reaction of bissulfone (**B18**) was performed at a relatively low temperature under static vacuum, rather than in a flow system typical of FVP. Some starting materials have no fluoranthene nucleus. Diyne (**B19**), reported by Zimmerman, was converted to **B1** after the removal of trimethylsilyl (TMS) groups.[12] Helicenes (**B21**) were also used in 1997 by Mehta and Panda although these conversions were not efficient.[13] After many possibilities were investigated, the best precursor for the synthesis of **B1** with FVP was found to be the dichloride (**B20**).[10]

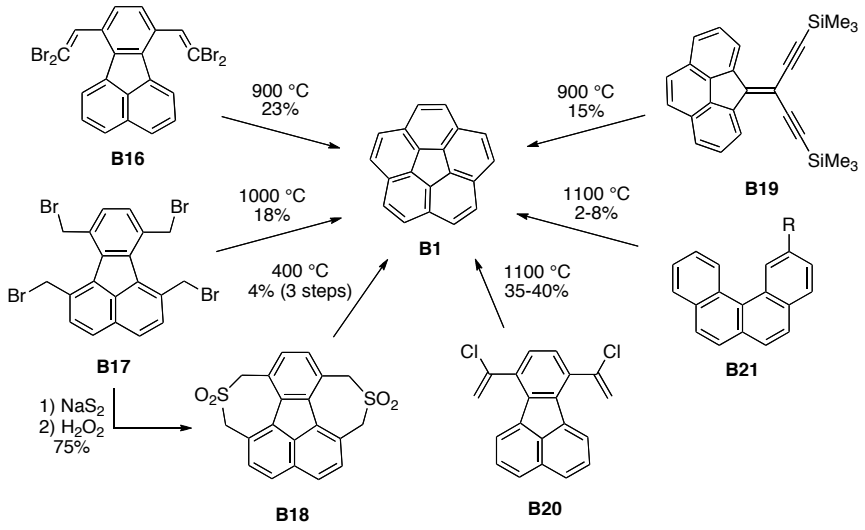

Scheme B5. Different routes to B1 by FVP.

2.1.3. Development of Efficient Solution-Phase Synthesis of B1

Although FVP gave a much better chemical yield than Lawton's first total synthesis of **B1**, there were some key problems for us as a general synthetic measure. First, the nature of the FVP equipment limits the large-scale synthesis. Second, there is almost no functional group tolerance because of the high temperature conditions. In addition, under high energy conditions, a possibility occurs to induce a thermal rearrangements of the molecule framework.[14] Therefore, to overcome these drawbacks of gas-phase synthesis, a mild solution-phase synthesis of **B1** was investigated.

The first solution-phase synthesis of a corannulene derivative was reported by Siegel in 1996 (Scheme B6).[15] The intermediate tetraalkylfluoranthene (**B24**) was prepared from the diketone **B22**.[11] The key step of this synthesis is a reductive coupling reaction of brominated fluoranthene derivative (**B25**) with low-valent titanium followed by dehydrogenation.

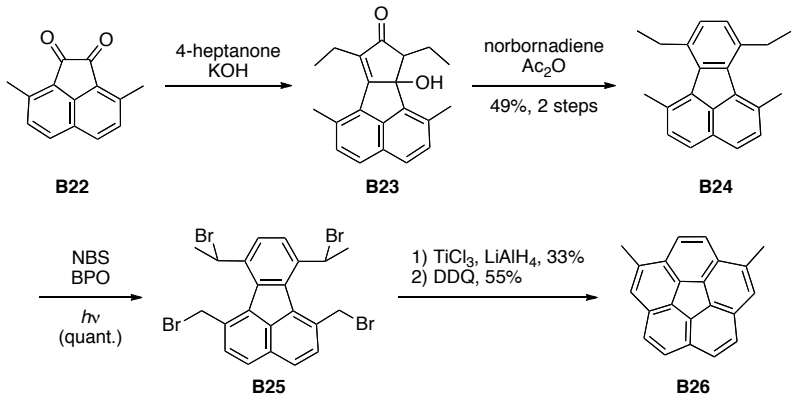

Scheme B6. First solution-phase synthesis of corannulene derivative.

The slightly modified methodology was applied for the synthesis of **B1** by Siegel and gave approximately 20% yield in 11 steps from commercially available 2,7-dimethylnaphthalene (**B27**) (Scheme B7).[16] At the same time, Rabideau reported the use of low-valent vanadium for the reductive coupling.[17]

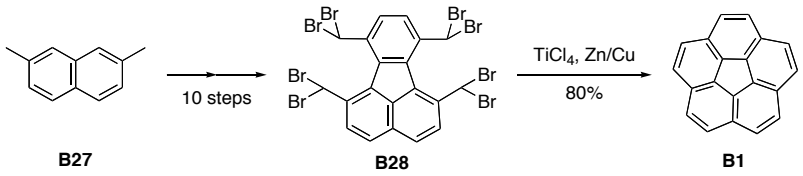

Scheme B7. Solution-phase synthesis of B1.

One disadvantage of reductive coupling with low-valent titanium or vanadium is the lack of functional group compatibility, and thus further refinement was desired. Sygula and Rabideau suggested the use of sodium hydroxide (Scheme B8)[18] and although this methodology is solvent dependent, large-scale synthesis is possible. When acetone and water were used as a solvent, complicated mixtures of dibrominated corannulenes (**B30**) were obtained and converted to **B1** using *n*-butyllithium followed by quenching with water. On the other hand, the use of a mixure of dioxane and water as a solvent produced only tetrabromocorannulene (**B31**) followed by the reductive removal of bromides with zinc metal and potassium iodide to afford **B1** in better yield.[18b] The expected mechanism in this reaction is benzylic hydrogen deprotonation followed by C-C bond formation.

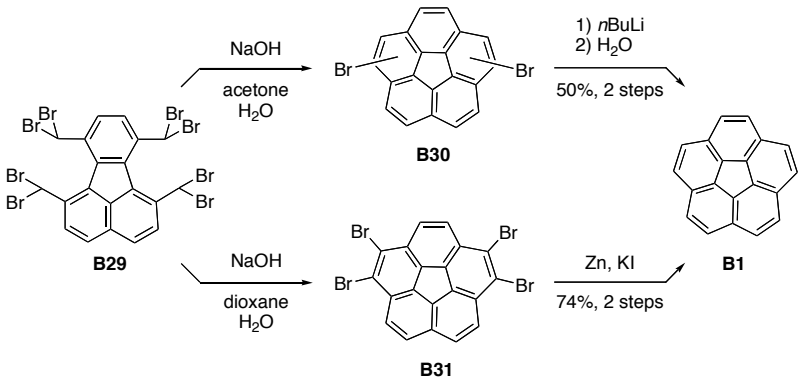

Scheme B8. Base catalyzed synthesis of B1 by Sygula and Rabideau.

Although reductive coupling with low-valent metal or sodium hydroxide produced many kinds of corannulene derivatives, the ester-functionalized corannulene derivatives were not synthesized because of its sensitibity. To overcome this problem, Sygula and Rabideau developed the extremely mild condition using nickel powder (Scheme B9).[19] The suggested intermediate is dibromide (**B34**) produced from the reductive coupling, which spontaneously converted to 1,2-dimethylcorannulene dicarboxylate (**B33**) under these reaction conditions.

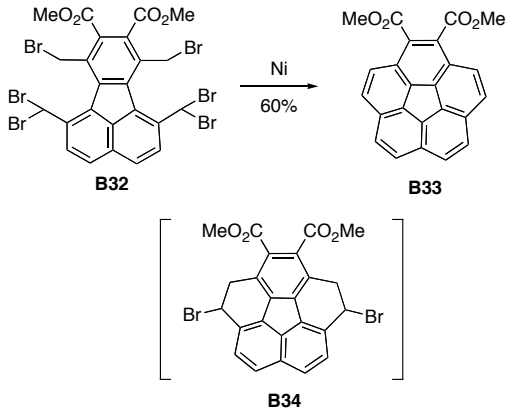

Scheme B9. Mild reaction conditions using nickel powder.

The following table summarizes the synthesis of different kinds of corannulene derivatives in three methodologies; reductive coupling with low-valent metals (titanium or vanadum), sodium hydroxide/zinc, and very mild nickel-mediated methods (Table B1).

Table B1. Synthesis of different kinds of corannulene derivatives under various conditions.

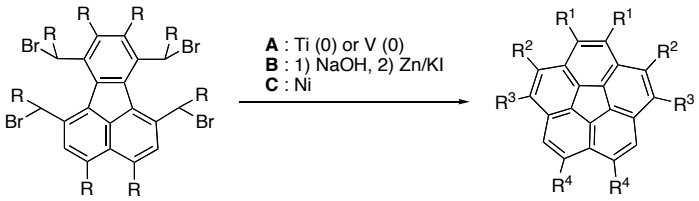

entry	R^1	R^2	R^3	R^4	method	yield (%)	ref
1	H	H	H	H	A (Ti)	80	16
2	H	H	H	H	A (V)	70-75	17
3	H	H	H	H	B	74	18
4	H	H	H	Cl	A (Ti)	85	16
5	H	Me	H	H	A (Ti)	24	15,16
6	H	H	Me	H	A (Ti)	48	16
7	H	H	Me	Cl	A (Ti)	45	16
8	H	Me	Me	H	A (Ti)	6	16
9	H	Me	H	H	B	66	20
10	H	2-BrPh	Br	H	B	96	21
11	CO_2Me	H	H	H	C	60	19
12	CO_2Me	H	H	Cl	C	49	22
13	CO_2Me, Ph	H	H	Cl	C	51	22

2.1.4. Substituted Corannulene Synthesized from Halocorannulenes

Halocorannulenes are some of the most promising candidates for introducing a broad spectrum of substituents into **B1**. Transition metal mediated coupling reactions for a variety of halide partners are now available. Some types of halocorannulene were synthesized and converted to corannulene derivatives using such reactions..

Bromocorannulene (**B35**) is prepared by bromination of **B1** with iron (III) bromide.[23] Methylcorannulene (**B36**) can be obtained from trimethylaluminium[16] or methylmagnesium bromide[24] in the presence of a catalytic amount of nickel (0) (Table B2). The reaction with organolithium reagents (R = *i*Pr, *t*Bu, or Bn) gives the intermediates, 1-alkyl-1,2-dehydrocorannulenes, and subsequent dehydrogenation produces the corresponding monoalkylcorannulene (**B37**).[25] The conversion of **B35** with *n*-butyllithium to the corannulyl lithium species and quenching with acetone affords the corresponding dimethylhydroxy-corannulene (**B38**).[26] The nickel-catalyzed Negishi coupling produces various monoarylcorannulenes (**B39**)[27] and trimethylsilylethynylcorannulene (**B40**) or phenylethylnyl-corannulene (**B41**) are accessible from **B35** by Sonogashira coupling.[28] Two σ-bond metal complexes have also been synthesized. Bis(1,5-cyclooctadiene) nickel(0) ($Ni(COD)_2$) addition to a mixture of triethylphosphine and **B35** results in the formation of *trans*-$Ni(PEt_3)_2(Br)$(corannulenyl) (**B42**).[29] On the other hand, the analogous platinum complex (**B43**) is readily obtained from the reaction of tetrakis-(triethylphosphine)platinum and **B35**.

Table B2. Synthesis of monosubstituted corannulenes.

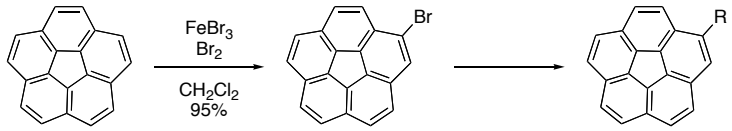

B1 **B35**

entry	product	R	condition	yield (%)	ref
1	**B36**	Me	$AlMe_3$, cat. $NiCl_2$(dppp) DME	90	16
2	**B36**	Me	MeMgBr, cat. $NiCl_2$(dppp) THF	63	24
3	**B37**	alkyl	1) RLi 2) Pd/C	—	25
4	**B38**	HO–	1) *n*BuLi 2) acetone	40	26
5	**B39**	Ar	ArZnCl, cat. $NiCl_2$(dppp) THF	—	27
6	**B40**	Me_3Si–	TMS-acetylene cat. $PdCl_2(PPh_3)_3$, CuI, NEt_3	97	28
7	**B41**	Ph–	phenylacetylene cat. $PdCl_2(PPh_3)_3$, CuI, NEt_3	67	28
8	**B42**	Et_3P, Br–Ni–, Et_3P	1) PEt_3, toluene 2) $Ni(COD)_2$, toluene	85	29
9	**B43**	Et_3P, Br–Pt–, Et_3P	$Pt(PEt_3)_4$, toluene	79	29

1,2,5,6-Tetrabromocorannulene (**B31**) and 1,2,5,6-tetraiodocorannulene (**B44**) are also useful for making corannulene derivatives (Scheme B10). The preparation and reactions of these compounds were reported by Sygula and Rabideau.[18] Using the reaction of trimethylaluminium, Sonogashira coupling, and Suzuki coupling, **B31**, which is a precursor of **B1**, can be converted to **B45**, **B46**, and **B47**, respectively. On the other hand, **B33** can also undergo the halogen-exchange reaction to afford **B44** as a better substrate for the Heck reaction. The Heck reaction of **B44** with methyl acrylate provides tetrakisethenylcorannulene (**B48**) and when styrene was used, the spontaneous cyclization/dehydrogenation process yields tetraphenyldibenzo-[a,g]-corannulene (**B49**).

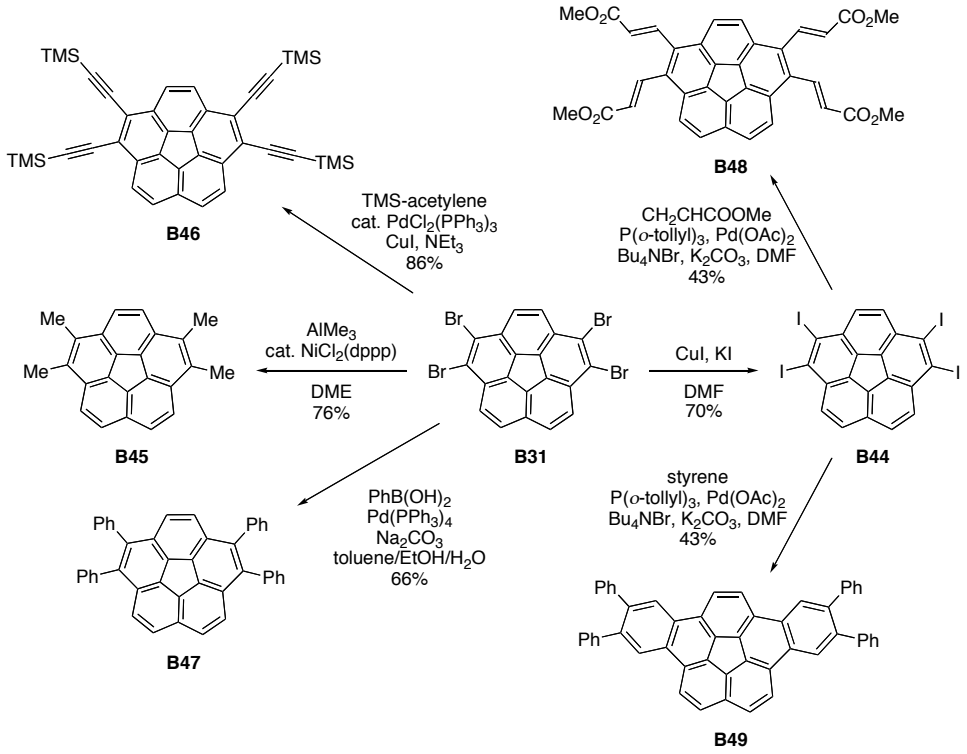

Scheme B10. Synthesis of 1,2,5,6-tetrasubstitutedcorannulenes.

2,3-Dichlorocorannulene (**B56**) was synthesized by Siegel starting with acenaphthalene (**B2**) (Scheme B11).[16] Treatment of **B56** with trimethylaluminium and catalytic amount of $NiCl_2$(dppp) yields 2,3-dimethylcorannulene (**B57**) (Table B3).[30] Under the same conditions, phenylmagnesium bromide produced 2,3-diphenylcorannulene (**B58**). The ethyleneglycol derivative (**B59**) can be prepared from the reaction with diethyleneglycol monomethylether with an excess of sodium hydride.

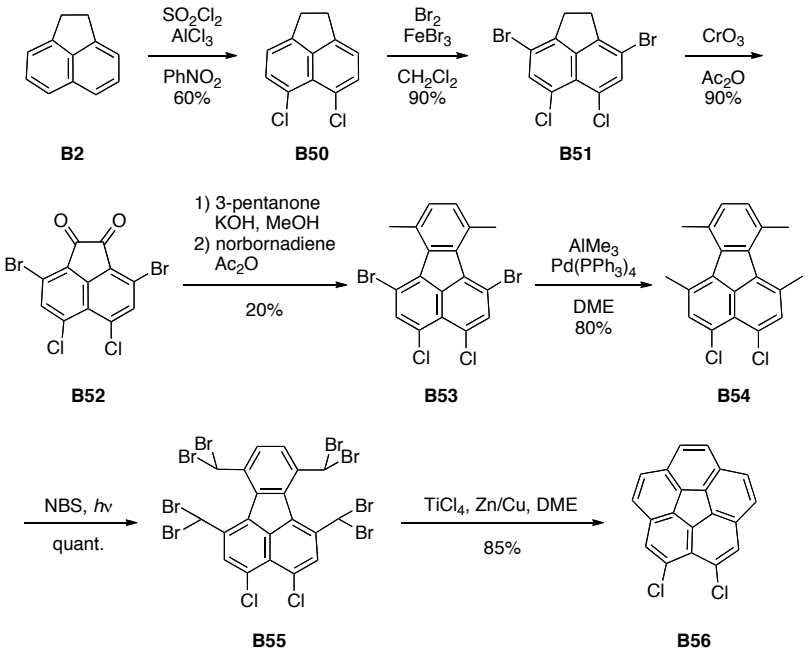

Scheme B11. Synthesis of 2,3-dichlorocorannulene (B56).

Table B3. Synthesis of 2,3-disubstitutedcorannulenes.

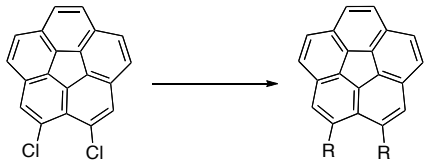

B56

entry	product	R	condition	yield (%)	ref
1	**B57**	Me	$AlMe_3$, cat. $NiCl_2$(dppp)	90	30
2	**B58**	Ph	PhMgBr, cat. $NiCl_2$(dppp)	40	30
3	**B59**	$O(CH_2CH_2O)_2CH_3$	NaOR, ROH	25	30

Two other chlorinated corannulenes, *sym*-pentachlorocorannulene (**B60**) and decachlorocorannulene (**B61**) can be synthesized from **B1** (Scheme B12). Treatment of **B1** with iodine monochloride produces **B60** in a 70-80% yield, along with impurities consisting of tri-, tetra-, hexasubstituted compounds, etc.[31] To make the decachlorinated derivative, a reaction using the Ballester-Molinet-Castaner reagent (sulfonyl chloride, sulfur dichloride, and aluminium chloride) gives **B61**.[32] This reaction also does not produce the pure compound but includes some amount of overchlorinated compounds. The overchlorinated compounds are rearomatized by heating at high temperature to produce **B61**.

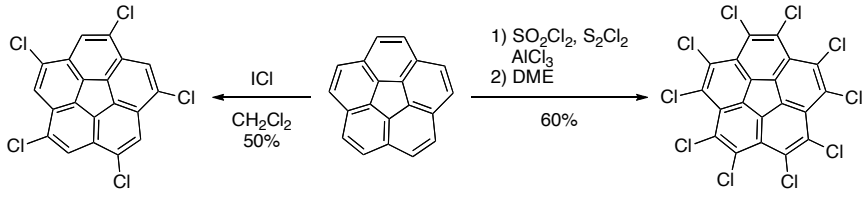

B60 **B1** **B61**

Scheme B12. Chlorinations of B1.

Once both chlorinated species are obtained, they can be converted to alkyl-, aryl-, and alkynyl-derivatives using organometallic chemistry (Table B4).[33] For example, the reaction of **B60** with trimethylaluminium and catalytic amount of $NiCl_2$(dppp) yields pentaalkylcorannulenes (**B62**), while some types of zinc-based Negishi coupling work moderately well to afford pentaarylcorannulenes (**B63**). However, because of the low reactivity of arylchlorides for the coupling reaction and steric hindrance of arylzincate, an extremely low yield (Ar = manisyl, 7%) is also obtained. *sym*-Pentakis(trimethylsilylacetylenyl)corannulene (**B64**) can be prepared from **B60** and a large excess amount of trimethylsilylethyne using Eberhard's method with the pincer catalyst (**B67**).[34]

Table B4. Synthesis of pentasubstitutedcorannulenes.

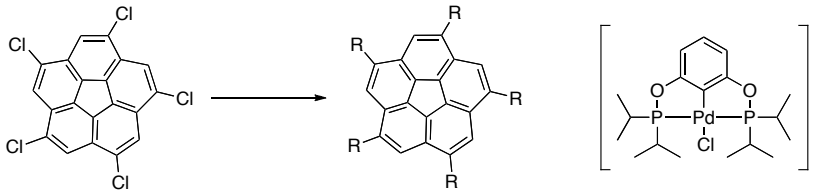

B60 **B67**

entry	product	R	condition	yield (%)	ref
1	**B62**	R	AlR_3, cat. $NiCl_2$(dppp) DME	31-51	33
2	**B63**	Ar	ArZnCl, cat. $NiCl_2$(dppp) THF	7-49	33
3	**B64**	Me_3Si—≡—	TMS-acetylene cat. **S77**, CuI, NEt_3	53	33
4	**B65**	SR or SAr	RSH, Na, DMEU	22-55	35
5	**B65**	SR or SAr	RSH, NaH, DMEU	36-38	33
6	**B66**	$O(CH_2CH_2O)_2CH_3$	ROH, NaH	41	33

Nucleophilic aromatic substitution is also useful for the preparation of pentasubstitutedcorannulene derivatives. Some kinds of thiocorannulenes (**B65**) were prepared from the corresponding thiols with sodium[35] or sodium hydride[33] in dimethylethanourea (DMEU). On the other hand, alkoxides are generally less nucleophilic than thiolates and thus their reactions need harsher conditions. The reaction of **B60** and sodium diethyleneglycolate monomethyl ether was performed at 180 ºC for two days to afford **B66**.[33]

B61 can also be converted to other types of derivatives (Scheme B13). Decamethylcorannulene (**B68**) was prepared by methylation with trimethylaluminium in the presence of nickel catalyst, but DME was replaced with DMEU as a solvent to heat to a higher temperature.[16] Various kinds of decaalkylthiocorannulenes (**B69**) were also synthesized by a nucleophilic aromatic substitution.[35b] One interesting molecule is pentakis(1,4-benzodithiino)-corannulene (**B70**) obtained from the reaction of **B61** with sodium 1,2-benzenethiolate.

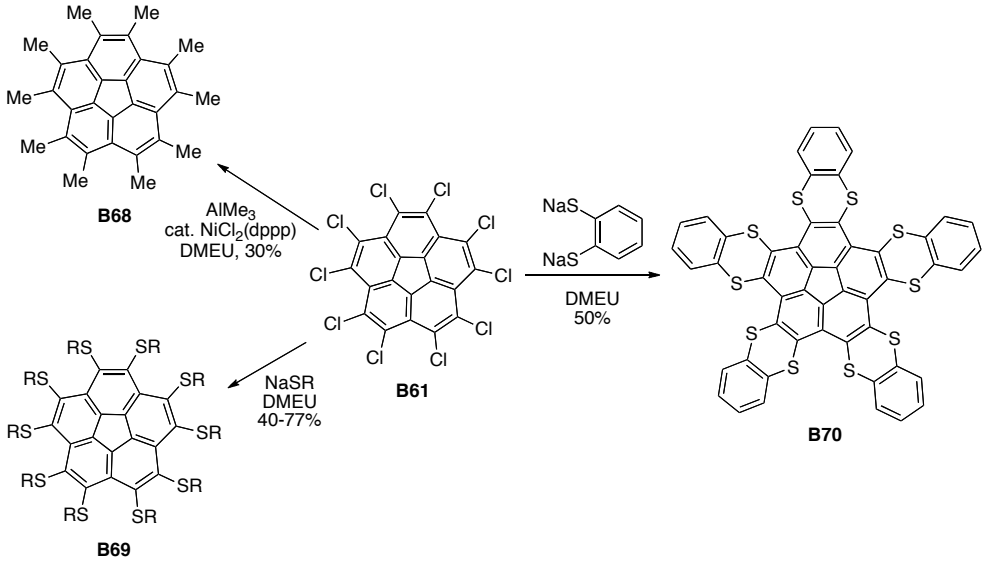

Scheme B13. Synthesis of decasubstitutedcorannulenes.

2.2. Present Work

2.2.1. Synthesis of *sym*-Pentaarylcorannulenes

From a geometrical point of view, *sym*-pentasubstitutedcorannulenes are quite attractive because of their five-fold symmetry and the bowl structure of the corannulene nucleus. As already mentioned, various kinds of *sym*-pentasubstitutedcorannulenes were already synthesized.[33] *sym*-Pentaarylcorannulene derivatives seem to be most promising in some applications for a number of reasons. First is their ease of syntheses. Generally, palladium- or nickel-catalyzed cross-coupling reactions tolerate various functional groups and thus, many kinds of substituents can be introduced.[36] Second, in the case of 2,6-disubstituted systems, five aryl rings will be perpendicular to the corannulene bowl to minimize steric repulsion and then introduced substituents will develop the three dimensional properties.

There are still problems associated with this type of reaction. For example, in the oxidative addition step of the cross-coupling reaction, chlorides are less reactive than the corresponding bromides. In addition, **B60** has five chlorides and therefore, low chemical yield for each coupling reaction will be fatal. In the case of manisyl substituents, the reported chemical yield was extremely low (only 7%) because of its steric bulkiness and electron donating groups (Scheme B14). Therefore, the optimization of the cross-coupling reaction was investigated.

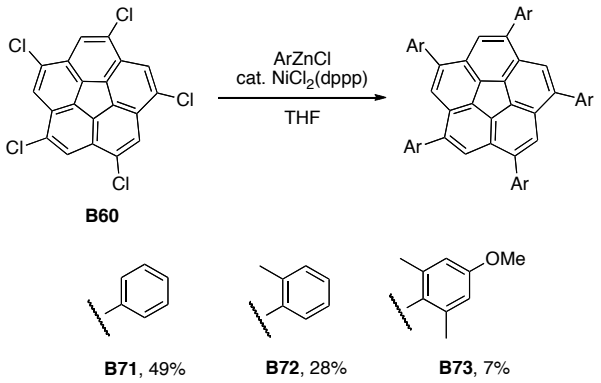

Scheme B14. Effect of steric hindrance for coupling reaction.

Considering steric bulkiness and electron donation, the following bromides (**B35**, **B74**-**80**) were chosen for the coupling partner with **B60** (Figure B1). Manisyl bromide (**S74**) and 1-bromo-2,6-diethylbenzene (**B76**) are commercially available, and 1-bromo-2,6-dimethoxybenzene (**B75**)[37] and **B35**[23] were prepared by literature procedures.

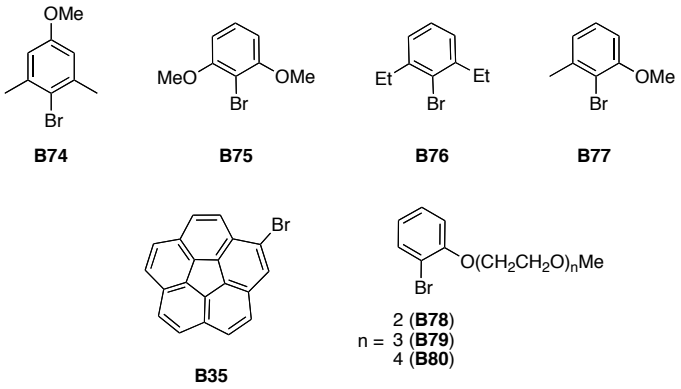

Figure B1. Selected bromides for the coupling reaction.

B75 was prepared in two steps (Scheme B15). The reaction of aryllithium from the ortho lithiation with dimethyltin dichloride in the presence of catalytic amounts of *N*,*N*,*N*',*N*'-tetramethylenediamine (TMEDA) afforded bis(2,6-dimethoxyphenyl)dimethyltin (**B82**). The bromination of **B82** with *N*-bromosuccinimide (NBS) yielded **B75**. 1-Bromo-2-methoxy-6-methylbenzene (**B77**) was simply prepared from aniline (**B83**) using the Sandmeyer reaction and **B35** was obtained from the bromination of **B1**. Long-chain bromides (**B78**-**80**) were synthesized by Williamson ether synthesis with the corresponding chlorides, potassium iodide, and potassium carbonate.

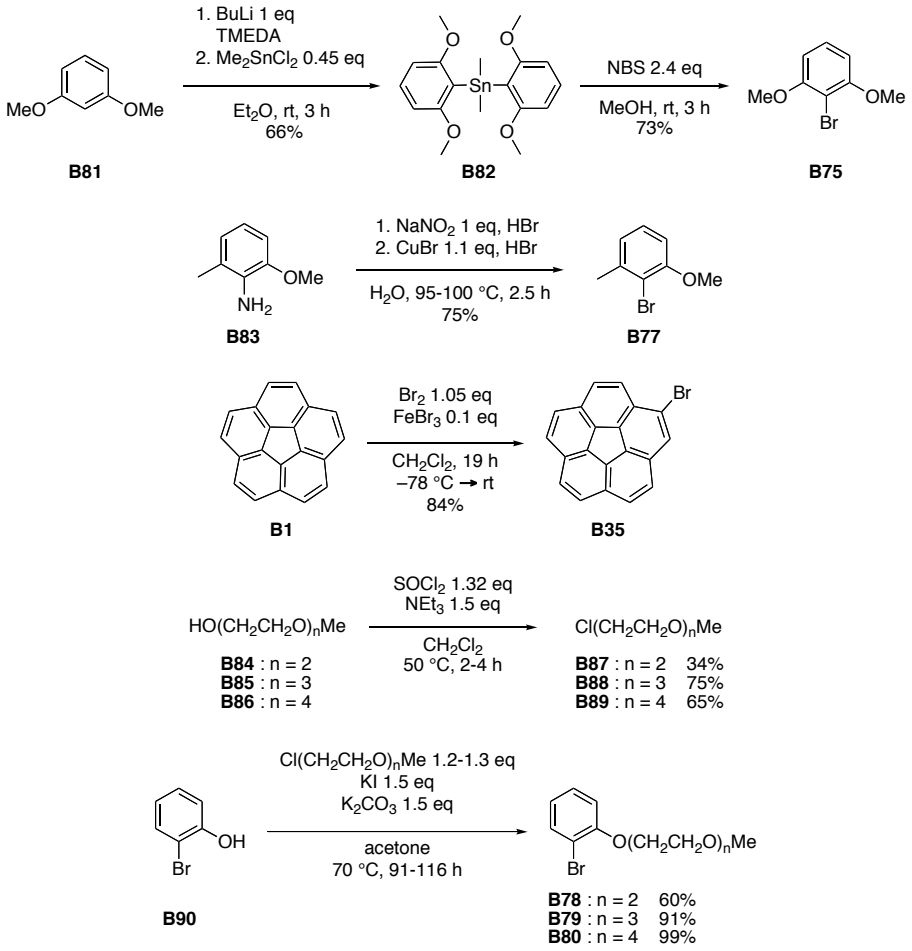

Scheme B15. Synthesis of bromides.

Today, two kinds of ligands are mainly used for the cross-coupling reaction. One is phosphines and the other is *N*-heterocyclic carbenes (NHCs).[38] Although the structural and electronic properties of the phosphine ligands are relatively well understood, they are highly toxic, oxygen-sensitive, and not easy to synthesize. On the other hand, the current understanding of the structural and electronic properties of NHCs is limited, but their toxicity is low and they are not oxygen-sensitive.[39] In addition, these compounds are very easy to prepare on a large scale.

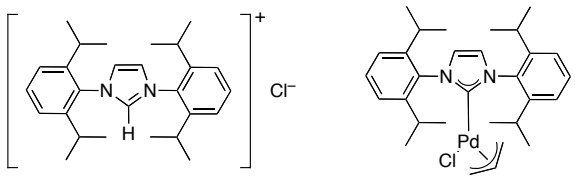

IPr-HCl **B91** (IPr)Pd(allyl)Cl **B92**

Figure B2. NHC ligand and its palladium complex.

The combination of *N*,*N*'-bis(2,6-diisopropylphenyl)imidazol-2-ylidene hydrogen chloride (IPr-HCl) (**B91**)[40] and palladium (II) acetate or NHC-palladium complex, (IPr)Pd(allyl)Cl (**B92**)[41] were used for our system (Figure B2, Scheme B16). The chemical yield of **B73** synthesis was generally improved compared with the Negishi coupling reaction using $NiCl_2$(dppp). Even in the case of *sym*-penta(2,6-dimethoxyphenyl)corannulene (**B93**), a moderately good yield was obtained in spite of its steric hindrance and highly electron rich properties. Although the chemical yield is very low, *sym*-penta(2,6-diethylphenyl)corannulene (**B94**) was also synthesized. In this reaction, relatively large amounts of mono-, di-, tri-, and tetrasubstituted compounds were confirmed, and thus the C-H insertion may occur during the coupling cycle. When the asymmetric substituents were used, an interesting result was found. The thin layer chromatography (TLC) of *sym*-penta(2-methoxy-6-methylphenyl)corannulene (**B95**) shows three spots and even if they are separated, isomerization occurs at room temperature. Probably it is because of the slow rotation of arylrings. The purification of *sym*-pentacorannulylcorannulene (**B96**) was extremely difficult work because of its low solubility. *sym*-Pentasubstitutedcorannulene (**B97**-**99**) having long chains were also synthesized.

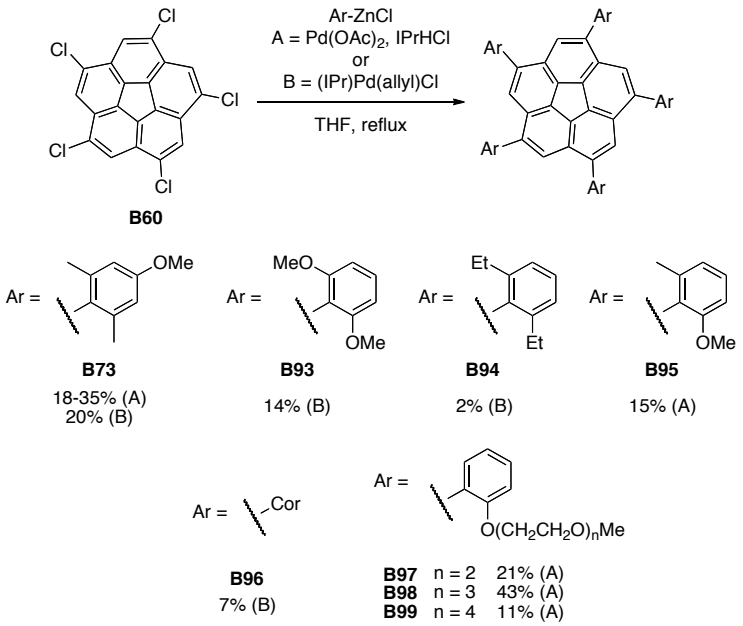

Scheme B16. Synthesis of *sym*-pentaarylcorannulenes.

B73, **B93**, and **B94** will be utilized for the study of the inversion energies in the third chapter. In the meanwhile, **B97-99** could be potentially used for making two-dimensional films on the water surface because they have five long hydrophilic tails.[42] Because **B96** has six corannulene nuclei, it may have an interesting electrochemistry.

2.2.2. Crystal Structures

The crystal structures of **B93** and **B94** were obtained from the mixture of *n*-propanol and dichloromethane (Figure B3 and Figure B4). These structures are similar to that of **B73**, and thus could be useful for the investigation of the relationship between bowl inversion and *endo* group effects.[43] This will be discussed in the following chapter.

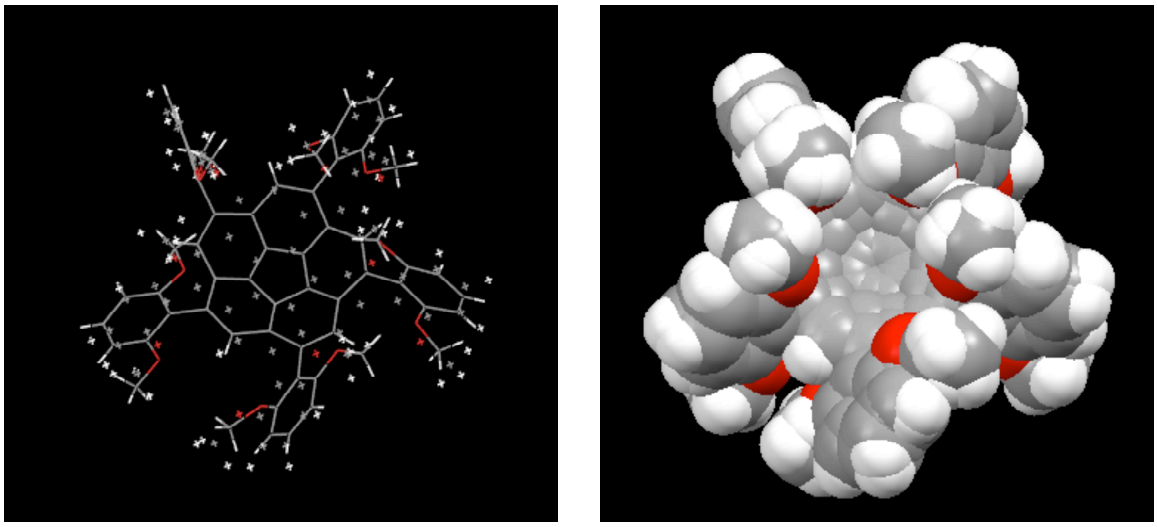

Figure B3. Crystal structure of B93.

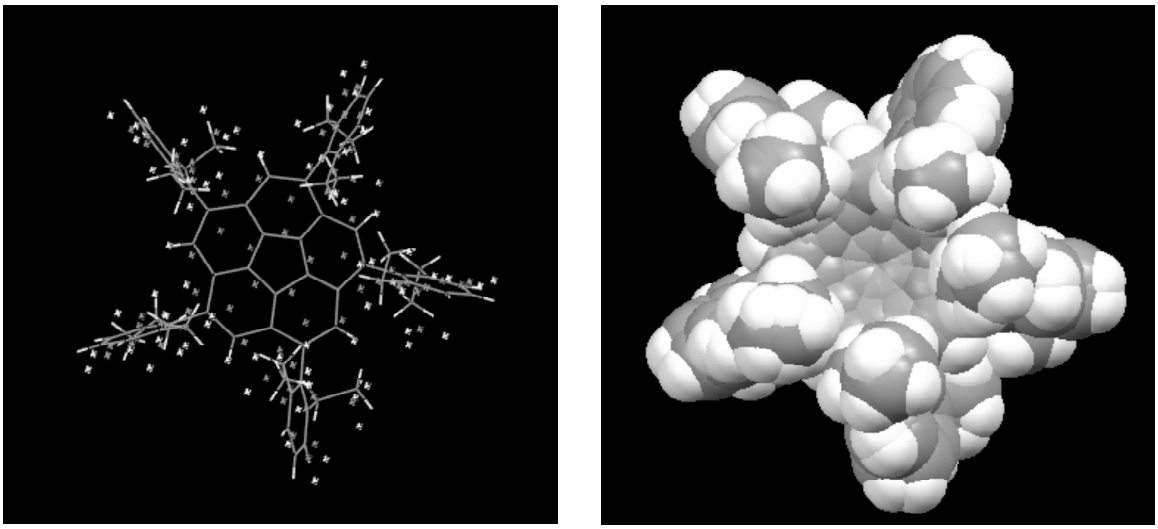

Figure B4. Crystal structure of B94.

2.2.3. Experimental Section

2.2.3.1. Materials and Methods

General: ^{1}H and ^{13}C NMR: Bruker AV-300 (300 and 75.5 MHz), AV2-400 (400 and 101 MHz), DRX-500 (126 MHz), AV-600 (600 and 151 MHz). – IR: Perkin Elmer Spectrum One (FT-IR). – EI- or CI- MS: Finnigan MAT95 MS, ESI-MS: Bruker EsquireLC MS, MALDI-MS: Bruker Autoflex I MALDI-TOF spectrometer. – X-ray structures were carried out by the X-ray analysis department of the Organic Chemistry Institute using a Nonius Kappa CCD diffractometer with MoKα radiation (λ = 0.71037 Å). – Chromatography: Merck silica gel 60 (230–400 mesh) or Fluka neutral alumina (Brockmann I, Activity II). – Melting points were measured to a maximum temperature of 350 °C. All experiments were carried out under nitrogen in freshly distilled anhydrous solvents unless otherwise noted. Solvents for chromatography were technical grade and freshly distilled before use. Corannulene (**B1**),[28] *sym*-pentachlorocorannulene (**B60**),[31] and *N*,*N*'-bis(2,6-diisopropylphenyl)imidazol-2-ylidene hydrogen chroride (IPr-HCl) (**B91**),[40] (IPr)Pd(allyl)Cl (**B92**)[41] were prepared according to the literature procedures. Other compounds, which are not mentioned, are commercially available.

2.2.3.2. Synthetic Procedures

Bis(2,6-dimethoxyphenyl)dimethyltin (B82)

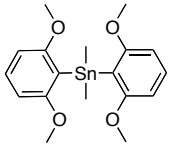

$C_{18}H_{24}O_4Sn$
Mol. Wt.: 423.0908

n-Butyllithium (1.5 M in hexane, 22 mL, 33 mmol) was added to the mixture of 1,3-dimethoxybenzene (**B81**) (4.56 g, 33 mol) and *N*,*N*,*N*',*N*'-tetramethylenediamine (0.12 mL) under nitrogen at 0 °C. The mixture was stirred at room temperature for 2 h to afford white suspension. The suspension was added under nitrogen to a suspension of dimethyltin dichloride (3.29 g, 15 mmol) in ether (2 mL) at 0 °C and the mixture was stirred at room temperature for 3 h. Water (20 mL) was added and the organic layer was separated, washed with water (20 mL × 2), dried with magnesium sulfate and evaporated. The product was purified by recrystallization with hexane to yield **B82** as a white solid (4.60 g, 66%). The spectroscopic data were identical with those reported.[37] Mp 93-94 °C (lit. 93-94 °C).[37]

1-Bromo-2,6-dimethoxybenzene (B75)

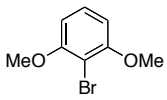

$C_8H_9BrO_2$
Mol. Wt.: 217.0599

The mixture of bis(2,6-dimethoxyphenyl)dimethyltin (**B82**) (4.24 g, 10 mmol) and *N*-bromosuccinimide (4.27 g, 24 mmol) in methanol (40 mL) was stirred at room temperature for 3 h. The resultant suspension was poured into aqueous hydrochloric acid (0.3 M, 80 mL) to afford white precipitate. The precipitate was filtered and washed with water to give white solid. The crude mixture was purified by recrystallization with methanol to yield **B75** as a white needle (3.16 g, 73%). The spectroscopic data were identical with those reported.[37] Mp 91-92 °C (lit. 90-92 °C).[37]

1-Bromo-2-methoxy-6-methylbenzene (B77)

C_8H_9BrO
Mol. Wt.: 201.0605

To a mixture of 2-methoxy-6-methylaniline (**B83**) (3.09 g, 22.5 mmol) and 10% aqueous hydrobromic acid (75 mL), a solution of sodium nitrite (1.55 g, 22.5 mmol) in water (15 mL) was added slowly dropwise at 0 °C in an ice bath. The mixture was stirred at 0 °C for 15 min. The mixture was added below the surface of a hot (95-100 °C) solution of cuprous bromide (3.55 g, 24.8 mmol) in 10% aqueous hydrobromic acid (30 mL). The mixture was stirred at 95-100 °C for 2.5 h. After cooling to room temperature, the mixture was extracted with dichloromethane (75 mL × 2). The organic layer was washed with water (75 mL × 2), 10 % aqueous hydrochloric acid (75 mL) and 10% aqueous sodium hydroxide (75 mL), dried with magnesium sulfate, and evaporated to yield **B77** as an orange solid (3.36 g, 75%). Mp 41-43 °C. ^{1}H-NMR (300 MHz, $CDCl_3$): δ ppm = 2.42 (s, 3H), 3.89 (s, 3H), 6.74 (d, ^3J = 8.1 Hz, 1H), 6.87 (d, ^3J = 8.1 Hz, 1H), 7.16 (t, ^3J = 8.1 Hz, 1H). ^{13}C-NMR (75.5 MHz, $CDCl_3$): δ ppm = 23.2 (CH_3), 56.2 (CH_3), 109.1 (CH), 114.1 (C), 122.9 (CH), 127.4 (CH), 139.6 (C), 155.9 (C). IR (KBr): ν cm^{-1} = 3435, 2967, 2839, 1933, 1569, 1453, 1255, 1095, 619. MS (EI): *m*/*z* (%): 200.0 (M^+). HRMS (EI): calcd for C_8H_9OBr: 199.9837; found: 199.9839.

Bromocorannulene (B35)

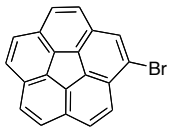

$C_{20}H_9Br$
Mol. Wt.: 329.1895

Bromine (67 mg, 0.42 mmol) in dichloromethane (5 mL) was added dropwise over 5 min to a solution of corannulene (**B1**) (100mg, 0.40 mmol) and iron (III) bromide (12 mg, 0.04 mmol) in dichloromethane (5 mL) at –78 °C in a dry ice/acetone bath. The solution was stirred at –78 °C for 5 h and allowed to warm to room temperature for 19 h. The mixture was washed with saturated sodium bisulfite (50 mL × 3) and water (50 mL), dried with magnesium sulfate, and evaporated. The product was purified by column chromatography on silica gel eluted with cyclohexane. The solvent was evaporated to yield **B35** as a white solid (110 mg, 84%) [R_f = 0.49 (SiO_2, cyclohexane)]. The spectroscopic data were identical with those reported.[16] Mp 176-177 °C (lit. 174-176 °C).[16]

2-(2-methoxyethoxy)ethoxy chloride (B87)

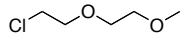

$C_5H_{11}ClO_2$
Mol. Wt.: 138.5926

To a mixture of 2-(2-methoxyethoxy)ethanol (**B84**) (10.0 g, 83.2 mmol) and triethylamine (12.6 g, 125 mmol) in dichloromethane (300 mL), thionyl chloride (13.1 g, 110 mmol) was added slowly. The mixture was refluxed in an oil bath for 2 h. After cooling to room temperature, the mixture was carefully poured into saturated sodium hydrogen carbonate (400 mL) and stirred for 5 min. The organic layer was separated and the aqueous layer was extracted with dichloromethane (200 mL × 2). The combined organic layer was washed with water (200 mL) and saturated sodium chloride (200 mL), dried with sodium sulfate, and evaporated. The product was purified by bulb-to-bulb distillation to yield **B87** as colorless oil (3.92 g, 34%). ^{1}H-NMR (400 MHz, $CDCl_3$): δ ppm = 3.38 (s, 3H), 3.54-3.57 (m, 2H), 3.62-3.68 (m, 4H), 3.73-3.76 (t, ^3J = 6.0 Hz, 2H). ^{13}C-NMR (101 MHz, $CDCl_3$): δ ppm = 42.7 (CH_3), 59.0 (CH_2), 70.6 (CH_2), 71.4 (CH_2), 71.9 (CH_2). IR (KBr): ν cm^{-1} = 3508, 2881, 1738, 1454, 1300, 1118, 850, 747, 666. MS (CI): *m*/*z* (%): 139.1 (M^+ + H). HRMS (CI): calcd for $C_5H_{12}O_2Cl$: 139.0526; found: 139.0526.

2-[2-(2-methoxyethoxy)ethoxy]ethoxy chloride (B88)

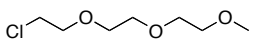

$C_7H_{15}ClO_3$
Mol. Wt.: 182.6452

To a mixture of 2-[2-(2-methoxyethoxy)ethoxy]ethanol (**B85**) (20.0 g, 120 mmol) and triethylamine (18.5 g, 183 mmol) in dichloromethane (600 mL), thionyl chloride (19.0 g, 159 mmol) was added slowly. The mixture was refluxed in an oil bath for 3 h. After cooling to room temperature, the mixture was carefully poured into saturated sodium hydrogen carbonate (800 mL) and stirred for 5 min. The organic layer was separated and the aqueous layer was extracted with dichloromethane (400 mL × 2). The combined organic layer was washed with water (400 mL) and saturated sodium chloride (400 mL), dried with sodium sulfate, and evaporated. The product was purified by bulb-to-bulb distillation to yield **B88** as pale yellow oil (16.6 g, 75%). ^{1}H-NMR (400 MHz, $CDCl_3$): δ ppm = 3.38 (s, 3H), 3.54-3.56 (m, 2H), 3.62-3.70 (m, 8H), 3.74-3.77 (t, ^3J = 6.0 Hz, 2H). ^{13}C-NMR (101 MHz, $CDCl_3$): δ ppm = 42.7 (CH_3), 59.0 (CH_2), 70.58 (CH_2), 70.61 (CH_2), 70.7 (CH_2), 71.4 (CH_2), 71.9 (CH_2). IR (KBr): ν cm^{-1} = 3517, 2878, 1954, 1636, 1456, 1300, 1200, 1110, 850, 745, 665. MS (CI): *m/z* (%): 183.1 (M^+ + H). HRMS (CI): calcd for $C_7H_{16}O_3Cl$: 183.0788; found: 183.0787.

2-[2-[2-(2-methoxyethoxy)ethoxy]ethoxy]ethoxy chloride (B89)

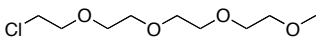

$C_9H_{19}ClO_4$
Mol. Wt.: 226.6978

To a mixture of 2-[2-[2-(2-methoxyethoxy)ethoxy]ethoxy]ethanol (**B86**) (2.50 g, 12 mmol) and triethylamine (1.82 g, 18 mmol) in dichloromethane (80 mL), thionyl chloride (1.88 g, 15.8 mmol) was added slowly. The mixture was refluxed in an oil bath for 4 h. After cooling to room temperature, the mixture was carefully poured into saturated sodium hydrogen carbonate (100 mL) and stirred for 5 min. The organic layer was separated and the aqueous layer was extracted with dichloromethane (50 mL × 2). The combined organic layer was washed with water (50 mL) and saturated sodium chloride (50 mL), dried with sodium sulfate, and evaporated. The product was purified by bulb-to-bulb distillation to yield **B89** as pale yellow oil (1.77g, 65%). ^{1}H-NMR (300 MHz, $CDCl_3$): δ ppm = 3.38 (s, 3H), 3.54-3.56 (m, 2H), 3.62-3.69 (m, 12H), 3.74-3.77 (t, ^3J = 6.0 Hz, 2H). ^{13}C-NMR (101 MHz, $CDCl_3$): δ ppm = 42.7 (CH_3), 59.0 (CH_2), 70.5 (CH_2), 70.60 (CH_2), 70.62 (CH_2), 70.65 (CH_2), 70.66 (CH_2), 71.4 (CH_2), 72.0 (CH_2). IR

(KBr): ν cm^{-1} = 3426, 2876, 1638, 1454, 1300, 1200, 1111, 852, 745, 665. MS (CI): *m/z* (%): 227.1 (M^+ + H). HRMS (CI): calcd for $C_9H_{20}O_4Cl$: 227.1050; found: 227.1053.

1-Bromo-[2-(2-methoxyethoxy)ethoxy]benzene (B78)

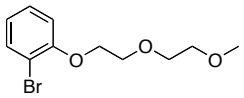

$C_{11}H_{15}BrO_3$
Mol. Wt.: 275.139

2-Bromophenol (**B90**) (1.73 g, 10 mmol), 2-(2-methoxyethoxy)ethoxy chloride (**B87**) (1.80 g, 13 mmol), potassium iodide (2.49 g, 15 mmol), and potassium carbonate (2.07 g, 15 mmol) in acetone (10 mL) were refluxed in an oil bath for 91 h. The mixture was filtered over celite and washed with ether. The organic layer was washed with aqueous sodium hydroxide (3 M, 20 mL × 3), dried with sodium sulfate, and evaporated. The product was purified by column chromatography on silica gel eluted with hexane/ether = 5/1 and 2/1, followed by bulb-to-bulb distillation to yield **B78** as pale yellow oil (1.64 g, 60%) [R_f = 0.23 (SiO_2, hexane/ether = 3:1)]. ^{1}H-NMR (300 MHz, $CDCl_3$): δ ppm = 3.37 (s, 3H), 3.55-3.58 (m, 2H), 3.76-3.79 (m, 2H), 3.89-3.92 (m, 2H), 4.19 (t, ^3J = 4.8 Hz, 2H), 6.83 (ddd, ^3J = 7.5, 7.8 Hz, ^4J = 1.5 Hz 1H), 6.90 (dd, ^3J = 8.4 Hz, ^4J = 1.5 Hz, 1H), 7.23 (ddd, ^3J = 7.5, 8.4 Hz, ^4J = 1.5 Hz, 1H), 7.51 (dd, ^3J = 7.8 Hz, ^4J = 1.5 Hz, 1H). ^{13}C-NMR (75.5 MHz, $CDCl_3$): δ ppm = 58.9 (CH_3), 69.0 (CH_2), 69.4 (CH_2), 70.9 (CH_2), 71.9 (CH_2), 112.2 (C), 113.5 (CH), 122.0 (CH), 128.3 (CH), 133.2 (CH), 155.2 (C). IR (KBr): ν cm^{-1} = 3506, 2925, 2878, 1587, 1481, 1278, 1249, 1110, 1059, 1030, 929, 850, 749, 666. MS (ESI): *m/z* (%): 299.0 (M^+ + Na). HRMS (ESI): calcd for $C_{11}H_{15}O_3NaBr$: 297.0102; found: 297.0100.

1-Bromo-[2-[2-(2-methoxyethoxy)ethoxy]ethoxy]benzene (B79)

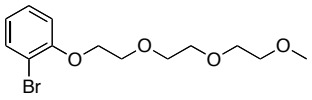

$C_{13}H_{19}BrO_4$
Mol. Wt.: 319.1916

2-Bromophenol (**B90**) (1.73 g, 10 mmol), 2-[2-(2-methoxyethoxy)ethoxy]ethoxy chloride (**B88**) (2.37 g, 13 mmol), potassium iodide (2.49 g, 15 mmol), and potassium carbonate (2.07 g, 15 mmol) in acetone (10 mL) were refluxed in an oil bath for 116 h. The mixture was filtered over celite and washed with ether. The organic layer was washed with aqueous sodium hydroxide (3

M, 10 mL × 3), dried with sodium sulfate, and evaporated. The product was purified by bulb-to-bulb distillation to yield **B79** as pale yellow oil (2.90 g, 91%). ^{1}H-NMR (300 MHz, $CDCl_3$): δ ppm = 3.38 (s, 3H), 3.55 (dd, ^{3}J = 3.5, 6.2 Hz, 2H), 3.66 (dd, ^{3}J = 3.5, 6.2 Hz, 2H), 3.69 (dd, ^{3}J = 3.8, 5.6 Hz, 2H), 3.80 (dd, ^{3}J = 3.8, 5.6 Hz, 2H), 3.92 (dd, ^{3}J = 4.5, 5.1 Hz, 2H), 4.19 (dd, ^{3}J = 4.5,5.1 Hz, 2H), 6.83 (td, ^{3}J = 7.8 Hz, ^{4}J = 1.5 Hz, 1H), 6.92 (dd, ^{3}J = 8.4 Hz, ^{4}J = 1.5 Hz, 1H), 7.24 (td, ^{3}J = 7.8 Hz, ^{4}J = 1.5 Hz, 1H), 7.53 (dd, ^{3}J = 8.4 Hz, ^{4}J = 1.5 Hz, 1H). ^{13}C-NMR (75.5 MHz, $CDCl_3$): δ ppm = 58.9 (CH_3), 68.9 (CH_2), 69.4 (CH_2), 70.4 (CH_2), 70.6 (CH_2), 71.0 (CH_2), 71.8 (CH_2), 112.2 (C), 113.6 (CH), 122.0 (CH), 128.3 (CH), 133.2 (CH), 155.2 (C). IR (KBr): ν cm^{-1} = 3060, 3026, 2922, 1942, 1601, 1492, 1451, 1029, 756, 701, 540. MS (ESI): *m*/*z* (%): 341.1 (M^+ + Na). HRMS (ESI): calcd for $C_{13}H_{19}O_4NaBr$: 341.0364; found: 341.0365.

1-Bromo-[2-[2-[2-(2-methoxyethoxy)ethoxy]ethoxy]ethoxy]benzene (B80)

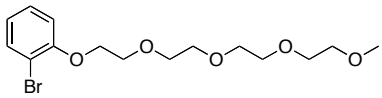

$C_{15}H_{23}BrO_5$
Mol. Wt.: 363.2441

2-Bromophenol (**B90**) (0.953 g, 5.51 mmol), 2-[2-[2-(2-methoxyethoxy)ethoxy]ethoxy]ethoxy chloride (**B89**) (1.50 g, 6.62 mmol), potassium iodide (1.37 g, 8.27 mmol), and potassium carbonate (1.14 g, 8.27 mmol) in acetone (10 mL) were refluxed in an oil bath for 91 h. The mixture was filtered over celite and washed with ether. The organic layer was washed with aqueous sodium hydroxide (3 M, 15 mL × 3), dried with sodium sulfate, and evaporated. The product was purified by column chromatography on silica gel eluted with ether to yield **B80** as yellow oil (2.03 g, 99%) [R_f = 0.45 (SiO_2, ether)]. ^{1}H-NMR (300 MHz, $CDCl_3$): δ ppm = 3.35 (s, 3H), 3.50-3.54 (m, 2H), 3.61-3.69 (m, 8H), 3.76-3.79 (m, 2H), 3.87-3.91 (m, 2H), 4.16 (t, ^{3}J = 4.8 Hz, 2H), 6.81 (ddd, ^{3}J = 7.2, 7.8 Hz, ^{4}J = 1.5 Hz 1H), 6.91 (dd, ^{3}J = 8.4 Hz, ^{4}J = 1.5 Hz, 1H), 7.23 (ddd, ^{3}J = 7.2, 8.4 Hz, ^{4}J = 1.5 Hz, 1H), 7.51 (dd, ^{3}J = 7.8 Hz, ^{4}J = 1.5 Hz, 1H). ^{13}C-NMR (75.5 MHz, $CDCl_3$): δ ppm = 58.8 (CH_3), 68.9 (CH_3), 69.3 (CH_3), 70.3 (CH_2), 70.4 × 2 (CH_2), 70.5 (CH_2), 70.9 (CH_2), 71.8 (CH_2), 112.1 (C), 113.5 (CH), 121.9 (CH), 128.3 (CH), 133.2 (CH), 155.1 (C). IR (KBr): ν cm^{-1} = 3519, 2875, 1953, 1587, 1480, 1443, 1278, 1249, 1108, 945, 851, 751, 666. MS (ESI): *m*/*z* (%): 387.1 (M^+ + Na), 403.1 (M^+ + K). HRMS (ESI): calcd for $C_{15}H_{23}O_5NaBr$: 385.0627; found: 385.0631.

***sym*-Pentamanisylcorannulene (B73)**

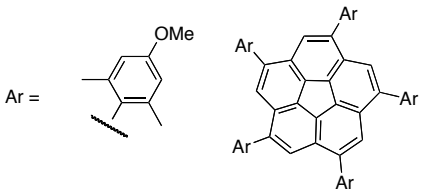

$C_{65}H_{60}O_5$
Mol. Wt.: 921.1689

Manisyl bromide (**B74**) (153 mg, 0.71 mmol) in THF (10 mL) was cooled to –78 °C in a dry ice/acetone bath and *n*-butyllithium (1.5 M in hexane, 0.52 mL, 0.78 mmol) was added dropwise. After 30 min, zinc chloride (146 mg, 1.07 mmol) in THF (5 mL) was transferred to the solution. After 10 min, the dry ice/acetone bath was removed. After 30 min, the resulting solution was transferred to the flask containing *sym*-pentachlorocorannulene (**B60**) (30 mg, 0.071 mmol) and (IPr)Pd(allyl)Cl (41 mg, 0.071 mmol) in THF (5 mL). The mixture was refluxed in an oil bath for 4 d. The cooled mixture was filtered over celite, washed with dichloromethane, and evaporated. The product was purified by column chromatography on aluminum oxide (5% deactivated with water) eluted with hexane/dichloromethane = 3/1, 2/1, and 1.5/1. The solvent was evaporated to yield **B73** as a yellow solid (13 mg, 20%) [R_f = 0.68 (Al_2O_3, hexane/dichloromethane = 1:1)]. The spectroscopic data were identical with those reported.[33]
^{1}H-NMR (300 MHz, $CDCl_3$): δ ppm = 1.98 (s, 30H), 3.80 (s, 15H), 6.66 (s, 10H), 7.08 (s, 5H).

***sym*-Penta(2,6-dimethoxyphenyl)corannulene (B93)**

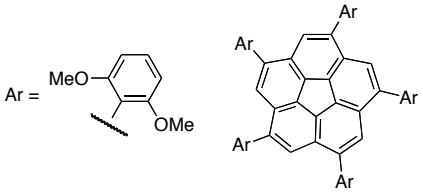

$C_{60}H_{50}O_{10}$
Mol. Wt.: 931.033

1-Bromo-2,6-dimethoxybenzene (**B75**) (618 mg, 2.86 mmol) in THF (40 mL) was cooled to –78 °C in a dry ice/acetone bath and *n*-butyllithium (1.5 M in hexane, 2.10 mL, 3.15 mmol) was added dropwise. After 40 min, zinc chloride (585 mg, 4.29 mmol) in THF (20 mL) was transferred to the solution. After 10 min, the dry ice/acetone bath was removed. After 40 min, the resulting solution was transferred to the flask containing *sym*-pentachlorocorannulene (**B60**) (120 mg, 0.286 mmol) and (IPr)Pd(allyl)Cl (246 mg, 0.429 mmol) in THF (20 mL). The mixture was refluxed in an oil bath for 5 d. The cooled mixture was filtered over celite, washed

with dichloromethane, and evaporated. The product was purified by column chromatography on aluminum oxide (5% deactivated with water) eluted with hexane/dichloromethane = 1/5, followed by preparative thin layer chromatography on silica gel eluted with hexane/dichloromethane = 1/7, 1/20, and 1/50. The solvent was evaporated to yield **B93** as a yellow solid (36 mg, 14%) [R_f = 0.38 (Al_2O_3, hexane/dichloromethane = 1:3)]. Mp > 350 °C. ^{1}H-NMR (300 MHz, $CDCl_3$): δ ppm = 3.58 (s, 30H), 6.61 (d, ^3J = 8.4 Hz, 10H), 7.25 (s, 5H), 7.25 (t, ^3J = 8.4 Hz, 5H). ^{13}C-NMR (151 MHz, $CDCl_3$): δ ppm = 55.8 (CH_3), 104.2 (CH), 118.3 (C), 127.7 (CH), 128.5 (CH), 130.3 (C), 131.9 (C), 134.9 (C), 158.7(C). IR (KBr): ν cm^{-1} = 3448, 2934, 2833, 1591, 1471, 1431, 1249, 1112, 782, 732, 612. MS (ESI): *m/z* (%): 931.4 (M^+). HRMS (ESI): calcd for $C_{60}H_{51}O_{10}$: 931.3482; found: 931.3482.

sym-Penta(2,6-diethylphenyl)corannulene (B94)

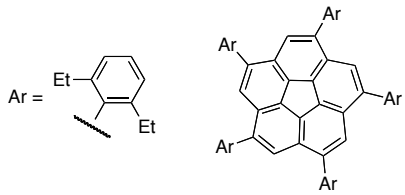

$C_{70}H_{70}$
Mol. Wt.: 911.3048

1-Bromo-2,6-diethylbenzene (**B76**) (303 mg, 1.42 mmol) in THF (20 mL) was cooled to –78 °C in a dry ice/acetone bath and *n*-butyllithium (1.5 M in hexane, 1.04 mL, 1.56 mmol) was added dropwise. After 40 min, zinc chloride (290 mg, 2.13 mmol) in THF (10 mL) was transferred to the solution. After 30 min, the dry ice/acetone bath was removed. After 30 min, the resulting solution was transferred to the flask containing *sym*-pentachlorocorannulene (**B60**) (60 mg, 0.142 mmol) and (IPr)Pd(allyl)Cl (122 mg, 0.213 mmol) in THF (10 mL). The mixture was refluxed in an oil bath for 4.5 d. The cooled mixture was filtered over celite, washed with dichloromethane, and evaporated. The product was purified by column chromatography on silica gel eluted with hexane/dichloromethane = 20/1, 10/1, and 5/1, followed by preparative thin layer chromatography on silica gel eluted with hexane/dichloromethane = 20/1 × 4. After evaporation of the solvent, the resulting solid was washed with ethanol to yield **B94** as a white solid (2 mg, 2%) [R_f = 0.50 (SiO_2, hexane/dichloromethane = 10:1)]. Mp > 350 °C. ^{1}H-NMR (300 MHz, $CDCl_3$): δ ppm = 0.97 (t, ^3J = 7.2 Hz, 30H), 2.31 (nonet, ^3J = 7.2 Hz, 20H), 7.14 (d, ^3J = 7.5 Hz, 10H), 7.16 (s, 5H), 7.28 (dd, ^3J = 7.5, 7.5 Hz, 5H). ^{13}C-NMR (126 MHz, $CDCl_3$): δ ppm = 15.6 (CH_3), 26.9 (CH_2), 125.5 (CH), 125.7(CH), 128.0 (CH), 130.0 (C), 134.2

(C), 137.5 (C), 139.6 (C), 143.0 (C). IR (KBr): ν cm^{-1} = 3059, 3026, 2923, 2850, 1942, 1601, 1492, 1451, 1371, 1028, 757, 701, 540. MS (EI): *m*/*z* (%): 910.6 (M^+).

sym-Penta(2-methoxy-6-methylphenyl)corannulene (B95)

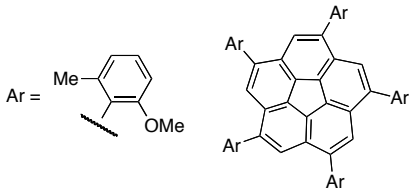

$C_{60}H_{50}O_5$
Mol. Wt.: 851.036

1-Bromo-2-methoxy-6-methylbenzene (**B77**) (284 mg, 1.42 mmol) in THF (20 mL) was cooled to –78 °C in a dry ice/acetone bath and *n*-butyllithium (1.5 M in hexane, 1.04 mL, 1.56 mmol) was added dropwise. After 30 min, zinc chloride (290mg, 2.13 mmol) in THF (10 mL) was transferred to the solution. After 30 min, the dry ice/acetone bath was removed. After 30 min, the resulting solution was transferred to the flask containing *sym*-pentachlorocorannulene (**B60**) (60 mg, 0.142 mmol), palladium (II) acetate (48 mg, 0.071 mmol), and IPr-HCl (60 mg, 0.142 mmol) in THF (10 mL). The mixture was refluxed in an oil bath for 4 d. The cooled mixture was filtered over celite, washed with dichloromethane, and evaporated. The product was purified by column chromatography on aluminum oxide (5% deactivated with water) eluted with hexane/dichloromethane = 3/1 and 2/1, followed by preparative thin layer chromatography on silica gel eluted with hexane/dichloromethane = 1/1 × 2. The solvent was evaporated to yield **B95** as a yellow solid (18 mg, 15%) [R_f = 0.02, 0.14, and 0.27 (Al_2O_3, hexane/dichloromethane = 2:1)]. Mp > 350 °C. ^{1}H-NMR (600 MHz, $CDCl_3$): δ ppm = 2.01-2.17 (m, 15H), 3.58-3.69 (m, 15H), 6.79-6.90 (m, 10H), 7.12-7.24 (m, 10H). IR (KBr): ν cm^{-1} = 3442, 2928, 2833, 1578, 1468, 1258, 1084, 776, 745, 611. MS (EI): *m*/*z* (%): 850.7 (M^+). HRMS (EI): calcd for $C_{60}H_{50}O_5$: 850.3658; found: 850.3648.

sym-Pentacorannulylcorannulene (B96)

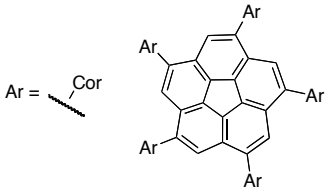

$C_{120}H_{50}$
Mol. Wt.: 1491.681

Bromocorannulene (**B35**) (267 mg, 0.811 mmol) in THF (15 mL) was cooled to –78 °C in a dry ice/acetone bath and *n*-butyllithium (1.5 M in hexane, 0.60 mL, 0.91 mmol) was added dropwise. After 30 min, zinc chloride (172mg, 1.26 mmol) in THF (5 mL) was transferred to the solution. After removal of the bath, the mixture was stirred for 30 min. The resulting solution was transferred to the flask containing *sym*-pentachlorocorannulene (**B60**) (38 mg, 0.091 mmol) and (IPr)Pd(allyl)Cl (52 mg, 0.091 mmol) in THF (15 mL). The mixture was refluxed in an oil bath for 5.5 d. The cooled mixture was filtered over celite, washed with dichloromethane, and evaporated. The product was purified by column chromatography on aluminum oxide (5% deactivated with water) eluted with hexane/toluene = 3.5/1, 3/1, 2/1, and 1/1 to yield **B96** as a yellow solid (10 mg, 7%) [R_f = 0.64 (Al_2O_3, hexane/toluene = 1:2)]. Mp > 350 °C. ^{1}H-NMR (600 MHz, $CDCl_3$): δ ppm = 7.67-8.18 (m, 50H). IR (KBr): ν cm^{-1} = 3441, 3059, 3026, 2923, 2849, 1942, 1601, 1492, 1451, 1028, 757, 701, 540. MS (MALDI): *m/z* (%): 1491.4 (M^+). HRMS (MALDI-FT-ICR): calcd for $C_{120}H_{50}$: 1490.3913; found: 1490.3910.

sym-Penta[[2-(2-methoxyethoxy)ethoxy]phenyl]corannulene (B97)

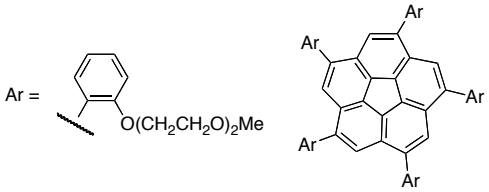

$C_{75}H_{80}O_{15}$
Mol. Wt.: 1221.4287

1-Bromo-[2-(2-methoxyethoxy)ethoxy]benzene (**B78**) (781 mg, 2.84 mmol) in THF (40 mL) was cooled to –78 °C in a dry ice/acetone bath and *n*-butyllithium (1.5 M in hexane, 2.08 mL, 3.12 mmol) was added dropwise. After 30 min, zinc chloride (580 mg, 4.26 mmol) in THF (10 mL) was transferred to the solution and the bath was removed. After 30 min, the resulting solution was transferred to the flask containing *sym*-pentachlorocorannulene (**B60**) (120 mg, 0.284 mmol), palladium (II) acetate (64 mg, 0.284 mmol), and IPr-HCl (120 mg, 0.284 mmol) in THF (20 mL). The mixture was refluxed in an oil bath for 4 d. The cooled mixture was filtered over celite, washed with dichloromethane, and evaporated. The product was purified by column chromatography on aluminum oxide (5% deactivated with water) eluted with dichloromethane/ethyl acetate = 8/1, 6/1, 4/1, and 2/1, followed by preparative thin layer chromatography on Alumina eluted with dichloromethane/ethyl acetate = 7/1 to yield **B97** as a yellow solid (75 mg, 21%) [R_f = 0.70 (Al_2O_3, dichloromethane/ethyl acetate = 6:1)]. Mp 70-

72 °C. ^{1}H-NMR (400 MHz, $CDCl_3$): δ ppm = 3.14 (s, 10H), 3.14 (s, 15H), 3.32 (s, 10H), 3.53 (s, 10H), 4.11 (s, 10H), 7.01 (t, ^{3}J = 8.0 Hz, 5H), 7.05 (d, ^{3}J = 8.0 Hz, 5H), 7.33-7.37 (m, 10H), 7.58 (s, 5H). ^{13}C-NMR (75.5 MHz, $CDCl_3$): δ ppm = 58.6 (CH_3), 68.2 (CH_2), 69.2 (CH_2), 70.5 (CH_2), 71.6 (CH_2), 112.7 (CH), 121.0 (CH), 127.2 (CH), 129.0 (CH), 129.1 (C), 130.4 (C), 132.3 (CH), 135.0 (C), 137.7 (C), 156.4 (C). IR (KBr): ν cm^{-1} = 3444, 2922, 2872, 1597, 1493, 1446, 1257, 1111, 935, 753, 648. MS (ESI): *m*/*z* (%): 1243.6 (M^+ + Na). HRMS (ESI): calcd for $C_{75}H_{80}O_{15}Na$: 1243.5395; found: 1243.5399.

sym-Penta[[2-[2-(2-methoxyethoxy)ethoxy]ethoxy]phenyl]corannulene (B98)

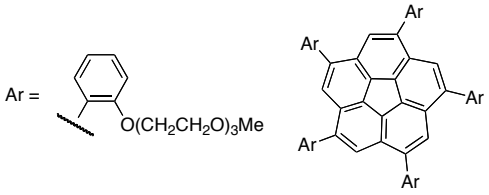

$C_{85}H_{100}O_{20}$
Mol. Wt.: 1441.6915

1-Bromo-[2-[2-(2-methoxyethoxy)ethoxy]ethoxy]benzene (**B79**) (453 mg, 1.42 mmol) in THF (20 mL) was cooled to –78 °C in a dry ice/acetone bath and *n*-butyllithium (1.5 M in hexane, 1.04 mL, 1.56 mmol) was added dropwise. After 30 min, zinc chloride (290 mg, 2.13 mmol) in THF (10 mL) was transferred to the solution and the bath was removed. After 30 min, the resulting solution was transferred to the flask containing *sym*-pentachlorocorannulene (**B60**) (60 mg, 0.142 mmol), palladium (II) acetate (32 mg, 0.142 mmol), and IPr-HCl (60 mg, 0.142 mmol) in THF (10 mL). The mixture was refluxed in an oil bath for 3 d. The cooled mixture was filtered over celite, washed with dichloromethane, and evaporated. The product was purified by column chromatography on aluminum oxide (5% deactivated with water) eluted with dichloromethane, ethyl acetate, ethyl acetate/ethanol = 4/1, followed by preparative thin layer chromatography on Alumina eluted with ethyl acetate × 2 to yield **B98** as a yellow solid (88 mg, 43%) [R_f = 0.50 (Al_2O_3, ethyl acetate)]. ^{1}H-NMR (400 MHz, $CDCl_3$): δ ppm = 3.29 (s, 15H), 3.34-3.35 (m, 10H), 3.37-3.43 (m, 30H), 3.51 (br s, 10H), 4.09 (br s, 10H), 7.01 (t, ^{3}J = 8.0 Hz, 5H), 7.06 (d, ^{3}J = 8.0 Hz, 5H), 7.32-7.36 (m, 10H), 7.58 (s, 5H). ^{13}C-NMR (101 MHz, $CDCl_3$): δ ppm = 58.9 (CH_3), 68.2 (CH_2), 69.3 (CH_2), 70.3 (CH_2), 70.4 (CH_2), 70.7 (CH_2), 71.8 (CH_2), 113.0 (CH), 121.1 (CH), 127.3 (CH), 129.1 (CH), 129.2 (C), 130.4 (C), 132.5 (CH), 135.2 (C), 137.8 (C), 156.5 (C). IR (KBr): ν cm^{-1} = 3059, 3026, 2923, 2850, 1942, 1601, 1492, 1451, 1371, 1028, 757, 701, 540. MS (ESI): *m*/*z* (%): 1464.5 (M^+ + Na). HRMS (ESI): calcd for

$C_{85}H_{100}O_{20}Na$: 1463.6706; found: 1463.6699.

***sym*-Penta[[2-[2-[2-(2-methoxyethoxy)ethoxy]ethoxy]ethoxy]phenyl]corannulene (B99)**

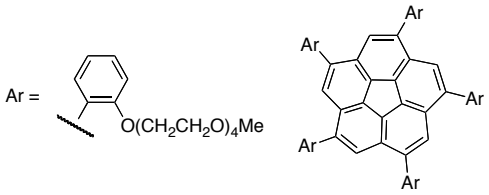

$C_{95}H_{120}O_{25}$
Mol. Wt.: 1661.9543

1-Bromo-[2-[2-[2-(2-methoxyethoxy)ethoxy]ethoxy]ethoxy]benzene (**B80**) (516 mg, 1.42 mmol) in THF (20 mL) was cooled to –78 °C in a dry ice/acetone bath and *n*-butyllithium (1.5 M in hexane, 1.04 mL, 1.56 mmol) was added dropwise. After 30 min, zinc chloride (290 mg, 2.13 mmol) in THF (10 mL) was transferred to the solution and the bath was removed. After 30 min, the resulting solution was transferred to the flask containing *sym*-pentachlorocorannulene (**B60**) (60 mg, 0.142 mmol), palladium (II) acetate (32 mg, 0.142 mmol), and IPr-HCl (60 mg, 0.142 mmol) in THF (10 mL). The mixture was refluxed in an oil bath for 3 d. The cooled mixture was filtered over celite, washed with dichloromethane, and evaporated. The product was purified by column chromatography on aluminum oxide (5% deactivated with water) eluted with dichloromethane, ethyl acetate, ethyl acetate/ethanol = 20/1 and 10/1, followed by preparative thin layer chromatography on Alumina eluted with ethyl acetate/ethanol = 40/1 × 2 to yield **B99** as yellow oil (26 mg, 11%) [R_f = 0.11 (Al_2O_3, ethyl acetate)]. ^{1}H-NMR (400 MHz, $CDCl_3$): δ ppm = 3.33 (s, 15H), 3.32-3.39 (m, 20H), 3.47-3.57 (m, 50H), 4.09 (br s, 10H), 7.01 (t, ^3J = 8.0 Hz, 5H), 7.07 (d, ^3J = 8.0 Hz, 5H), 7.32-7.37 (m, 10H), 7.59 (s, 5H). ^{13}C-NMR (75.5 MHz, $CDCl_3$): δ ppm = 58.9 (CH_3), 68.1 (CH_2), 69.2 (CH_2), 70.3 × 4 (CH_2), 70.6 (CH_2), 71.8 (CH_2), 112.9 (CH), 121.0 (CH), 127.2 (CH), 129.0 (CH), 129.1 (C), 130.3 (C), 132.4 (CH), 135.1 (C), 137.7 (C), 156.4 (C). IR (KBr): ν cm^{-1} = 3444, 2872, 1597, 1493, 1448, 1252, 1112, 937, 755, 647. MS (ESI): *m*/*z* (%): 1684.9 (M^+ + Na), 1699.9 (M^+ + K). HRMS (ESI): calcd for $C_{95}H_{120}O_{25}Na$: 1683.8016; found: 1683.8019.

2.2.3.3. UV and Fluorescent spectra

All spectra were recorded in spectroscopic grade solvents and are uncorrected. Absorption spectra were recorded on a Perkin Elmer Lamda 19 UV/Vis/NIR Spectrometer and emission spectra were recorded on an Edinburgh Instruments FLS920 Combined Steady State and Lifetime Spectrometer. Lifetime decays were measured using time-correlated single photon counting (TCSPC) with the nF900 nanosecond flash-lamp. Quantum yields are relative to 9,10-diphenylanthracene ($\Phi_f = 0.95$) in ethanol and calculated by the reference.[44]

***sym*-Pentacorannulylcorannulene (B96)**

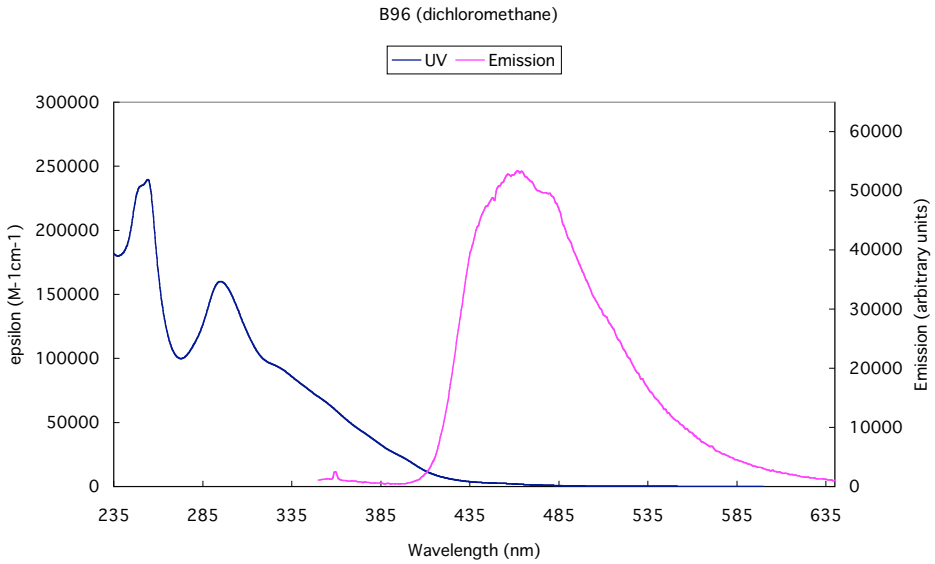

[lifetime] $\tau 1 = 5.34$ (ns), $\chi 2 = 1.17$, [quantum yield] $\Phi_f = 0.181$

2.3. Appendix

2.3.1. Crystallographic Data of B93

Crystallised from		*n*-PrOH / CH_2Cl_2
Empirical formula		$C_{62.5}H_{56}Cl_2O_{10.5}$
Formula weight [g mol^{-1}]		1046.03
Crystal colour, habit		colourless, plate
Crystal dimensions [mm]		0.02 × 0.23 × 0.25
Temperature [K]		160(1)
Crystal system		monoclinic
Space group		*C*2/*c* (#15)
Z		8
Reflections for cell determination		6629
2θ range for cell determination [°]		4–44
Unit cell parameters	*a* [Å]	55.144(2)
	b [Å]	14.5976(5)
	c [Å]	14.0050(5)
	α [°]	90
	β [°]	102.677(2)
	γ [°]	90
	V [Å^3]	10998.7(6)
F(000)		4392
D_x [g cm^{-3}]		1.263
μ(Mo *K*α) [mm^{-1}]		0.178
Scan type		ϕ and ω
2$\theta_{(max)}$ [°]		44
Total reflections measured		34016
Symmetry independent reflections		6668
R_{int}		0.056
Reflections with $I > 2\sigma(I)$		4329
Reflections used in refinement		6667
Parameters refined; restraints		1283; 3780
Final *R*(*F*) [$I > 2\sigma(I)$ reflections]		0.1331
wR(F^2) (all data)		0.4102
Weights:	$w = [\sigma^2(F_o^2) + (0.2000P)^2]^{-1}$ where $P = (F_o^2 + 2F_c^2)/3$	
Goodness of fit		1.633

Secondary extinction coefficient	0.009(1)
Final Δ_{max}/σ	0.029
$\Delta\rho$ (max; min) [e Å^{-3}]	0.57; -0.58
$\sigma(d_{(C-C)})$ [Å]	0.004 – 0.007 (small due to restraints)

2.3.2. Crystallographic Data of B94

Crystallised from		CH_2Cl_2 / *n*-PrOH
Empirical formula		$C_{70}H_{70}$
Formula weight [g mol^{-1}]		911.32
Crystal colour, habit		pale yellow, prism
Crystal dimensions [mm]		0.20 × 0.22 × 0.32
Temperature [K]		160(1)
Crystal system		triclinic
Space group		$P\bar{1}$ (#2)
Z		2
Reflections for cell determination		9162
2θ range for cell determination [°]		4 – 50
Unit cell parameters	a [Å]	12.4515(4)
	b [Å]	15.4637(4)
	c [Å]	15.7348(4)
	α [°]	105.922(2)
	β [°]	110.722(1)
	γ [°]	97.884(2)
	V [Å^3]	2630.9(1)
$F(000)$		980
D_x [g cm^{-3}]		1.150
μ(Mo $K\alpha$) [mm^{-1}]		0.0644
Scan type		ω
$2\theta_{(max)}$ [°]		50
Total reflections measured		41697
Symmetry independent reflections		9286
R_{int}		0.060
Reflections with $I > 2\sigma(I)$		5171
Reflections used in refinement		9284
Parameters refined; restraints		1163; 3956

Final $R(F)$ [$I > 2\sigma(I)$ reflections]	0.1215
$wR(F^2)$ (all data)	0.3825
Weights:	$w = [\sigma^2(F_o^2) + (0.1695P)^2 + 4.5133P]^{-1}$ where $P = (F_o^2 + 2F_c^2)/3$

Goodness of fit	1.036
Secondary extinction coefficient	0.010(3)
Final Δ_{max}/σ	0.001
$\Delta\rho$ (max; min) [e Å^{-3}]	0.87; -0.47
$\sigma(d_{(C-C)})$ [Å]	0.003 – 0.005 (small due to restraints)

2.4. References

[1] Wu, Y.-T.; Siegel, J. S. *Chem. Rev.* **2006**, *106*, 4843.

[2] Tsefrikas, V. M.; Scott, L. T. *Chem. Rev.* **2006**, *106*, 4868.

[3] (a) Barth, W. E.; Lawton, R. G. *J. Am. Chem. Soc.* **1966**, 88, 380. (b) Barth, W. E.; Lawton, R. G. *J. Am. Chem. Soc.* **1971**, *93*, 1730.

[4] Janata, J.; Gendell, J.; Ling, C.; Barth, W. E.; Backes, L.; Mark, H. B.; Lawton, R. G. *J. Am. Chem. Soc.* **1967**, *89*, 3058.

[5] Hanson, J. C.; Nordman, C. E. *Acta. Crystallogr. B* **1976**, *B32*, 1147.

[6] Davy, J. R.; Iskander, M. N.; Reiss, J. A. *Tetrahedron Lett.* **1978**, *42*, 4085.

[7] Craig, J. T.; Robins, M. D. W. *Aust. J. Chem.* **1968**, *21*, 2237.

[8] Scott, L. T.; Hashemi, M. M.; Meyer, D. T.; Warren, H. B. *J. Am. Chem. Soc.* **1991**, *113*, 7082.

[9] (a) Brown, R. F. C.; Eastwood, F. W.; Jackman, G. P. *Aust. J. Chem.* **1977**, *30*, 1757. (b) Brown, R. F. C. *Recl. Trav. Chim. Pays-Bas* **1988**, *107*, 655.

[10] Scott, L. T.; Cheng, P.-C.; Hashemi, M. M.; Bratcher, M. S.; Meyer, D. T.; Warren, H. B. *J. Am. Chem. Soc.* **1997**, *119*, 10963.

[11] Borchardt, A.; Fuchicello, A.; Kilway, K. V.; Baldridge, K. K.; Siegel, J. S. *J. Am. Chem. Soc.* **1992**, *114*, 1921.

[12] Zimmermann, G.; Nuechter, T.; Hagen, S.; Nuechter, M. *Tetrahedron Lett.* **1994**, *35*, 4747.

[13] Mehta, G.; Panda, G. *Tetrahedron Lett.* **1997**, *38*, 2145.

[14] Reisch, H. A.; Bratcher, M. S.; Scott, L. T. *Org. Lett.* **2000**, *2*, 1427.

[15] Seiders, T. J.; Baldridge, K. K.; Siegel, J. S. *J. Am. Chem. Soc.* **1996**, *118*, 2754.

[16] Seiders, T. J.; Elliot, E. L.; Grube, G. H.; Siegel, J. S. *J. Am. Chem. Soc.* **1999**, *121*, 7804.

[17] Sygula, A.; Rabideau, P. W. *J. Am. Chem. Soc.* **1999**, *121*, 7800.

[18] (a) Sygula, A.; Rabideau, P. W. *J. Am. Chem. Soc.* **2000**, *122*, 6323. (b) Xu, G.; Sygula, A.; Marcinow, Z.; Rabideau, P. W. *Tetrahedron Lett.* **2000**, *41*, 9931. (c) Sygula, A.; Xu, G.; Marcinow, Z.; Rabideau, P. W. *Tetrahedron* **2001**, *57*, 3637.

[19] Sygula, A.; Karlen, S. D.; Sygula, R.; Rabideau, P. W. *Org. Lett.* **2002**, *4*, 3135.

[20] Maag, R. Diplomarbeit, University of Zurich, Zurich, 2006.

[21] Marcinow, Z.; Grove, D. I.; Rabideau, P. W. *J. Org. Chem.* **2002**, *67*, 3537.

[22] Wu, Y.-T.; Hayama, T.; Baldridge, K. K.; Linden, A.; Siegel, J. S. *J. Am. Chem. Soc.* **2006**, *128*, 6870.

[23] Cheng, P.-C. Ph.D. Dissertation, Boston College: Boston, MA, 1996; p212.

[24] Aprahamian, I.; Eisenberg, D.; Hoffman, R. E.; Sternfeld, T.; Matsuo, Y.; Jackson, E. A.; Nakamura, E.; Scott, L. T.; Sheradsky, T.; Rabinovitz, M. *J. Am. Chem. Soc.* **2005**, *127*, 9581.

[25] Sygula, A.; Sygula, R.; Fronczek, F. R.; Rabideau, P. W. *J. Org. Chem.* **2002**, *67*, 6487.

[26] Scott, L. T.; Hashemi, M. M.; Bratcher, M. S. *J. Am. Chem. Soc.* **1992**, *114*, 1920.

[27] Jones, C. S.; Bandera, D.; Siegel, J. S. Sbmitted for publication.

[28] Jones, C. S.; Elliott, E.; Siegel, J. S. *Synlett.* **2004**, 187.

[29] Lee, H. B.; Sharp, P. R. *Organometallics* **2005**, *24*, 4875.

[30] Seiders, T. J.; Baldridge, K. K.; Grube, G. H.; Siegel, J. S. *J. Am. Chem. Soc.* **2001**, *123*, 517.

[31] Scott. L. T. *Pure Appl. Chem.* **1996**, *68*, 291.

[32] (a) Huang, R.; Huang, W.; Wang, Y.; Tang, Z.; Zheng, L. *J. Am. Chem. Soc.* **1997**, *119*, 5954. (b) Samdal, S.; Hedberg, L.; Hedberg, K.; Richardson, A. D.; Bancu, M.; Scott, L. T. *J. Phys. Chem.* **2003**, *107*, 411.

[33] Grube, G. H.; Elliott, E. L.; Steffens, R. J.; Jones, C. S.; Baldridge, K. K.; Siegel, J. S. *Org. Lett.* **2003**, *5*, 713.

[34] Eberhard, M. R.; Wang, Z; Jensen, C. M. *Chem. Commun.* **2002**, 818.

[35] (a) Mizyed, S.; Georghiou, P. E.; Bancu, M.; Cuadra, B.; Rai, A. K.; Cheng, P.; Scott, L. T. *J. Am. Chem. Soc.* **2001**, *123*, 12770. (b) Bancu, M.; Rai, A. K.; Cheng, P.-C.; Gilardi, R. D.; Scott, L. T. *Synlett.* **2004**, 173.

[36] Hegedus, L. S. *Transition Metals in the Synthesis of Complex Organic Molecules*; University Science Books, New York, 1999, Chapter 2 and 4.

[37] Wada, M.; Wakamori, H.; Hiraiwa, A.; Erabi, T. *Bull. Chem. Soc. Jpn.* **1992**, *65*, 1389.

[38] For review on NHC, see: (a) Regitz, M. *Angew. Chem. Int. Ed. Engl.* **1996**, *35*, 725. (b) Bourissou, D.; Guerret, O.; Gabbai, F. P.; Bertrand, G. *Chem. Rev.* **2000**, *100*, 39.

[39] For revies, see: (a) Herrmann, W. A. *Angew. Chem. Int. Ed. Engl.* **2002**, *41*, 1290. (b) Scott, N. M.; Nolan, S. P. *Eur. J. Inorg. Chem.* **2005**, 1815.

[40] (a) Arduengo, A. J. III; Krafczyk, R.; Schmutzler, R. *Tetrahedron* **1999**, *55*, 14523. (b) Jafarpour, L.; Stevens, E. D.; Nolan, S. P. *J. Organomet. Chem.* **2000**, *606*, 49.

[41] (a) Viciu, M. S.; Germaneau, R. F.; Navarro-Fernandez, O.; Stevens, E. D.; Nolan, S. P. *Organometallics* **2002**, *21*, 5470. (b) Viciu, M. S.; Germaneau, R. F.; Nolan, S. P. *Org. Lett.* **2002**, *4*, 4053. (c) Navarro, O.; Kaur, H.; Mahjoor, P.; Nolan, S. P. *J. Org. Chem.* **2004**, *69*, 3173.

[42] Ulman, A. *An Introduction to Ultrathin Organic Films: from Langmuir-Blodgett to Self-Assembly*; Academic Press, San Diego, CA, 1991.

[43] (a) Hayama, T.; Siegel, J. S; et al. Submitted for publication. (b) Hayama, T. Diplomarbeit, University of Zurich, Zurich, 2005.

[44] Crosby, G. A.; Demas, J. N. *J. Phys. Chem.* **1971**, *75*, 991.

Chapter 3. Bowl-to-Bowl Inversion

3.1. Introduction

The bowl shape of corannulene (**C1**) affects its bowl inversion process (Figure C1). In this chapter, the relationship between bowl depth and inversion energy ($\Delta G^{\ddagger}_{inv}$), the influence of substituents, and the solvent effect will be discussed.

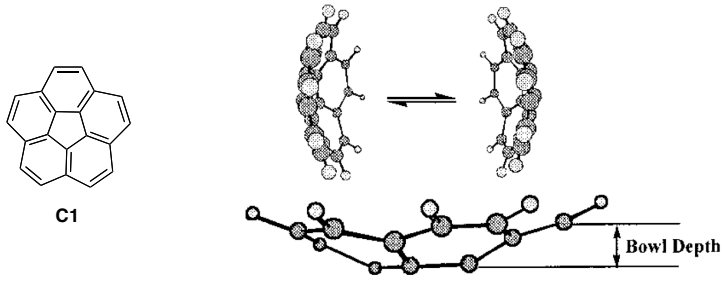

Figure C1. Bowl inversion of C1.

3.1.1. Correlation between Structure and Inversion Energy

By comparing a series of corannulene derivatives, a structure-energy correlation between bowl depth and inversion barrier was developed.[1] The calculated inversion barriers for a number of corannulene derivatives correspond to this trend. The bowl depth is measured from the mean plane of the hub carbons to the mean plane of the rim carbons (Figure C1). The correlation between structures and $\Delta G^{\ddagger}_{inv}$ can be simply described as in Figure C2. Repulsive *peri* interactions flatten the bowl and cause a decrease in $\Delta G^{\ddagger}_{inv}$ (**Class I**). This interaction is seen in derivatives with sterically demanding groups. On the other hand, attractive *peri* interactions deepen the bowl and cause an increase in $\Delta G^{\ddagger}_{inv}$ (**Class II**). This interaction is seen in derivatives with the substitutions tethered together (Table C1).

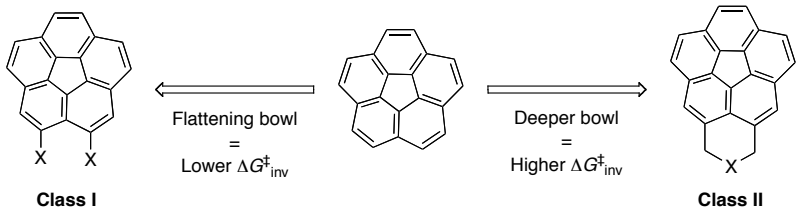

Figure C2. Correlation between structures and $\Delta G^{\ddagger}_{inv}$.

Table C1. Bowl depths and $\Delta G^{\ddagger}_{inv}$ for various corannulene derivatives.

structure		number	bowl depth (Å)	$\Delta G^{\ddagger}_{inv}$ (kcal/mol)	ref
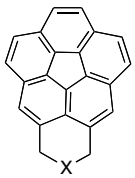		**C2**	(1.05),[b] (1.08)[c]	(30.9),[a] (29.2),[b] (27.7)[c]	1
		**C3**	(1.04),[b] (1.07)[c]	27.7, (28.9),[a] (26.6),[b] (25.6)[c]	1,2
		**C4**	(0.914),[b] (0.947)[c]	17.3, (16.9),[a] (14.8),[b] (14.7)[c]	1
		**C5**	(0.903),[b] (0.935)[c]	16.1, (16.4),[a] (14.3),[b] (13.9)[c]	1,3
		**C6**	—	16.7	1
	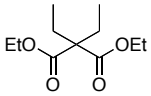	**C7**	—	15.5	1
		**C8**	(0.863),[b] (0.898)[c]	13.9, (14.5),[a] (12.1),[b] (11.8)[c]	1
		**C9**	—	13.0	1
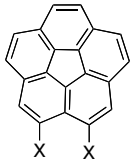		**C10**	—	9.4	1
		**C11**	(0.782),[b] (0.822)[c]	(9.1),[a] (7.5),[b] (7.4)[c]	1
		**C12**	(0.789),[b] (0.830)[c]	(9.6),[a] (7.7),[b] (7.7)[c]	1
	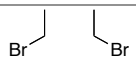	**C13**	—	9.1	1
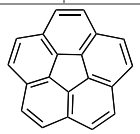		**C14**	0.88, (0.834),[b] (0.877)[c]	11.5,[d] (11.0),[a] (9.2),[b] (9.2)[c]	1,4,5
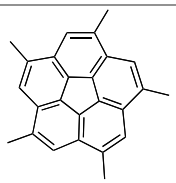		**C15**	(0.81),[b] (0.85)[c]	(11.3),[a] (8.9),[b] (8.7)[c]	1,5
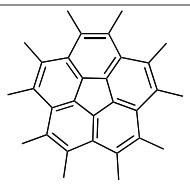		**C16**	(0.54),[b] (0.58)[c]	(1.3),[a] (2.0),[b] (2.2)[c]	1,5
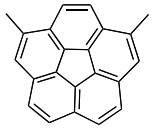		**C17**	(0.825),[b] (0.866)[c]	(11.1),[a] (9.1),[b] (9.0)[c]	1

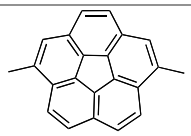	**C18**	(0.825),[b] (0.865)[c]	(11.1),[a] (9.1),[b] (9.0)[c]	1
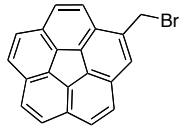	**C19**	—	11.0	1
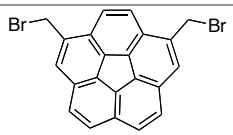	**C20**	—	10.4	1
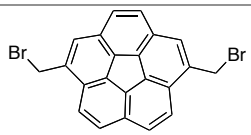	**C21**	—	10.5	1
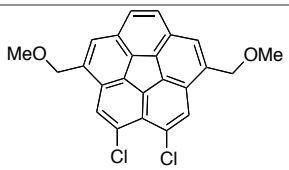	**C22**	—	8.7	1
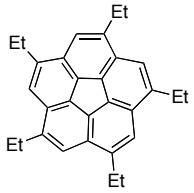	**C23**	—	11.0	6
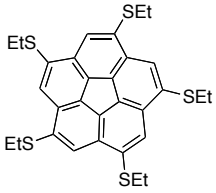	**C24**	—	10.5	6
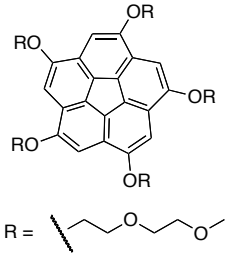	**C25**	—	11.5	6

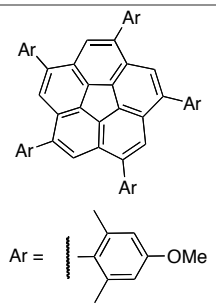	**C26**	—	12.1	6

[a]() was calculated using MP2/cc-pVDZ. [b]() was calculated using RHF/cc-pVDZ. [c]() was calculated using B3LYP/cc-pVDZ. [d]Estimation base on inversion barriers for **C19**-**C21**.

Structure-energy correlations, proposed by Bürgi and Dunitz, are important tools for elucidating reaction mechanisms and for describing stereoelectronic effects along a reaction path.[7] To visualize the structural changes that occur for a particular process, a series of related compounds are needed. Ideally perturbations within the series are designed to simulate the distortions along the potential energy surface for the process in question. In the case of the inversion process for **C1**, corannulene derivatives having different bowl depths were used. These compounds allow one to visualize the inversion process.

Experimental and calculated inversion barriers were plotted versus calculated bowl depth (Figure C3). Each calculated structure was fully optimized using the B3LYP/cc-pVDZ hybrid density functional method and additional single point energy computations of the ground and transition state structures were computed using MP2/cc-pVDZ. In both cases, a fourth order function eq 1 was fitted well.

$$\Delta E = -ax_o^4 \qquad (1)$$

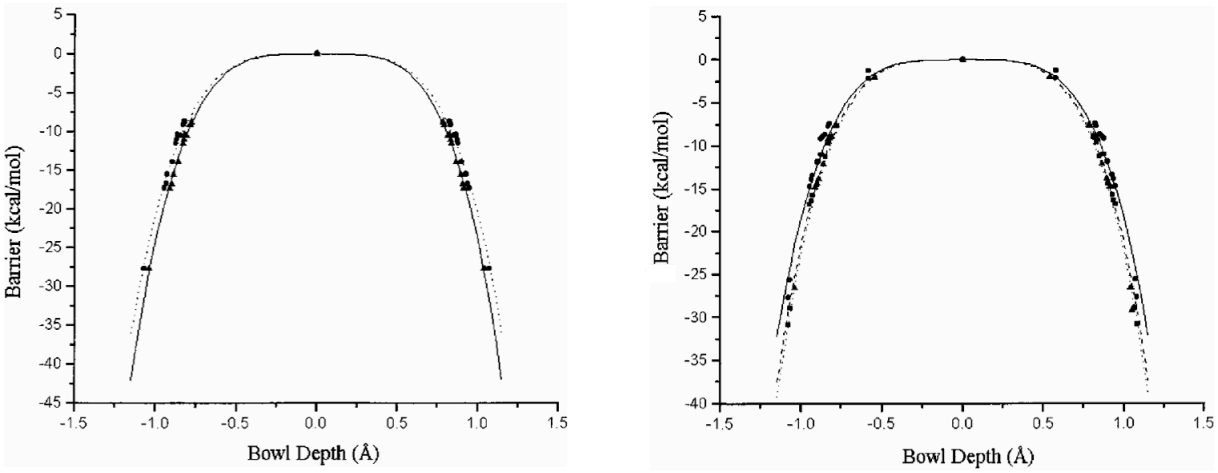

Figure C3. Structure-energy correlation of experimental (left) and calculated (right) $\Delta G^{\ddagger}_{inv}$ versus calculated bowl depth.

The observed differences in activation energy of the corannulene derivatives are attributed to a mixture of ground-state and transition-state effects. Destabilization of bowl-shaped structure through repulsive interactions raises the ground state energy and consequently decreases the activation energy. In contrast, relative stabilization of the bowl-shaped structure through attractive tethering interactions leads to an increase in transition state strain. Therefore changes of the ground state and transition state energy are at the heart of dynamic rate acceleration.

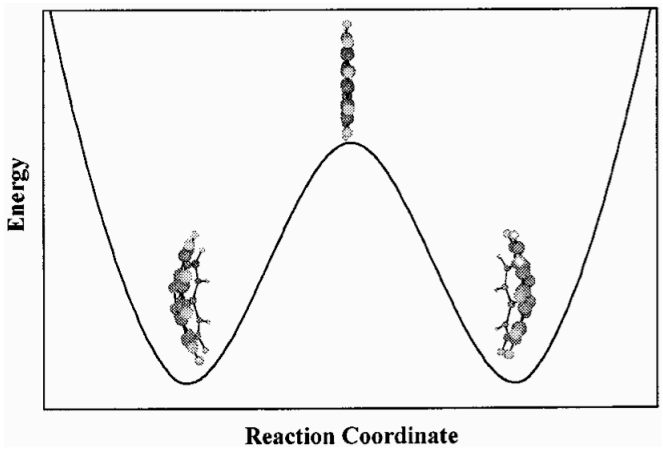

Figure C4. Energy diagram of the bowl-to-bowl inversion process of C1 (eq 2).

Although those correlations relate structure and energy within a series of corannulene derivatives, the reaction profile of an individual molecule is left unaccounted for. For **C1**, the potential energy surface (PES) for bowl-to-bowl inversion is described by two symmetry-equivalent minima connected through a common transition state (Figure C4). The transition states for simple corannulene derivatives have been calculated to be planar. On the basis of the report concerning NH_3 inversion by Dunitz,[8] the inversion of **C1** was assumed to fit a quartic function eq 2. The coefficients *a* and *b* tailor the shape of each profile (Figure C5). Solving for *a* and *b*, by evaluating the derivative of eq 2 (eq 3) at the extrema (eq 4), leads to the quartic relationship of inversion energy (ΔE) with bowl depth (x_o) (eq 5), which corresponds to eq 1.

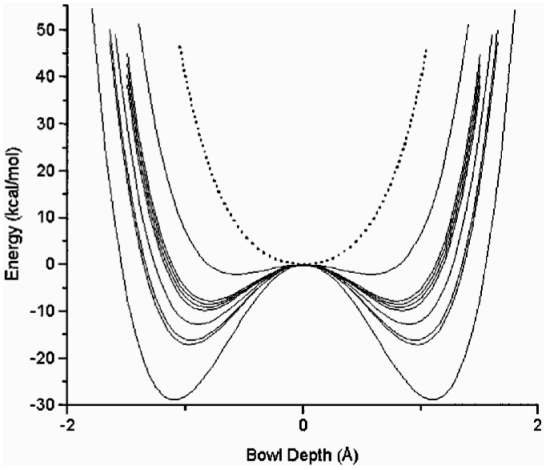

Figure C5. Reaction profiles representing the perturbation of corannulene derivatives.

$$E = ax^4 - bx^2 \tag{2}$$

$$\frac{dE}{dx} = 4ax^3 - 2bx = 0 \tag{3}$$

$$x = 0, \quad b = 2a(x_o)^2 \tag{4}$$

$$\Delta E = E_{x_o} - E_{eq} = a(x_o)^4 - 2a(x_o)^2(x_o)^2 = -ax_o^4 \tag{5}$$

Similar structure-energy correlations involving **C1** and seven singularly fused benzannulated corannulene derivatives were reported by Dinadayalane and Satry (calculated Φ_{POAV} versus calculated inversion barrier) (Figure C6).[9] As previously explained, the POAV angle is an effective measurement to gauge the pyramidalization at a given sp^2 center.[10] They have taken the average of the hub-POAV as an idealized description of curvature. Each structure was fully optimized using the B3LYP/6-31* hybrid density functional method and additional single point energies were obtained for each transition state. In spite of the relatively small basis set used and the lack of electron correlation, the data fit well to eq 1. These results suggest that singularly fused benzannulations of the corannulene nucleus flatten the bowl and reduce the barrier to inversion by a destabilization of the ground state.

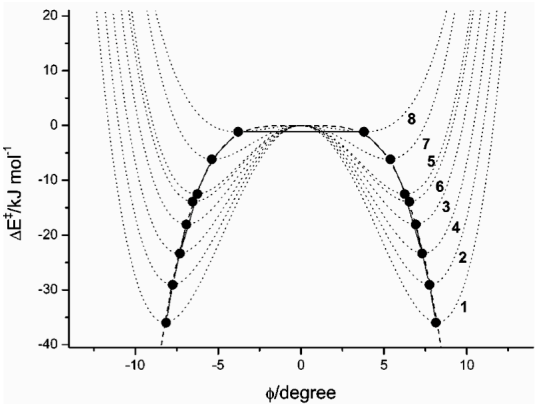

Figure C6. Correlation of Φ_{POAV} and bowl-to-bowl inversion barrier.

3.1.2. Influence of *endo* Groups of *sym*-Pentamanisylcorannulene (C26)

Although almost all corannulene derivatives follow the structure-energy correlation that more ring substitution tends to lower the inversion barrier, one interesting exception exists. The inversion barrier of **C26** is about 12.1 kcal/mol by the coalescence approximation in dichloromethane (aromatic proton: 12.1 kcal/mol, methyl proton: 12.0 kcal/mol).[6] This value is approximately 2.5 kcal/mol higher than that expected based on extrapolation from the monomanisylcorannulene. In addition, the inversion energy of monomanisylcorannulene (11.1 kcal/mol) follows the normal trend. Density functional computations at the B3LYP/cc-pVDZ level of theory were carried out and predicted a barrier to inversion of 8.5 kcal/mol, substantially lower than what was found experimentally. Addition of dynamic correlation is essential for realistic prediction of barriers in this system, for example MP2/cc-pVDZ//B3LYP/cc-pVDZ. These computations predicted a barrier of 14.6 kcal/mol.

This computational result suggested that the anomalous increase in barrier height arises from van der Waals (vdW) attractive forces among the *endo* methyl groups in **C26** (Figure C7). These attractive interactions are not present among the methyls of the *exo* face or the methyls in the transition state structure. Therefore breaking such noncovalent bonds would contribute to the higher barrier to inversion.

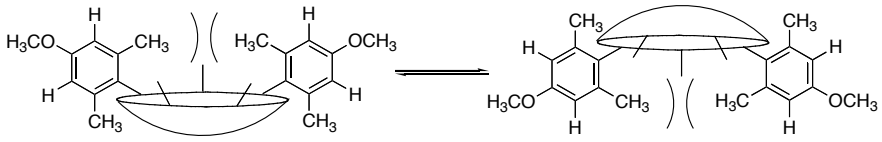

Figure C7. VdW attractive forces among the *endo* methyl groups.

A study about the correlations between the isotopic effect and $\Delta G^{\ddagger}_{inv}$ in **C26** were also reported (Table C2).[11] In this report, the X-ray crystallographic data on **C26** and the difference of $\Delta G^{\ddagger}_{inv}$ in **C27** and **C28**, suggested that the vdW interaction of CD_3//CD_3 is stronger than that of CH_3//CH_3.

Table C2. Inversion energies of C27 and C28.

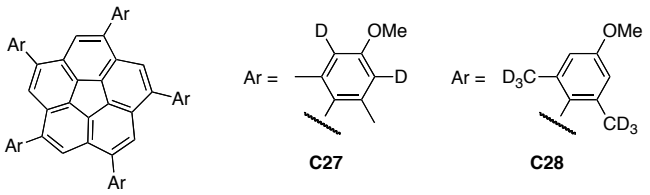

C27 **C28**

	T_c [a] (K)	$\Delta G^{\ddagger}_{T250}$ (kcal/mol)	$\Delta G^{\ddagger}_{Tc}$ (kcal/mol)
C27 (CH_3)	266.1	11.62 ± 0.015	11.60 ± 0.011
C28 (CH_3)	251.0	11.72 ± 0.011	11.72 ± 0.010

[a] T_c : coalescence temperature.

3.2. Present Work

3.2.1. Solvent Effect on Inversion Energies

The vdW attractive forces of *endo* groups of **C26** suggest the probability of other interactions in similar *sym*-pentaarylcorannulenes. In addition, the investigation of $\Delta G^{\ddagger}_{inv}$ in various kinds of solvents would give information about the kinds of interaction because of their different physical properties.

The *sym*-pentaarylcorannulenes (**C26**, **C29**, and **C30**) and monosubstitutedcorannulene (**C19**) were chosen for the solvent effect study (Figure C8). **C19** was prepared from bromocorannulene (**C32**) by a reported procedure (Scheme C1).[12]

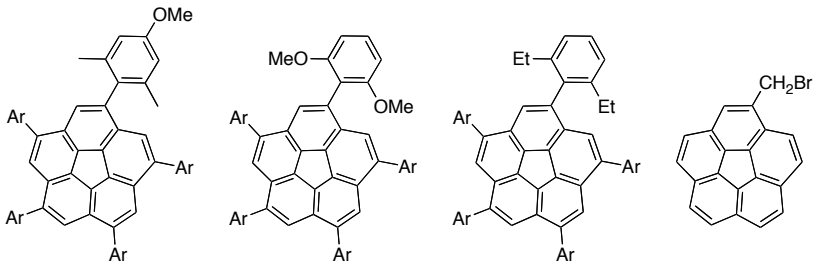

C26 **C29** **C30** **C19**

Figure C8. Selected corannulene derivatives for solvent effect study.

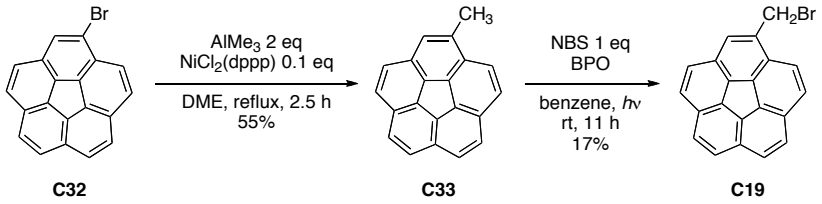

Scheme C1. Synthesis of C19.

The variable temperature ^{1}H-NMR spectra were measured in several different solvents. For the evaluation of rate parameters, the line shape analysis (LSA) or coalescence approximation (CA) were used. The experimental line shapes, temperature, and rates were analyzed with the computer program WINDNMR.[13] The program was provided with the chemical shifts at slow exchange and the digitized NMR spectrum.

Standard activation parameters were obtained from the linear least squares fit of the experimental rate data to the Eyring equation (Table C3). To remove the differential temperature effect associated with coalescence data comparisons, the free energy at a temperature in the middle of the temperature range was selected (T = 235 K).

Table C3. $\Delta G^{\ddagger}_{inv}$ in different kinds of solvents.

solvent	LSA, $\Delta G^{\ddagger}_{T235}$ [a] (stdev[d])			CA, $\Delta G^{\ddagger}_{T211}$ [a] (stdev[d])
	C26	C29	C19	C30
Toluene-d_8	10.48 (0.027)	10.63 (0.053)	10.61 (0.014)	—
Chlorobenzene-d_5	10.33 (0.007)	—	—	—
Chloroform-d	11.00 (0.013)	10.70 (0.032)	11.02 (0.017)	9.770 (0.115)
Dibromomethane-d_2	11.89 (0.025)	—	—	—
Dichloromethane-d_2	11.73 (0.017)[e]	11.50 (0.018)	10.88 (0.008)	—
Acetone-d_6	11.07 (0.017)	12.41 (0.020)	10.87 (0.012)	—
DCFM-d[c]	11.20 (0.029)	—	—	—
Bowl Depth[b]	0.94 [0.56]	0.91 [0.54]	—	0.82 [0.50]

[a](kcal/mol). [b](Å), from X-ray crystal structures. [] is the value from the mean plane of the hub carbons to the mean plane of the spoke atoms. [c]DCFM : dichlorofluoromethane. [d]For the calculation of errors, see experimental section. [e]12.0 kcal/mol at 268 K was reported by coalescence approximation.[6]

Generally, when solvent effects are considered, there are two kinds of factors. The first are electronic factors: polarity or polarization. The other is nonelectronic factors: cavitation, dispersion forces, or solvent dispositions.[14] The former tends to depend on the polarity of solvent. On the other hand, one of the nonelectronic factors, the dispersion forces, has a dependency on the volume of the molecule. Normally, a larger molecule has a larger polarizability and exerts a greater dispersion force. The physical properties of some solvents are listed on Table C4.

Table C4. Some physical properties of solvents.

solvent	M_T [a]	**ρ** [b] **(g/cm³)**	V [c] **(Å³)**	ε_r [d]	α [e] **10^{-24}(cm³)**
Toluene	92.14	0.8669	176	2.379	12.26, 11.8
Chlorobenzene	112.56	1.1058	169	5.6895	14.1, 12.3
Chloroform	119.38	1.4832	134	4.8069	9.5, 8.23
Dibromomethane	173.83	2.4969	116	7.77	9.32, 8.62
Dichloromethane	84.93	1.3266	106	8.93	7.93, 6.48
Acetone	58.08	0.7899	122	21.01	6.4, 6.39, 6.33
DCFM	102.92	1.405	122	—	9.5, 6.82

[a] M_T : molecular weight. [b] ρ : density at 20°C (9°C for DCFM).[15] [c] V : volume, $V = \frac{M_T}{\rho} \times \frac{1}{N_A} \times 10^{24}$.

[d] ε_r : dielectric constant.[15] [e] α : polarizability.[15]

One observation is that the $\Delta G^{\ddagger}_{inv}$ of **C19** in four solvents are almost the same, while those of **C26** or **C29** depend on the solvent. This suggests the existence of some interactions in *endo* groups that have a dependency on the solvent properties. The activation parameters, $\Delta H^{\ddagger}_{inv}$ and $\Delta S^{\ddagger}_{inv}$, also do not show a large difference in **C19** (Table C5).

Table C5. Activation parameters of C19.

solvent	LSA		
	$\Delta G^{\ddagger}_{T235}$ (stdev[a]) (kcal/mol)	$\Delta H^{\ddagger}$ (stdev[a]) (kcal/mol)	$\Delta S^{\ddagger}$ (stdev[a]) (cal/mol·K)
Toluene-d_8	10.61 (0.014)	10.8 (0.19)	0.9 (0.87)
Chloroform-d	11.02 (0.017)	10.7 (0.19)	–1.5 (0.89)
Dichloromethane-d_2	10.88 (0.008)	11.3 (0.08)	1.9 (0.36)
Acetone-d_6	10.87 (0.012)	12.0 (0.14)	4.7 (0.65)

[a]For the calculation of errors, see experimental section.

In the case of **C26**, the dipole moments of the ground state (bowl) and the transition state (plane) were 1.5 and 0 D from calculations (MP2/DZV(2d, p)//B3LYP/cc-pVDZ). As such a polarity dependency of $\Delta G^{\ddagger}_{inv}$ is possible, but this kind of correlation was not found (the Pearson regression factor (R^2) = 0.0733 ($\Delta G^{\ddagger}_{inv}$-$\varepsilon_r$, except DCFM)). On the other hand, when $\Delta G^{\ddagger}_{inv}$ was plotted against the solvent volume, there seemed to be a trend (Figure C9). The R^2 value of $\Delta G^{\ddagger}_{inv}$-V plot is 0.8306 and moderately high (the empirical volume was calculated from the density). This correlation suggests that the smaller solvent had a larger $\Delta G^{\ddagger}_{inv}$.

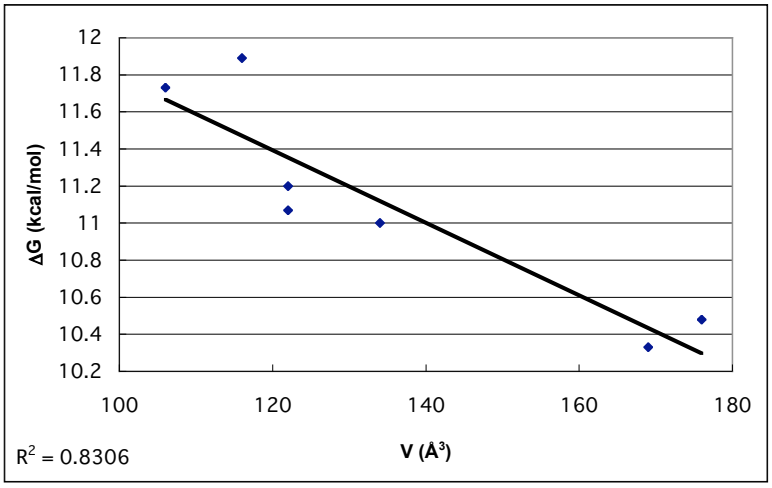

Figure C9. Relationship between $\Delta G^{\ddagger}_{inv}$ and the solvent volume in C26.

It seems difficult to understand this result. In the meanwhile, activation parameters $\Delta H^{\ddagger}_{inv}$ and $\Delta S^{\ddagger}_{inv}$ can also be utilized because $\Delta G^{\ddagger}_{inv}$ was originally calculated from those values by LSA. The table shows almost constant values of $\Delta H^{\ddagger}_{inv}$ (Table C6). The computational value of $\Delta H^{\ddagger}_{inv}$ in the gas phase is 12.5 kcal/mol. Generally, the reliability of $\Delta G^{\ddagger}_{inv}$ is higher than those of $\Delta H^{\ddagger}_{inv}$ and $\Delta S^{\ddagger}_{inv}$ due to the covariance.[16] Therefore, small differences of $\Delta H^{\ddagger}_{inv}$ might be ignored. Now if the influence of solvent effect on $\Delta H^{\ddagger}_{inv}$ is removed, $\Delta S^{\ddagger}_{inv}$ should show the same trend as that of $\Delta G^{\ddagger}_{inv}$ because of the equation $\Delta G^{\ddagger}_{inv} = \Delta H^{\ddagger}_{inv} - T\Delta S^{\ddagger}_{inv}$.

Table C6. Activation parameters of C26.

solvent	ε_r	V (Å^3)	LSA		
			$\Delta G^{\ddagger}_{T235}$ (stdev[a]) (kcal/mol)	$\Delta H^{\ddagger}$ (stdev[a]) (kcal/mol)	$\Delta S^{\ddagger}$ (stdev[a]) (cal/mol·K)
Toluene-d_8	2.379	176	10.48 (0.027)	13.7 (0.24)	13.6 (1.04)
Chlorobenzene-d_5	5.6895	169	10.33 (0.007)	11.0 (0.17)	2.7 (0.75)
Chloroform-d	4.8069	134	11.00 (0.013)	12.0 (0.19)	4.5 (0.79)
Dibromomethane-d_2	7.77	116	11.89 (0.025)	13.0 (0.24)	4.5 (0.94)
Dichloromethane-d_2	8.93	106	11.73 (0.017)[e]	13.4 (0.11)	6.9 (0.42)
Acetone-d_6	21.01	122	11.07 (0.017)	12.0 (0.31)	4.0 (1.27)
DCFM-d[c]	—	122	11.20 (0.029)	11.3 (0.14)	0.2 (0.46)
				average (exptl $\Delta H^{\ddagger}$) = 12.3; calc $\Delta H^{\ddagger}$ = 12.5	

[a]For the calculation of errors, see experimental section.

The degree of association of molecules in a liquid can be estimated by means of the Trouton constant.[17] This constant equals the entropy of vaporization at the boiling point $\Delta S_{vap}(T_{bp})$ and is calculated from the enthalpy of vaporization (Table C7). This rule works best for apolar, quasi-spherical molecules. Large deviations occur when chemical association is involved (*e.g.* carboxylic acids), from molecular dipolarity (*e.g.* dimethyl sulfoxide), and from molecular asphericity (*e.g.* neopentane/*n*-pentane).

Table C7. Enthalpy and entropy of vaporization.

solvent	bp[a] (K)	$\Delta H_{vap}(T_{bp})$[b] (kcal/mol)	$\Delta S_{vap}(T_{bp})$[c] (cal/mol·K)
Toluene	383.78	7.929	20.66
Chlorobenzene	404.87	8.409	20.77
Chloroform	334.32	6.988	20.90
Dibromomethane	370.15	7.867	21.25
Dichloromethane	313.15	6.706	21.41
Acetone	329.2	6.954	21.12
DCFM	282.05	6.022	21.35

[a]bp : boiling point.[15] [b]$\Delta H_{vap}(T_{bp})$: enthalpy of vaporization at the boiling point.[15]

[c] [b]$\Delta S_{vap}(T_{bp})$: entropy of vaporization at the boiling point, $\Delta S_{vap}(T_{bp}) = \frac{\Delta H_{vap}(T_{bp})}{T_{bp}}$.

When $\Delta G^{\ddagger}_{inv}$ was plotted against $\Delta S_{vap}(T_{bp})$, there is a correlation (Figure C10). R^2 is 0.7535 and is not so high. However, when it is considered that there are different shapes of solvent molecules, this correlation seems to exist. The correlation shows that $\Delta G^{\ddagger}_{inv}$ is larger in the solvent having larger $\Delta S_{vap}(T_{bp})$. If the supposition $\Delta S^{\ddagger}_{inv} \approx \Delta G^{\ddagger}_{inv}$ is added to this correlation, it will imply an interpretation. In the bowl inversion of **C26**, the entropy of inversion ($\Delta S^{\ddagger}_{inv}$) is larger in more associated solvents (larger $\Delta S_{vap}(T_{bp})$). This relationship sounds reasonable because if solvent molecules associated strongly with each other, the entropy of the ground state of **C26** will be smaller due to the hard solvent cage (Figure C11). Naturally, there would be an influence of the solvent cage also in the transition state, but this effect would be larger in the ground state because of the energy profile of the bowl inversion process (Figure C4). Since the transition state is highly unstable, the solvent cage would be easily broken. Although the further studies are probably desirable, a kind of understanding of the experimental results of the solvent effect on **C26** seems to be achieved for the present.

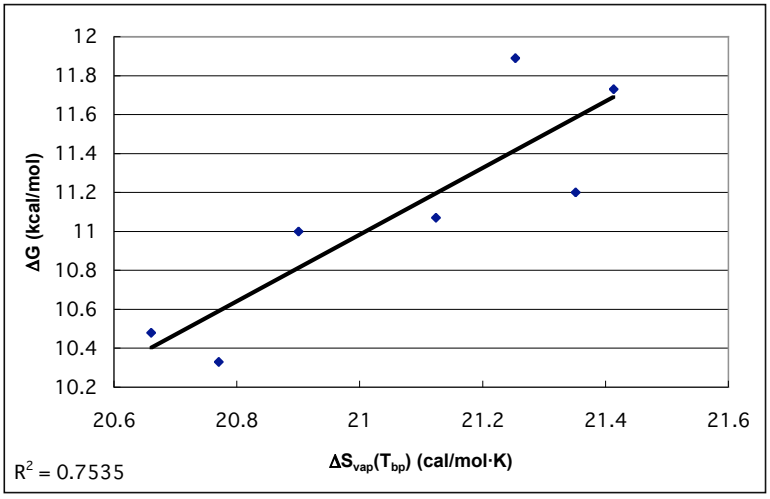

Figure C10. Relationship between $\Delta G^{\ddagger}_{inv}$ and $\Delta S_{vap}(T_{bp})$ in C26.

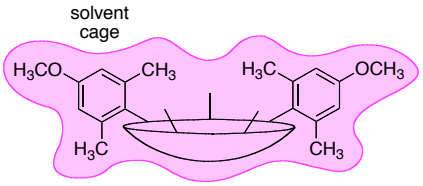

Figure C11. Solvent cage fixes the movement of C26, especially in the ground state.

In the meanwhile, $\Delta G^{\ddagger}_{inv}$ of **C29** shows a correlation with the solvent polarity, especially dielectric constant ε_r (or relative permittivity), not volume. The parameter ε_r represents the ability of a molecule to separate charge and to orient its dipoles. Because both ε_r and the dipole moment μ are important complementary solvent properties, organic solvents are sometimes classified according to their product $\varepsilon_r \cdot \mu$ which takes into account the influence of both properties.[18] The solvent polarity generally consists of many factors; dipole moment, dielectric constant, and the sum of all other molecular properties responsible for all the interaction forces between solvent and solute molecules (for example, Coulombic, directional, inductive, dispersion, hydrogen-bonding, etc).[19] The Reichart parameter $E_T(30)$ is an empirical solvent polarity parameter based on the transition energy for the longest-wavelength solvatochromic absorption band of the pyridinium *N*-phenolate betaine dye.[20] $E_T(30)$ includes all kinds of factors related with the solvent polarity and thus, it is used as a comprehensive index of the solvent polarity. Some parameters of solvent polarity are listed in Table C8.

Table C8. Polarity parameters of solvents.

solvent	ε_r	μ^a **(D)**	$\varepsilon_r \cdot \mu$ **(D)**	$E_T(30)^b$ **(kcal/mol)**
Toluene	2.379	0.37	176	33.9
Chlorobenzene	5.6895	1.69	169	36.8
Chloroform	4.8069	1.04	134	39.1
Dibromomethane	7.77	1.43	116	39.4
Dichloromethane	8.93	1.6	106	40.7
Acetone	21.01	2.88	122	42.2
DCFM	—	—	—	—

[a] μ : electric dipole moment.[15] [b] $E_T(30)$: Reichardt solvent polarity parameter.[20]

The R^2 value of $\Delta G^{\ddagger}_{inv}$-$\varepsilon_r$ plot is 0.9605 which shows a very good correlation (Figure C12). The correlations of $\Delta G^{\ddagger}_{inv}$ with other polarity parameters are 0.9454 ($\Delta G^{\ddagger}_{inv}$-$\mu$), 0.9143 ($\Delta G^{\ddagger}_{inv}$-$\varepsilon_r \cdot \mu$), and 0.6453 ($\Delta G^{\ddagger}_{inv}$-$E_T(30)$). These values suggest that ε_r or μ has a high influence on $\Delta G^{\ddagger}_{inv}$ in the solvent polarity parameters.

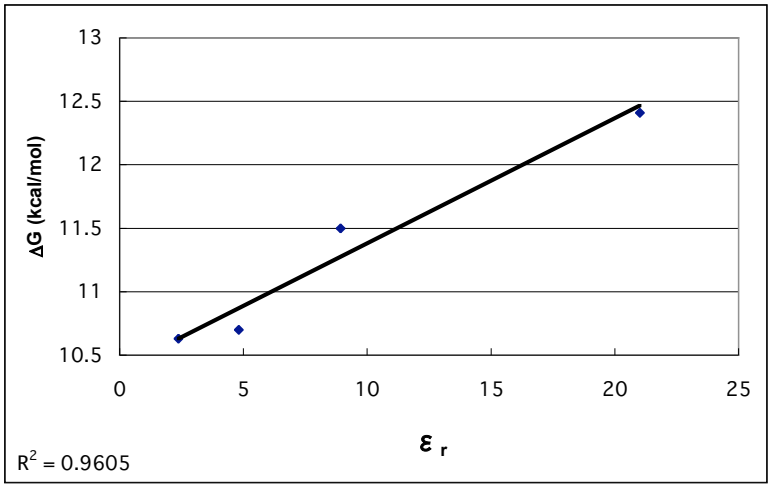

Figure C12. Relationship between $\Delta G^{\ddagger}_{inv}$ and dielectric constant in C29.

More useful information can be obtained from the activation parameters (Table C9). Although a quantitative treatment of $\Delta H^{\ddagger}_{inv}$ and $\Delta S^{\ddagger}_{inv}$ is generally difficult because of errors, there are obviously inverse trends with the solvent polarity. The R^2 values of the correlations of $\Delta H^{\ddagger}_{inv}$ with polarity parameters are 0.9061 ($\Delta H^{\ddagger}_{inv}$-$\varepsilon_r$), 0.9770 ($\Delta H^{\ddagger}_{inv}$-$\mu$), 0.8192 ($\Delta H^{\ddagger}_{inv}$-$\varepsilon_r \cdot \mu$), and 0.8705 ($\Delta H^{\ddagger}_{inv}$-$E_T(30)$). On the other hand, the R^2 values of the correlations of $\Delta S^{\ddagger}_{inv}$ with polarity parameters are 0.8932 ($\Delta S^{\ddagger}_{inv}$-$\varepsilon_r$), 0.7769 ($\Delta S^{\ddagger}_{inv}$-$\mu$), 0.9583 ($\Delta S^{\ddagger}_{inv}$-$\varepsilon_r \cdot \mu$), and 0.3542 ($\Delta S^{\ddagger}_{inv}$-$E_T(30)$). These correlations show that in a highly polar solvent, $\Delta H^{\ddagger}_{inv}$ and $\Delta S^{\ddagger}_{inv}$ are larger (Figure C13, Figure C14).

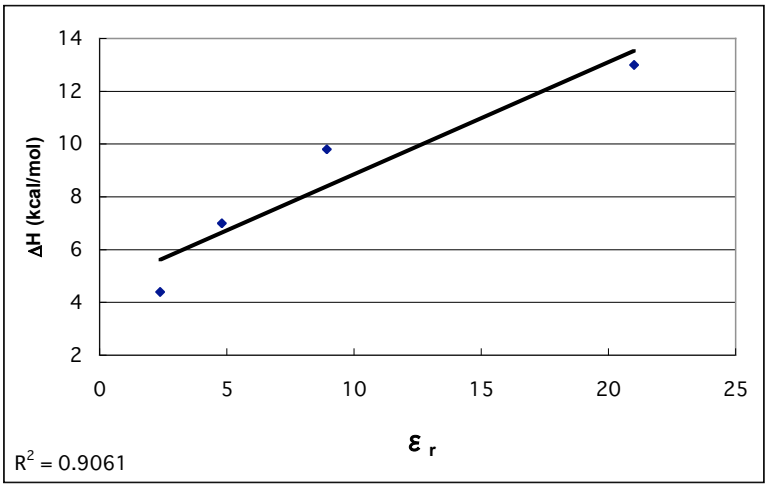

Figure C13. Relationship between $\Delta H^{\ddagger}_{inv}$ and dielectric constant in C29.

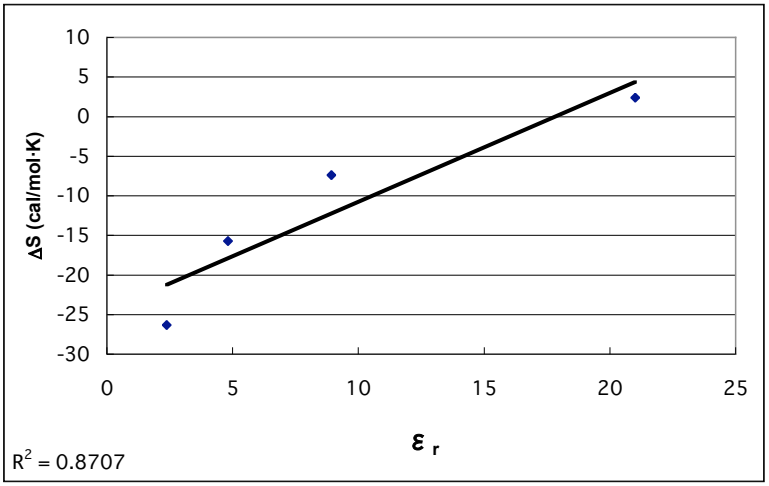

Figure C14. Relationship between $\Delta S^{\ddagger}_{inv}$ and dielectric constant in C29.

Table C9. Activation parameters of C29.

solvent	ε_r	LSA		
		$\Delta G^{\ddagger}_{T235}$ (stdev[a]) (kcal/mol)	$\Delta H^{\ddagger}$ (stdev[a]) (kcal/mol)	$\Delta S^{\ddagger}$ (stdev[a]) (cal/mol·K)
Toluene-d_8	2.379	10.63 (0.053)	4.4 (0.06)	–26.3 (0.26)
Chloroform-d	4.8069	10.70 (0.032)	7.0 (0.11)	–15.7 (0.46)
Dichloromethane-d_2	8.93	11.50 (0.018)	9.8 (0.13)	–7.4 (0.49)
Acetone-d_6	21.01	12.41 (0.020)	13.0 (0.15)	2.4 (0.55)

[a]For the calculation of errors, see experimental section.

We can consider solvent effects on $\Delta H^{\ddagger}_{inv}$ and $\Delta S^{\ddagger}_{inv}$ separately because both terms are independent of each other. **C29** would have different dipole moments in the ground state (bowl) and in the transition state (plane). The former is 3.2 D and the latter is 0 D because of the symmetric structure. Based on the difference of the dipole moments, one interpretation is possible. In a highly polar solvent, the ground state will be stabilized by solvent molecules. This means that the enthalpy of the ground state (H_G) will be smaller. Because $\Delta H^{\ddagger}_{inv} = H_T - H_G$, if the enthalpy of the transition state (H_T) is the same, $\Delta H^{\ddagger}_{inv}$ will become larger. The stabilization by solvent molecules will lead to an increased order in the solvent cage or smaller vibrational movement of **C29** in the ground state, which gives a smaller entropy of the ground state (S_G) (Figure C15). Because $\Delta S^{\ddagger}_{inv} = S_T - S_G$, if the entropy of the transition state (S_T) is the same, $\Delta S^{\ddagger}_{inv}$ will become larger in polar solvents.

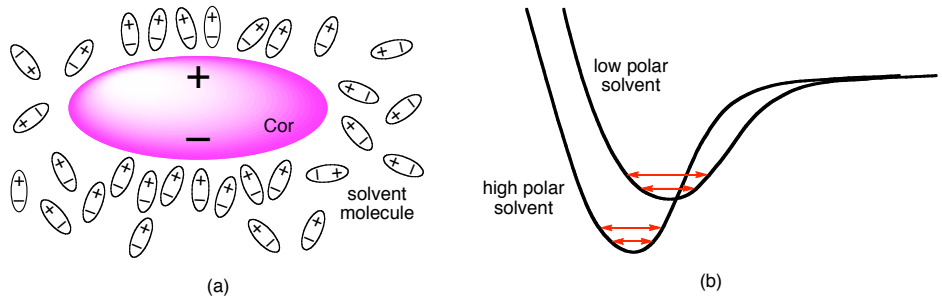

Figure C15. In a highly polar solvent, (a) an ordered solvent cage or (b) smaller vibrational movement of C29 in the ground state will give a smaller S_G.

This interpretation explains the trends of $\Delta H^{\ddagger}_{inv}$ and $\Delta S^{\ddagger}_{inv}$, but there still remains an unsolved problem. In low polar solvents, $\Delta S^{\ddagger}_{inv}$ is large and negative. This means that S_G is larger than S_T. To explain the trend of $\Delta S^{\ddagger}_{inv}$, the influence of the stabilization by solvent molecules was used. Now when this contribution supposed to be $\Delta S^{\ddagger}_{solv}$, this value should be always positive because there is no dipole moment in the transition state and thus no effect ordering solvent molecules (Figure C16). In this case, to explain the negative values of $\Delta S^{\ddagger}_{inv}$, an additional term $\Delta S^{\ddagger}_{x}$ would be desired. This term must be relatively constant and could come from something like the volume change of **C29** itself. The experimental results imply the existence of this kind of contribution by $\Delta S^{\ddagger}_{x}$.

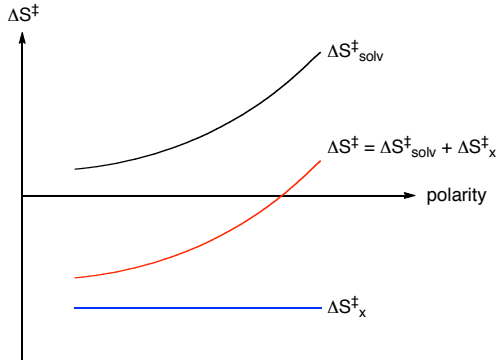

Figure C16. An additional term, $\Delta S^{\ddagger}_{x}$ should be large and negative.

Although only one solvent was used, $\Delta G^{\ddagger}_{inv}$ of **C30** is *ca*. 1 kcal/mol lower than that of **C29**. Such a difference of $\Delta G^{\ddagger}_{inv}$ (**C30**) and $\Delta G^{\ddagger}_{inv}$ (**C29**) could come from the different conformations of ethyl and methoxy groups. The conformational energies of anisole and ethylbenzene have been reported already.[21] In ethylbenzene the out-of-plane conformation is favored by *ca*. 1.0 kcal/mol, whereas in anisole the in-plane conformation around the C—O bond is favored by *ca*. 2.7 kcal/mol (Figure C17). These kind of conformational effects and the difference of the bowl depth of 0.91 Å (**C29**) and 0.82 Å (**C30**) suggest the steric repulsion of methyl groups in **C30**.

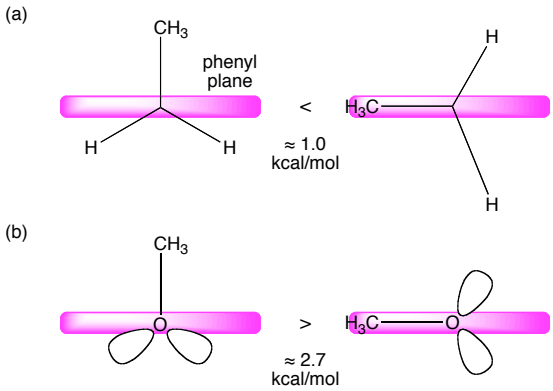

Figure C17. Conformations of (a) ethylbenzene and (b) anisole.

3.2.2. Experimental Section

3.2.2.1. Variable Temperature ^{1}H-NMR Spectra

Spectra were recorded on a Bruker DRX-500 at 500 MHz or DRX-600 at 600 MHz. In the case of coalescence approximation of **C30**, the proton decoupling technique for CH_2 of ethyl groups was used. For the evaluation of rate parameters of **C26**, **C29** and **C19**, the corresponding proton peaks were used by fitting the experimental data with the computer program WINDNMR.[13] The program was provided with the proton chemical shifts at slow exchange and the digitized NMR spectrum (FID files). Full-width-at-half-heights (FWHHs) were supposed to be 2.0 Hz for **C26** and **C29**, and 2.5 Hz for **C19**. Standard activation parameters were obtained from the linear least squares fit of the experimental rate data to Eyring equations. The variables, k, R, k_b, and h are the rate constant, the universal gas constant (8.314 J/mol·K), Boltzmann's constant (1.381×10^{-31} J/K), Plank's constant (6.626×10^{-34} J·s), respectively. Dichlorofluoromethane-*d* (DCFM-*d*) was prepared according to the literature procedure.[22] Other deuterated solvents are commercially available.

3.2.2.2. Eyring Eqation

Eyring equation 1 was used to obtain the activation parameters.

$$k = r\frac{k_B T}{h}e^{-\Delta G^{\ddagger}/RT} \tag{1}$$

Assuming the transmission coefficient *r*, which is defined as the fraction of the reactant reaching the transition state that proceeds to the product, to be unity, eq 2 is obtained.

$$\Delta G^{\ddagger} = RT\left\{\ln\left(\frac{k_b}{h}\right) - \ln\left(\frac{k}{T}\right)\right\} \tag{2}$$

3.2.2.3. Coalescence Approximation

At the coalescence temperature, the following equation can be used.

$$k = k_c = \frac{\pi\delta\nu}{\sqrt{2}} \tag{3}$$

Combination of eqs 2 and 3 gives eq 4.

$$\Delta G^{\ddagger} = RT_c\left\{\ln\left(\frac{k_b}{h}\right) - \ln\left(\frac{k_c}{T}\right)\right\} \tag{4}$$

Equation 4 was used for activation parameters of the coalescence approximation.

3.2.2.4. Line Shape Analysis

Substituting $\Delta G^{\ddagger} = \Delta H^{\ddagger} - T\Delta S^{\ddagger}$, eq 1 becomes eq 5.

$$k = \frac{k_B T}{h}e^{\frac{-\Delta H^{\ddagger}}{RT}}e^{\frac{-\Delta S^{\ddagger}}{R}} \tag{5}$$

Dividing eq 5 by *T* then linearizing it affords eq 6.

$$\ln\left(\frac{k}{T}\right) = -\frac{\Delta H^{\ddagger}}{RT} + \frac{\Delta S^{\ddagger}}{R} + \ln\left(\frac{k_b}{h}\right) \tag{6}$$

Equation 6 can now be linearly fit, and then the activation parameters are related to the slope *m* and *y*-intercept *b*, by the following equations:

$$m = -\frac{\Delta H^{\ddagger}}{R} \tag{7}$$

$$b = \frac{\Delta S^{\ddagger}}{R} + \ln\left(\frac{k_b}{h}\right) \tag{8}$$

Equation 7 and 8 were used for activation parameters of the line shape analysis.

3.2.2.5. Calculation of Errors[23]

In a function $F(x, y, z)$, if the errors Δx, Δy, Δz are small, the resulting error in F can be approximated by eq 9 and the variance in F by eq 10.

$$\Delta F = \frac{\partial F}{\partial x}\Delta x + \frac{\partial F}{\partial y}\Delta y + \frac{\partial F}{\partial z}\Delta z \tag{9}$$

$$\begin{aligned} VarF = (\Delta F)^2 = &\left(\frac{\partial F}{\partial x}\Delta x\right)^2 + \left(\frac{\partial F}{\partial y}\Delta y\right)^2 + \left(\frac{\partial F}{\partial z}\Delta z\right)^2 \\ &+2\frac{\partial F}{\partial x}\cdot\frac{\partial F}{\partial y}\Delta x\Delta y + 2\frac{\partial F}{\partial x}\cdot\frac{\partial F}{\partial z}\Delta x\Delta z + 2\frac{\partial F}{\partial y}\cdot\frac{\partial F}{\partial z}\Delta y\Delta z \end{aligned} \tag{10}$$

If the variables x, y, z are completely independent, eq 10 reduces to eq 11.

$$VarF = (\Delta F)^2 = \left(\frac{\partial F}{\partial x}\Delta x\right)^2 + \left(\frac{\partial F}{\partial y}\Delta y\right)^2 + \left(\frac{\partial F}{\partial z}\Delta z\right)^2 \tag{11}$$

The standard deviation in F, σF, is then obtained as the square root of eqs 10 or 11. In the coalescence approximation, since k and T are independent, eq 12 can be used.

$$\begin{aligned} Var\Delta G^{\ddagger} &= \left(\frac{\partial\left(\Delta G^{\ddagger}\right)}{\partial k}\Delta k\right)^2 + \left(\frac{\partial\left(\Delta G^{\ddagger}\right)}{\partial T}\Delta T\right)^2 \\ &= \left(RT\right)^2\left[\left\{\frac{\Delta T}{T}\left(\ln\frac{k_b T}{hk}+1\right)\right\}^2 + \left(\frac{\Delta k}{k}\right)^2\right] \end{aligned} \tag{12}$$

On the other hand in the line shape analysis, the errors were calculated by the following equation 13:

$$\begin{aligned} Var\Delta G^{\ddagger} = &\left(\frac{\partial\left(\Delta G^{\ddagger}\right)}{\partial\left(\Delta H^{\ddagger}\right)}\Delta\left(\Delta H^{\ddagger}\right)\right)^2 + \left(\frac{\partial\left(\Delta G^{\ddagger}\right)}{\partial\left(\Delta S^{\ddagger}\right)}\Delta\left(\Delta S^{\ddagger}\right)\right)^2 + \left(\frac{\partial\left(\Delta G^{\ddagger}\right)}{\partial\left(\Delta T\right)}\Delta\left(\Delta T\right)\right)^2 \\ &+2\frac{\partial\left(\Delta G^{\ddagger}\right)}{\partial\left(\Delta H^{\ddagger}\right)}\cdot\frac{\partial\left(\Delta G^{\ddagger}\right)}{\partial\left(\Delta S^{\ddagger}\right)}\Delta\left(\Delta H^{\ddagger}\right)\Delta\left(\Delta S^{\ddagger}\right) \\ &+2\frac{\partial\left(\Delta G^{\ddagger}\right)}{\partial\left(\Delta H^{\ddagger}\right)}\cdot\frac{\partial\left(\Delta G^{\ddagger}\right)}{\partial\left(\Delta T\right)}\Delta\left(\Delta H^{\ddagger}\right)\Delta\left(\Delta T\right) \\ &+2\frac{\partial\left(\Delta G^{\ddagger}\right)}{\partial\left(\Delta S^{\ddagger}\right)}\cdot\frac{\partial\left(\Delta G^{\ddagger}\right)}{\partial\left(\Delta T\right)}\Delta\left(\Delta S^{\ddagger}\right)\Delta\left(\Delta T\right) \end{aligned} \tag{13}$$

Since $\Delta S^{\ddagger}$ and $\Delta H^{\ddagger}$ are not independent, eq 13 becomes eq 14.

$$Var\Delta G^{\ddagger} = \left(\frac{\partial\left(\Delta G^{\ddagger}\right)}{\partial\left(\Delta H^{\ddagger}\right)}\Delta\left(\Delta H^{\ddagger}\right)\right)^2 + \left(\frac{\partial\left(\Delta G^{\ddagger}\right)}{\partial\left(\Delta S^{\ddagger}\right)}\Delta\left(\Delta S^{\ddagger}\right)\right)^2 + \left(\frac{\partial\left(\Delta G^{\ddagger}\right)}{\partial\left(\Delta T\right)}\Delta\left(\Delta T\right)\right)^2$$
$$+2\frac{\partial\left(\Delta G^{\ddagger}\right)}{\partial\left(\Delta H^{\ddagger}\right)}\cdot\frac{\partial\left(\Delta G^{\ddagger}\right)}{\partial\left(\Delta S^{\ddagger}\right)}\Delta\left(\Delta H^{\ddagger}\right)\Delta\left(\Delta S^{\ddagger}\right) \tag{14}$$

Here $\Delta(\Delta H^{\ddagger})$ and $\Delta(\Delta S^{\ddagger})$ are $\sigma(\Delta H^{\ddagger})$ and $\sigma(\Delta S^{\ddagger})$, respectively. Substituting $\Delta G^{\ddagger} = \Delta H^{\ddagger} - T\Delta S^{\ddagger}$, gives eq 15.

$$\begin{aligned} Var\Delta G^{\ddagger} &= \left(\sigma\left(\Delta G^{\ddagger}\right)\right)^2 \\ &= \left(\sigma\left(\Delta H^{\ddagger}\right)\right)^2 + \left(-T\sigma\left(\Delta S^{\ddagger}\right)\right)^2 + \left(-\Delta S^{\ddagger}\Delta T\right)^2 - 2T\sigma\left(\Delta H^{\ddagger}\right)\sigma\left(\Delta S^{\ddagger}\right) \end{aligned} \tag{15}$$

The errors on $\Delta H^{\ddagger}$ and $\Delta S^{\ddagger}$ can now be defined as follows:

$$\sigma\left(\Delta H^{\ddagger}\right) = R\sigma(m) \tag{16}$$

$$\sigma\left(\Delta S^{\ddagger}\right) = R\sigma(b) \tag{17}$$

The errors on m and b, $\sigma(m)$ and $\sigma(b)$, are derived from the linear least square fit of the data to the Eyring function. Errors on k_b, h, and R are assumed to be 0. Temperature settings of the spectrometer were calibrated to within 1°C by reference to a methanol standard.

3.2.2.6. Eyring Plots

***sym*-Pentamanisylcorannulene (C26)**

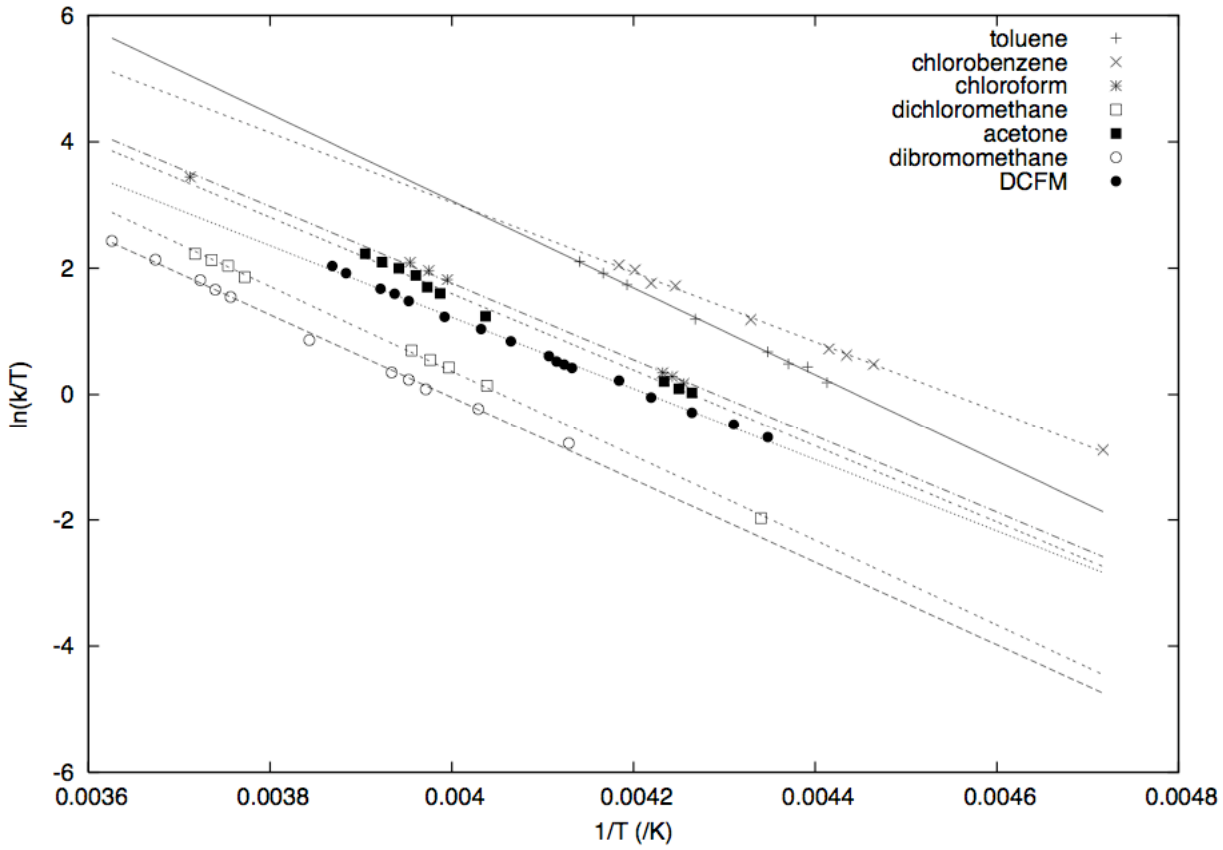

Figure C18. Eyring plot of bowl inversion process monitored through methyl peaks.

The Pearson regression factors (R^2) are 0.9981 (toluene-d_8), 0.9983 (chlorobenzene-d_5), 0.9987 (chloroform-d_3), 0.9969 (dibromomethane-d_2), 0.9993 (dichloromethane-d_2), 0.9946 (acetone-d_6), and 0.9978 (DCFM-*d*).

***sym*-Penta(2,6-dimethoxyphenyl)corannulene (C29)**

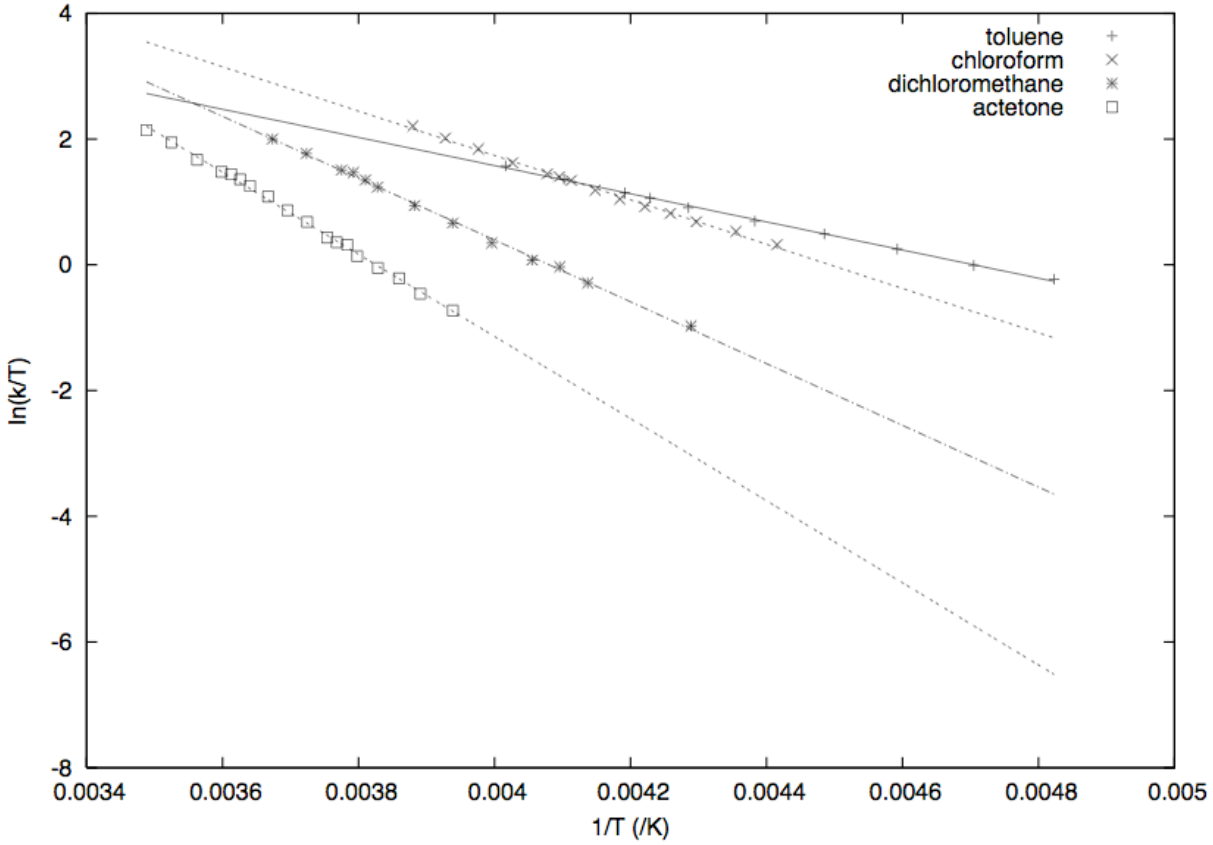

Figure C19. Eyring plot of bowl inversion process monitored through methoxy peaks.

R^2 are 0.9986 (toluene-d_8), 0.9970 (chloroform-d_3), 0.9982 (dichloromethane-d_2), and 0.9979 (acetone-d_6).

1-(Bromomethyl)benzene (C19)

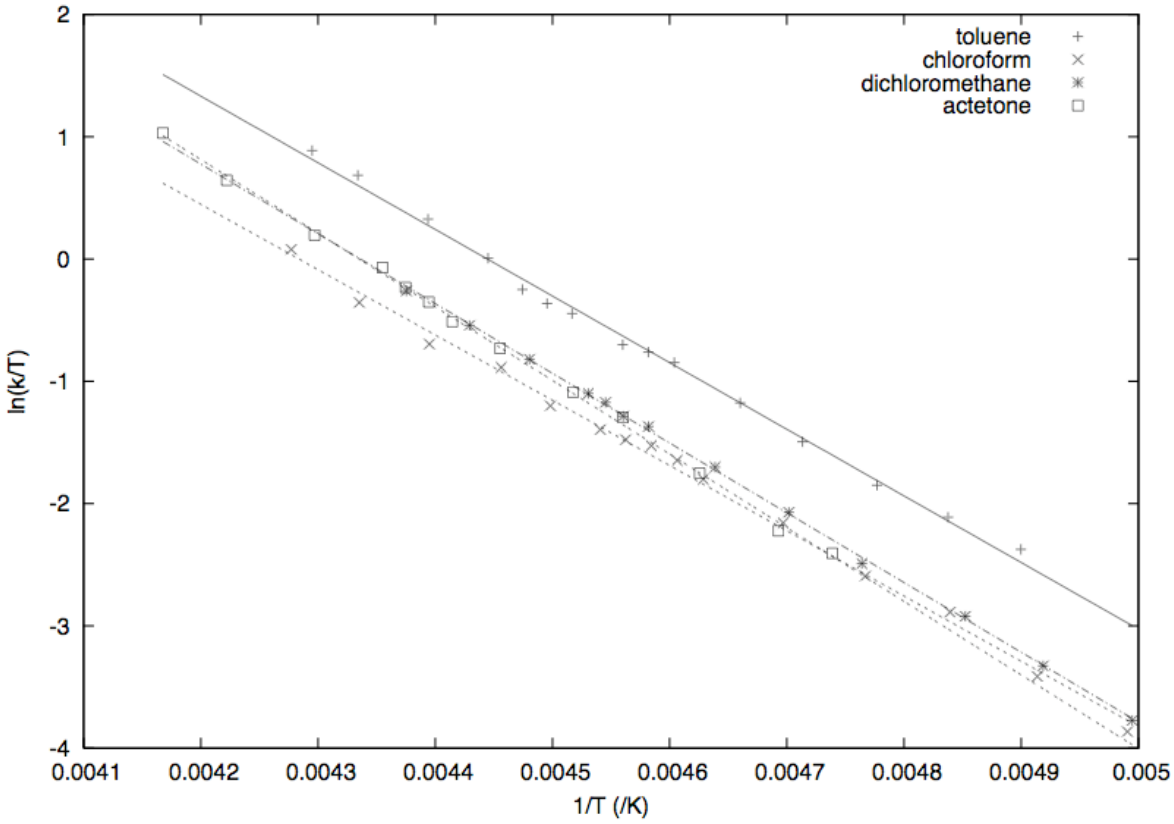

Figure C20. Eyring plot of bowl inversion process monitored through methylene peaks.

R^2 are 0.9960 (toluene-d_8), 0.9967 (chloroform-d_3), 0.9995 (dichloromethane-d_2), and 0.9988 (acetone-d_6).

3.2.2.7. Materials and Methods

Chromatography: Merck silica gel 60 (230–400 mesh). All experiments were carried out under nitrogen in freshly distilled anhydrous solvents unless otherwise noted. Solvents for chromatography were technical grade and freshly distilled before use. Bromocorannulene (**C32**) was prepared in the chapter 2. Other compounds, which are not mentioned, are commercially available.

3.2.2.8. Synthetic Procedures

Methylcorannulene (C33)

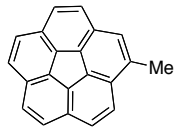

$C_{21}H_{12}$
Mol. Wt.: 264.32

Trimethylaluminium (2.0 M in hexane, 0.13 mL, 0.261 mmol) was added dropwise to a solution of bromocorannulene (**C32**) (43 mg, 0.131 mmol) and 1,3-bis(diphenylphosphino)-nickel (II) chloride (7 mg, 0.013mmol) in DME (15 mL) at room temperature. The mixture was refluxed for 2.5 h. The mixture was cooled to room temperature and quenched slowly with ethanol (5 mL), diluted with dichloromethane (50 mL), washed with water (100 mL × 3), dried with magnesium sulfate, and evaporated. The product was purified by column chromatography on silica gel eluted with hexane to yield **C33** as a yellow solid (19 mg, 55%) [R_f = 0.24 (SiO_2, hexane)]. The spectroscopic data were identical with those reported.[12] Mp 125-128 °C (lit. 123-129 °C).[12]

1-(Bromomethyl)benzene (C19)

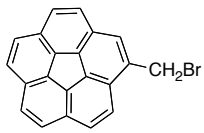

$C_{21}H_{11}Br$
Mol. Wt.: 343.216

To methylcorannulene (**C33**) (18 mg, 0.068 mmol) in benzene (10 mL), *N*-bromosuccinimide (12 mg, 0.068 mmol) and benzoyl peroxide (2 mg) were added. The mixture was stirred at room temperature under irradiation with a tungsten lamp for 11 h. The reaction was quenched with water (10 mL). The organic layer was separated, washed with water (10 mL × 3), dried with magnesium sulfate, and evaporated. The product was purified by column chromatography on

silica gel eluted with hexane/dichloromethane = 5/1 to yield **C19** as a white solid (4 mg, 17%) [R_f = 0.33 (SiO_2, hexane/dichloromethane = 10:1)]. The spectroscopic data were identical with those reported.[24] ^{1}H-NMR (300 MHz, $CDCl_3$): δ ppm = 5.08 (s, 2H), 7.76 (d, ^3J = 9.0 Hz, 1H), 7.79-7.84 (m, 6H), 7.90 (d, ^3J = 9.0 Hz, 1H), 8.07 (d, ^3J = 9.0 Hz, 1H).

3.3. References

[1] Seiders, T. J.; Baldridge, K. K.; Grube, G. H.; Siegel, J. S. *J. Am. Chem. Soc.* **2001**, *123*, 517.

[2] Sygula, A.; Abdourazak, A. H.; Rabideau, P. W. *J. Am. Chem. Soc.* **1996**, *118*, 339.

[3] Steffens, R. J.; Baldridge, K. K.; Siegel, J. S. *Helv. Chim. Acta* **2000**, *83*, 2644.

[4] Sevryugina. Y.; Rogachev, A. Y.; Jackson, E. A.; Scott, L. T.; Petrukhina, M. A. *J. Org. Chem.* **2006**, *71*, 6615.

[5] Seiders, T. J.; Baldridge, K. K.; Elliott, E. L.; Grube, G. H.; Siegel, J. S. *J. Am. Chem. Soc.* **1999**, *121*, 7439.

[6] Grube, G. H.; Elliott, E. L.; Steffens, R. J.; Jones, C. S.; Baldridge, K. K.; Siegel, J. S. *Org. Lett.* **2003**, *5*, 713.

[7] (a) Bürgi, H. B.; Dubler-Steudle, K. C. *J. Am. Chem. Soc.* **1988**, *110*, 4953. (b) Bürgi, H. B.; Dubler-Steudle, K. C. *J. Am. Chem. Soc.* **1988**, *110*, 7291.

[8] Ha, T. K.; Dunitz, J. D. *Helv. Chim. Acta.* **1990**, *73*, 583.

[9] Dinadayalane, T. C.; Sastry, G. N. *J. Org. Chem.* **2002**, *67*, 4605.

[10] Haddon, R. C. *J. Am. Chem. Soc.* **1986**, *108*, 2837.

[11] (a) Hayama, T.; Siegel, J. S; et al. Submitted for publication. (b) Hayama, T. Diplomarbeit, University of Zurich, Zurich, 2005.

[12] Seiders, T. J.; Elliot, E. L.; Grube, G. H.; Siegel, J. S. *J. Am. Chem. Soc.* **1999**, *121*, 7804.

[13] Reich, H. J. *WINDNMR Version 7.1.6* 2002.

[14] Cramer, C. J.; Truhlar, D. G. *Reviews in Computational Chemisry 6*; VCH Publishiers, Inc., New York, 1995, Chapter 1.

[15] Lide, D. R. *CRC Handbook of Chemistry and Physics*, 1999; CRC Press, Florida, 1999.

[16] see Experimental Section.

[17] Nash, L. K. *J. Chem. Educ.* **1984**, *61*, 981.

[18] Dack, M. R. J. *The influence of Solvent on Chemical Reactivity*, Dack, M. R. J. (ed), Vol. VIII, Part II, p95., in Weissberger, A. (ed) *Techniques of Chemistry*, Wiley-Interscience, New York, 1976.

[19] Kováts, E. sz. *Chimia* **1968**, *22*, 459.

[20] Reichardt, C. *Solvents and Solvent Effects in Organic Chemistry*; Wiley-VCH: Weinheim, 2003; Chapter 7.

[21] Lofthagen, M.; Siegel, J. S. *J. Org. Chem.* **1995**, *60*, 2885 and references cited therein.

[22] Siegel, J. S.; Anet, F. A. L. *J. Org. Chem.* **1988**, *53*, 2629.

[23] Sandström, J. *Dynamic NMR Spectroscopy*; Academic Press: New York, 1982; Chapter 7.

[24] Seiders, T. J. Ph.D. Dissertation, University of California, San Diego, CA, 1999; p179.

Chapter 4. Passage to Nanotube

4.1. Introduction

This chapter covers the trial to make carbon-based nanotube structures from corannulene derivatives. In addition, the production and structure analysis of an astonishing open-ring corannulene derivative will be presented.

4.1.1. Carbon Nanotubes (CNTs)

Since the striking report by Iijima about carbon nanotubes (CNTs),[1] CNTs have been fascinating various fields of researchers because of their usefulness. They have unique electronic and mechanical properties with chemical stability, and therefore can be utilized for many applications: electronic devices, field emitters, or mechanical strengthening.[2]

The structure of CNTs is cylindrical with at least one end-capped with a hemisphere of the buckybowl structure. Their chemical bonding consists of sp^2 carbon atoms similar to those of graphite. Generally, CNTs separate into two classes; single-walled nanotubes (SWNTs) and multi-walled nanotubes (MWNTs). The former is made of a single graphite layer rolled up into a hollow cylinder and the latter is composed of several concentrically arranged cylinders. Generally, the diameter of CNTs is on the nanometer scale and the length is in the millimeter scale.

Many different kinds of synthetic methods for CNTs have been reported for the large-scale preparation; electric arc-discharge, laser ablation, high-pressure CO conversion (HiPCO) or catalytic vapour deposition (CVD).[3] However, in these synthetic methods, the products have a Gaussian distribution of diameters d with mean diameters $d_0 \approx 1.0\text{-}1.5$ nm. Today, the most promising method in terms of large-quantities for industrial applications is CVD, due to the relative ease with which it is possible to upscale both the preparation and the purification methods.[4]

Many applications utilizing SWNTs require chemical modification to exploit their properties.[5] However, since the popular synthetic methods for growing nanotubes produce samples yielding a mixture of many different diameters and chiralities of nanotubes that are moreover contaminated with metallic and amorphous impurities, the purification method to separate a single compound is problematic. Therefore, a synthetic method to make a single compound is desired to investigate the physical properties of nanotubes, even if it requires many steps with low chemical yield.

4.1.2. From Buckybowl to Buckytube

The formula $C_{10n}H_{10}$ includes a series of bowl-shaped carbon-rich structures where in corannulene (**D1**) n = 2, and the simplest capped nanotube, $C_{40}H_{10}$ (**D2**), n = 4 (Figure D1). In 1997, Baldridge and Siegel reported a computer simulation of the transition from a buckybowl to buckytube (Figure D2).[6] In this paper, they concluded based on the POAV angles and dipole moments that $C_{50}H_{10}$ (**D4**) ends the bowl property and **D2** begins the tube property.

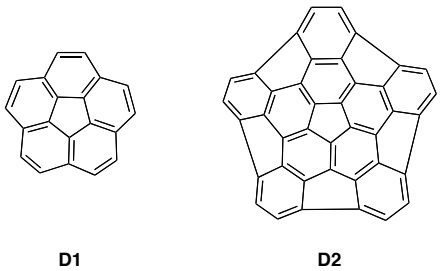

Figure D1. Corannulene (D1) and carbon-nanotube isomer $C_{40}H_{10}$ (D2).

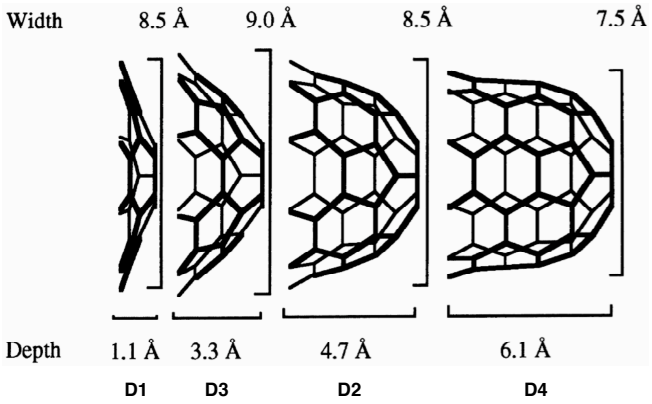

Figure D2. From buckybowl to buckytube ($C_{10n}H_{10}$, n = 1, 2, 3, and 4).

In spite of the enormous power of modern organic synthetic chemistry, **D2-D4** presently cannot be prepared. Especially, **D2** is the first member of the series of five-fold symmetric SWNTs, and therefore the synthesis of **D2** would give extremely important information about the physical properties of the nanotube structure.

4.1.3. Exploitation of Acetylene Chemistry

From the thermodynamical point of view, the carbon-carbon triple bond shows a tendency to open up and form another bond (Figure D3).[7] This is due to the relative weakness of the triple bond compared with the carbon-carbon double bond. In addition, in the case of the formation of a new aromatic ring, further stability will be obtained. However, since there is an activation energy in a reaction, some types of acetylene moieties could be kinetically stable. Therefore, they can be introduced to store energy and utilized to make various kinds of functional groups.

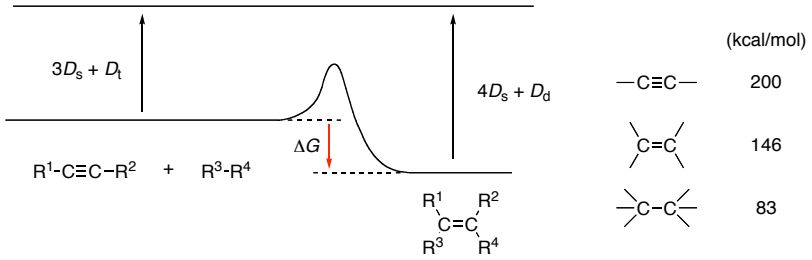

Figure D3. Energy gain (Δ*G*) from the dissociation energies (*D*) of carbon-carbon bonds.

Carbon rich compounds based on per-ethynylation of a basic carbon functional group tend to be high-energy metastable organic compounds with unusual reactivity and photophysical properties.[8] Molecular constructs manifesting subunits like tetraethynyl enthylene (**D5**)[9] or hexaethynyl benzene (**D7**)[10] appear in hundreds of variations in the current literature (Figure D4). Such compounds are often kinetically unstable and decompose readily. For example, at 25 °C **D5** becomes rapidly brown even in the absence of oxygen and polymerizes to a black solid with metallic luster. **D7** also turns brown slowly in the absence of air but rapidly in its presence. Substituted derivatives **D6** or **D8** are relatively stable, which implies the usefulness of substituents to synthesize per-ethylnylated compounds.

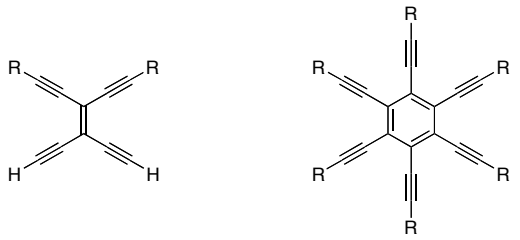

D5: R = H
D6: R = Si*i*Pr$_3$

D7: R = H
D8: R = SiMe$_3$

Figure D4. Tetraethynylethenes (D5 and D6) and hexaethynylbenzenes (D7 and D8).

For the synthesis of per-ethylnylated compounds, organometallic reactions are often used. For example, **D7** is produced from the commercially available perhalobenzenes (Br or I) and trimethylsiliyalkyne via Sonogashira couplings followed by removal of the silyl groups. Higher order per-ethynylated polycyclic aromatic hydrocarbons (PAHs) like decaethynylcorannulene (**D9**) should in principle be accessible by similar synthetic methods, if the perhalo compounds were easy to obtain (Figure D5).[11]

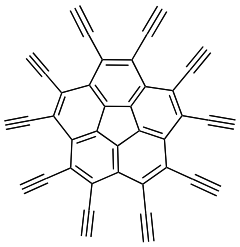

D9

Figure D5. Decaethynylcorannulene (D9) as an example of the per-ethynylated PAHs.

4.2. Present Work

A simple bond energy estimate for the energetics of **D9** compared with **D2** results in a remarkable value of 300-400 kcal/mol in favor of **D2**, and could lead one to question the feasibility of isolating **D9** as an inert material.[12] In contrast, the conceptual synthesis of **D3** from **D1** via decachlorocorannulene (**D10**) and the potential of **D9** as a direct precursor to **D2**, is so attractive in its simplicity as to be irresistible. Such an approach would open a solution phase method to the synthesis of mono-dispersed single-walled carbon nanotubes (SWCNT) from per-ethynylcorannulenes. Thus, the following retrosynthetic scheme was suggested (Scheme D1).

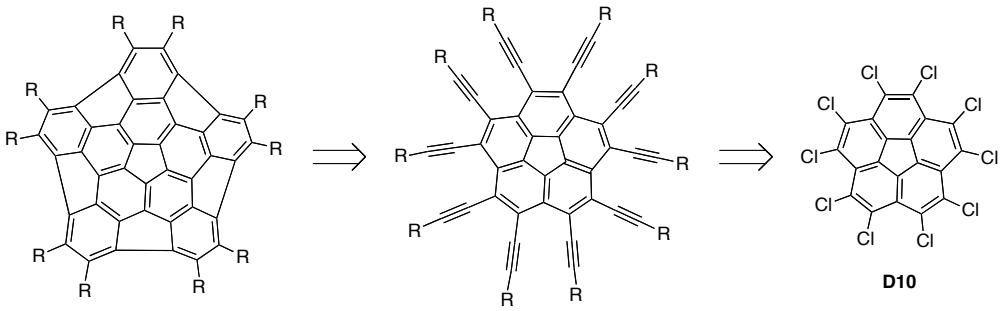

Scheme D1. Retrosynthetic analysis of D2 derivatives.

4.2.1. Synthesis of Decapentynylcorannulene (D12)

Classical per-halogenation conditions like those of Balister allows the preparation of even the sterically congested **D10**[13] in one step from **D1**, which is now available on a multigram scale in five steps (Scheme D2). Therefore, **D10** can be used as a starting material to enlarge the corannulene ring.

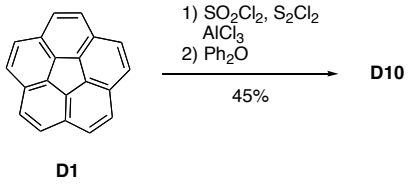

Scheme D2. Synthesis of decachlorocorannulene (D10).

The key remaining hurdles are the limited solubility of **D10** and the low reactivity of chloro-substituents. Implementation of stannylalkynes as Sonogashira partners in higher boiling solvents overcomes these problems. Thus, reaction of excess trimethylstannylpentyne (**D11**) with **D10** under palladium mediated catalysis yields decapentynylcorannulene (**D12**) directly, albeit in modest yield (10%) and an additional product (**D13**) (18%) of similar R_f value by TLC, which has the same molecular weight as that of **D12** (Scheme D3). The propyl groups endow **D12** with appreciable solubility in organic solvents, which makes chromatographic isolation much simpler.

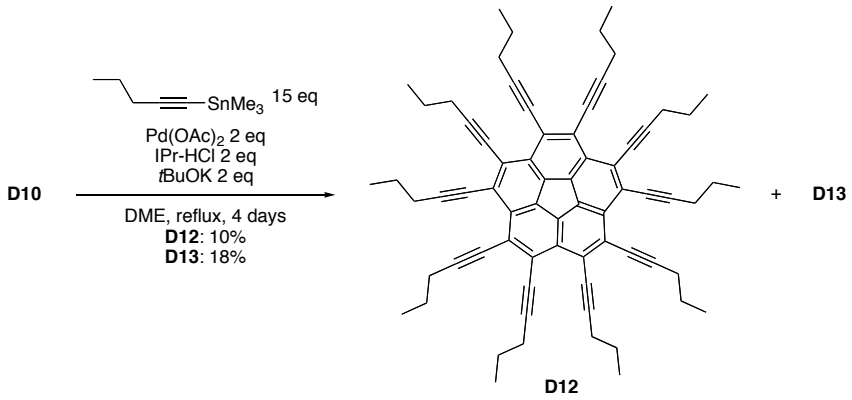

Scheme D3. Synthesis of decapentynylcorannulene (D12).

Slow evaporation of dichloromethane/*n*-propanol solution of **D12** produced crystals suitable for X-ray diffraction analysis (Figure D6). Key features of the structure are the distribution of bond lengths and the bowl depth (Table D1). The structure of **D12** is flatter than **D1** and has a longer rim bond, but is otherwise similar. The core crystallographic structure of **D12** agrees with that calculated for **D9** (B3LYP/cc-pVDZ) within 1 pm for bond lengths and ca. 1° for bond angles.[14] The geometrical patterns and trends are the same. Similar computations on **D2** (B3LYP/cc-pVDZ) show that the bowl depth and [5]radialene character are monotonic and increasing for the series, **D9** (**D12**), **D1**, **D2**. The bowl depth and radialene character of the closed fullerenes, C_{60} and C_{70}, are less than for **D2**. MP2/cc-pVDZ//B3LYP/cc-pVDZ computational energy differences of **D2** and **D9** (388.3 (364.5 ZPE) kcal/mol) support the estimates made using simple bond energy arguments. Nonetheless, **D12** (decapropyl-**D9**) appears to be kinetically inert to the formation of **D14** (decapropyl-**D2**) up to 100 °C (Scheme D4).

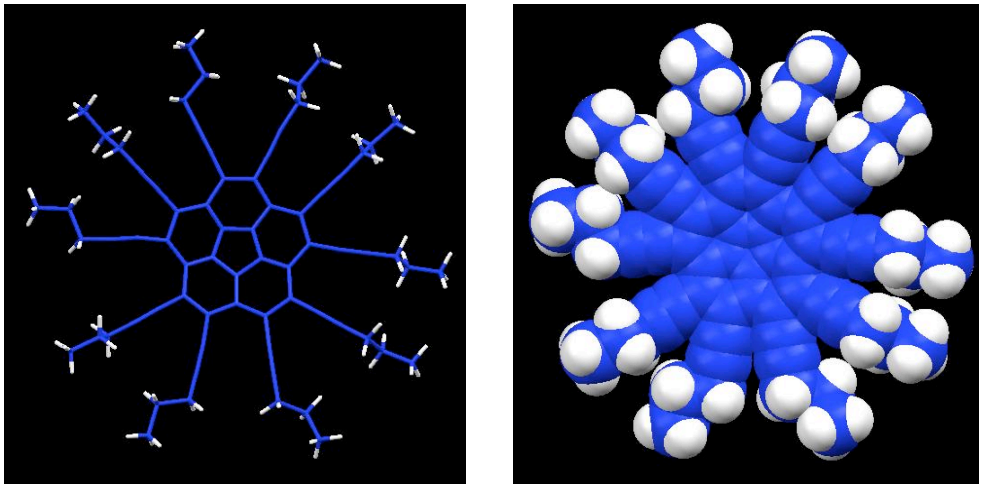

Figure D6. Skeleton and space filling models of D12.

Table D1. Geometry of D1, D2, D9, and D12.

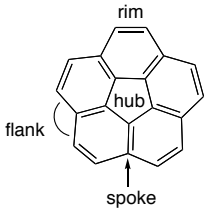

	D1[a]	**D1**[b]	**D2**[b]	**D9**[b]	**D12**[b]
hub (Å)	1.415(2)	1.420	1.453 (1.453)	1.412	1.403(6)
spoke (Å)	1.379(2)	1.388	1.392 (1.410)	1.378	1.376(6)
flank (Å)	1.446(2)	1.449	1.444 (1.445)	1.464	1.455(6)
rim (Å)	1.383(2)	1.392	1.402 (1.416)	1.436	1.430(6)
rim/flank (deg)	121.2(1)	122.0	119.5 (119.6)	121.7	121.5(3)
flank/flank (deg)	129.9(1)	130.1	106.8 (107.0)[d]	133.6	132.9(4)
rim-sp (Å)	—	—	—	1.426	1.430(7)
acetylenic (Å)	—	—	—	1.214	1.190(7)
$\delta_{hub\text{-}spoke}$ (Å)	0.036(3)	0.032	0.061 (0.044)	0.034	0.027(8)
$depth_{hub/rim}$ (Å)	0.87	0.87	1.53 (1.54)[d]	0.58[d]	0.60[d]

[a]ref15. [b]Calcd B3LYP/cc-pVDZ(MP2/cc-pVDZ). [c]Exptl avg from this work. [d]Mearured on the C_{20} core.

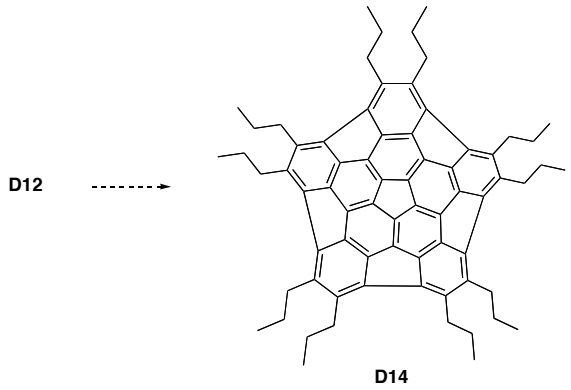

Scheme D4. Conversion into the nanotube derivative (D14).

4.2.2. Biscumulenyl[10]annulene (D13)

Careful chromatography allows the isolation of **D13** cleanly. Curiously, its mass spectrum is identical to that of **D12** indicating that **D13** is an isomer of **D12**. A first suspicion would be that **D14** formed under the reaction conditions, but the ^{1}H and ^{13}C NMR spectra of **D13** pointed to a compound of C*s* symmetry. Additional 2D NMR work gave confidence that **D13** is a pure compound and an isomer of **D12** with only C*s* symmetry.

Re-running the reaction several times consistantly reproduced the isomer mixture and provided enough material to afford large well-formed crystals of **D13** from dichloromethane/*n*-propanol mixture, which diffracted poorly on our in house instrument. As such, the crystals were taken to the Paul Scherrer Institute and measured using the synchrotron light source. Three molecular units are seen in the asymmetric unit. Stacking disorder is evident from the observed diffuse scattering. Difference *Fourier* maps revealed at least three orientations for two of the molecular units and two for the third; the non-polar disc form of **D13** allows it to pack in nearly random orientations. A model of these eight orientations was refined using bond length and angle similarity restraints (R = 0.12) (Figure D7). The structure of **D13** is planar, the first [10]annulene of its type,[16] comprising two cumulenyl groups (Figure D8).

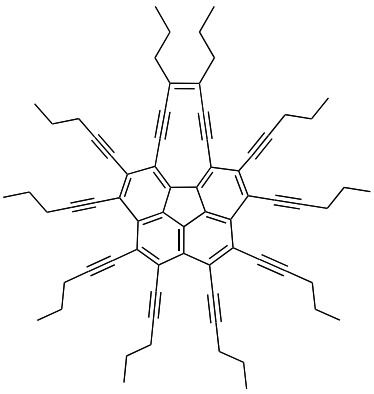

D13

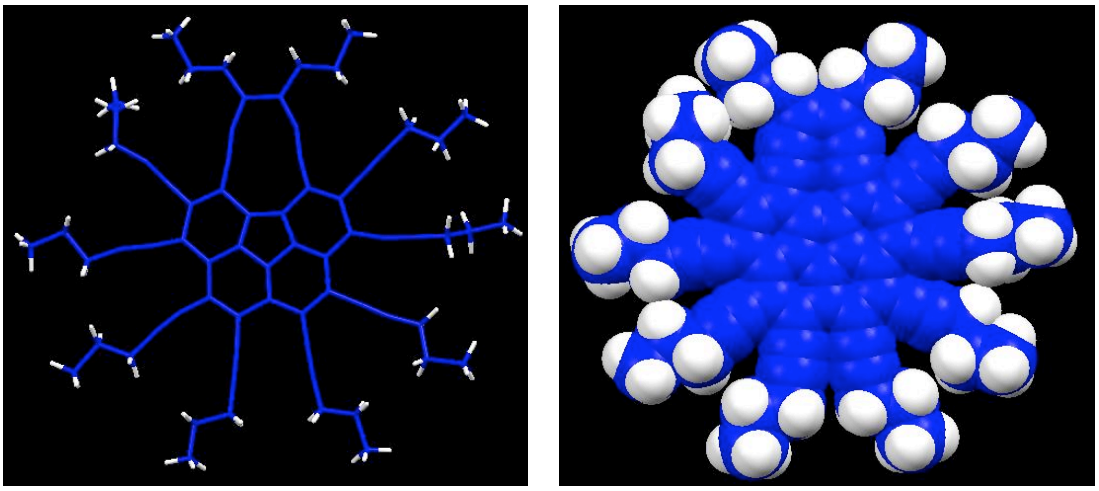

Figure D7. Skeleton and space filling models of D13.

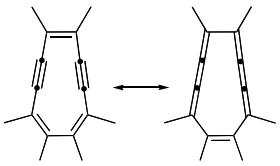

Figure D8. Two resonance forms of the [10]annulene fragment of D13.

Quantum mechanical and X-ray crystallographic geometries of **D13** suggest that the alkynyl resonance form dominates (Table D2). The alkynyl form would retain the [5]radialene core found generally for corannulene derivatives. The cumulene/alkynyl linkages kink in such a way as to betray a substantial transannular interaction, and give rise to a short "non-bonded" carbon-carbon contact "r" (ca. 3.1 Å). The question of alkynyl vs. cumulyl forms has been addressed in the context of cyclic polyynes.[17]

Table D2. Geometrical parameters of the [10]annulene fragment of D13.

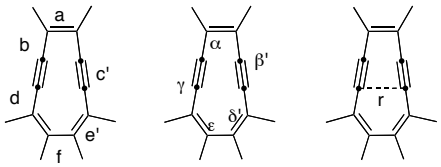

length (Å)	exptl avg[a]	calcd	angle (deg)	exptl avg	calcd[a]
a	1.387(9)	1.384 (1.401)	α/α'	116.4	118.5 (118.5)
b/b'	1.427(9)	1.398 (1.399)	β/β'	164.6	162.1 (160.7)
c/c'	1.203(9)	1.228 (1.257)	γ/γ'	176.5	177.9 (179.9)
d/d'	1.411(9)	1.404 (1.403)	δ/δ'	123.8	123.3 (122.7)
e/e'	1.401(9)	1.411 (1.423)	ε/ε'	137.5	138.2 (138.1)
f	1.475(9)	1.481 (1.469)			
r	3.113(9)	3.170 (3.139)			

[a]Calcd B3LYP/cc-pVDZ(MP2/cc-pVDZ).

The formation of **D13** can be deduced to have arisen from the very enediyne cyclization anticipated for the formation of **D2** from **D9**.[18] In this case, the diradical intermediate, instead of entering into a radical cyclization cascade or picking up two hydrogen atoms from the surroundings, homolytically opens the central bond of the *in situ* formed naphthyldiradical unit to yield **D13**. Despite the novel nature of the cumulyl functions, the [10]annulene is expected to benefit energetically from a reduction of overall ring strain and the stabilization associated with a 10-electron aromatic ring. Indeed, computations place **D16** ca. 21.5 (18.8 ZPE) kcal/mol lower in energy than **D9** (Scheme D5). This value is a tiny fraction of the nearly 400 kcal/mol thermodynamic potential which produces **D14**. Curiously, a comparison of computational energies for 1,2-diethynylbenzene ($C_{10}H_6$) and its dicumulenyl[10]annulene isomer ($C_{10}H_6$) suggests that the parent rearrangement would be ca. 17.8 (18.7 ZPE) kcal/mol endothermic. Thus, this fragment seems to be stabilized by its incorporation into the alkynylated PAH network.

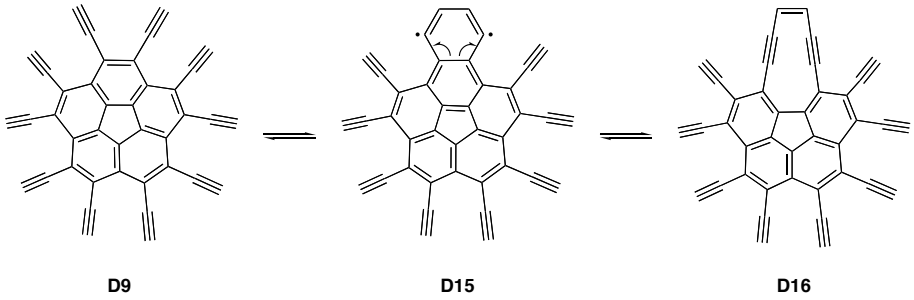

Scheme D5. Conceptual enediyne cyclization of D9 to [10]annulene (D16) via the diradical (D15).

Two compounds have already been reported as a similar [10]annulene derivatives; 5,6,9,10-tetradehydrobenzo[7,8]cyclodeca[1,2,3,4-*def*]biphenylene (**D17**)[19] and 3,4-benzocyclodeca-3,7,9-triene (**D18**) (Figure D9).[20,21] In **D17**, the rigid bridged biphenylene moiety prevents the Bergman cyclization and formation of the highly reactive diradical, and thus this compound is thermally stable even at room temperature. On the other hand, in the case of **D18**, prepared as a mixture in the gas-phase, Sander and coworkers suggested the rapid equilibrium at room temperature between **D18** and its diradical form, because of the low activation energy (Figure D10).[21a] This also explains the failure of the synthesis of **D18** attempted by Masamune in 1971.[22]

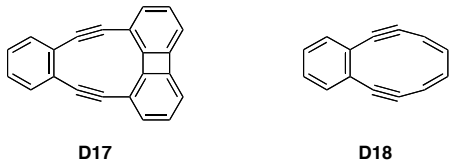

Figure D9. [10]annulene derivatives, D17 and D18.

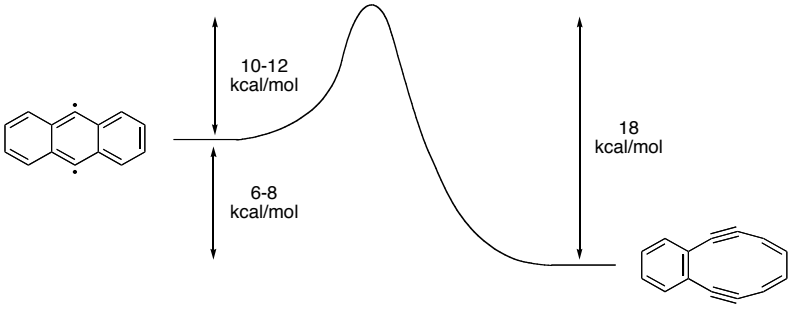

Figure D10. Relative energies of D18 and its diradical.

A possible explanation for the novel reactivity of diradical (**D19**) as an intermediate is that the flanking alkyne groups, which should engage in the cyclization cascade, are just outside the range for reaction under these conditions; however, they are close enough to block the proximity of the diradical from interactions with solvent or other hydrogen donor sources (Figure D11). Under such conditions, the ring-opening pathway becomes kinetically viable. Given that the energy for the two isomers **D9** and **D16** is computed to be close enough to be kinetically accessible, the challenge arises to find conditions where an equilibrium between **D12** and **D13** through the diradical intermediate **D19**, leads the reaction to its thermodynamic endpoint: **D14**.

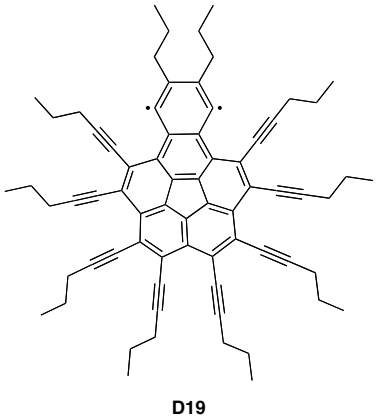

Figure D11. Diradical intermediate (D19).

Computed physical properties of derivatives of **D2** (e.g. near IR absorption at 550 and 894 nm, dipole moment of 5.6 D, and thermal stability) all speak for the possibilities for this structure to be of great use in materials chemistry. Indeed, **D2** and cognates can be viewed as the first members in the series of five-fold symmetric SWCNT, and potential seed compounds for the preparation of monodisperse higher order SWCNT. Given the efficient synthesis of **D1** and the relatively short path from **D1** via **D10** to **D12**, there would seem to be good reasons to be optimistic about finding efficient conditions for larger scale synthesis of SWCNT by solution phase methods.

4.2.3. Experimental Section

4.2.3.1. Materials and Methods

General: ^{1}H and ^{13}C NMR: Bruker AV-300 (75.5 MHz), AV2-400 (400 and 101 MHz), AV-700 (700 MHz). – IR: Perkin Elmer Spectrum One (FT-IR). – MALDI-MS: Bruker Autoflex I MALDI-TOF spectrometer. – X-ray structures were carried out by the X-ray analysis department of the Organic Chemistry Institute using a Nonius Kappa CCD diffractometer with MoKα radiation (λ = 0.71037 Å). – Chromatography: Merck silica gel 60 (230–400 mesh) or Fluka neutral alumina (Brockmann I, Activity II). – Melting points were measured to a maximum temperature of 350 °C. Ethylene glycol dimethylether (DME) and ether were distilled from sodium/benzophenone. Solvents for chromatography were technical grade and freshly distilled before use. **D10**[13] and *N*,*N*'-bis(2,6-diisopropylphenyl)imidazol-2-ylidene hydrogen chroride (IPr-HCl)[23] were prepared according to the literature procedures. Other compounds, which are not mentioned, are commercially available.

4.2.3.2. Synthetic Procedures

Trimethylstannylpentyne (D11)

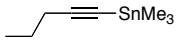

$C_8H_{16}Sn$
Mol. Wt.: 230.9226

To a solution of 1-pentyne (1.41 g, 20.7 mmol) in ether (20 mL), methyllithium (1.5M in ether, 12.4 mL, 18.6 mmol) was added dropwise at –20 °C. The mixture was stirred at –20 °C for 1 h. After warming to 0 °C, trimethyltin chloride (3.51 g, 17.6 mol) in ether (20 mL) was added slowly and warmed to room temperature for 8 h. After the filtration of white solid, ether was evaporated. The product was purified by bulb-to-bulb distillation to yield **D11** as colorless oil (3.41 g, 84%). The spectroscopic data were identical with those reported.[24] ^{1}H-NMR (300 MHz, $CDCl_3$): δ ppm = 0.26 (s, 9H), 0.98 (t, ^{3}J = 7.2 Hz, 3H), 1.54 (sext, ^{3}J = 7.2 Hz, 2H), 2.22 (t, ^{3}J = 6.9 Hz, 2H).

Decapentynylcorannulene (left, D12) and biscumulenyl[10]annulene (right, D13)

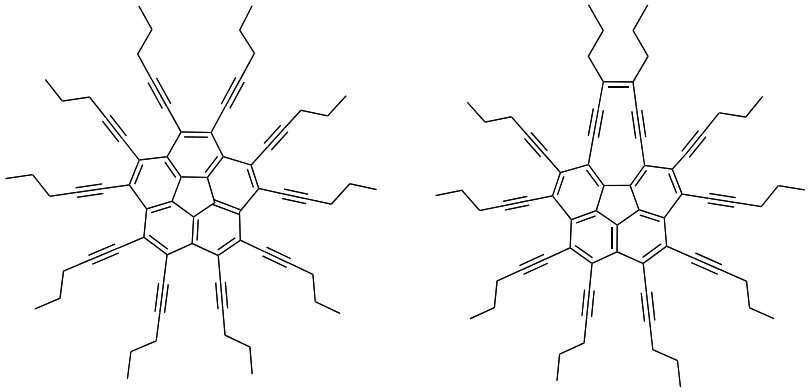

$C_{70}H_{70}$
Mol. Wt.: 911.3048

$C_{70}H_{70}$
Mol. Wt.: 911.3048

The mixture of decachlorocorannulene (**D10**) (50 mg, 0.0848 mg), palladium (II) acetate (37 mg, 0.170 mmol), IPr-HCl (70 mg, 0.170 mmol), and potassium *tert*-butoxide (19 mg, 0.170 mmol) in DME (11 mL) was stirred at 50 °C in an oil bath for 30 min. Trimethylstannylpentyne (**D11**) (294 mg, 1.27 mmol) in DME (4 mL) was added to the solution and the mixture was refluxed for 4 d. After cooling to room temperature, the solvent was evaporated. The product was purified by column chromatography on aluminum oxide (5% deactivated with water) eluted with hexane, hexane/dichloromethane = 3/1, 2/1, and 1/1. The solvent was evaporated to yield **D12** as a black solid (8 mg, 10%) [R_f = 0.52 (Al_2O_3, hexane/dichloromethane = 1:1)] and **D13** as a dark orange solid (14 mg, 18%) [R_f = 0.43 (Al_2O_3, hexane/dichloromethane = 1:1)].

D12

Mp 79-81 °C. ^{1}H-NMR (400 MHz, $CDCl_3$): δ ppm = 1.14 (t, ^3J = 8.0 Hz, 30H), 1.78 (sextet, ^3J = 8.0 Hz, 20H), 2.63 (t, ^3J = 8.0 Hz, 20H). ^{13}C-NMR (75.5 MHz, $CDCl_3$): δ ppm = 14.0-14.3 (br, CH_3), 22.8 (CH_2), 23.1 (CH_2), 80.3 (C), 103.2 (C), 127.1 (C), 128.3 (C), 130.6 (C). IR (KBr): ν cm^{-1} = 3417, 2960, 2214, 1720, 1461, 1386, 750. MS (MALDI): *m*/*z* (%): 910.5 (M^+).

D13

Mp 221-223 °C. ^{1}H-NMR (700 MHz, $CDCl_3$): δ ppm = 1.13 (t, ^3J = 7.0 Hz, 6H), 1.18 (t, ^3J = 7.0 Hz, 12H), 1.21 (t, ^3J = 7.0 Hz, 6H), 1.22 (t, ^3J = 7.0 Hz, 6H), 2.03 (sextet, ^3J = 7.0 Hz, 4H), 1.79-1.88 (m, 16H), 2.69 (t, ^3J = 7.0 Hz, 8H), 2.71 (t, ^3J = 7.0 Hz, 4H), 2.72 (t, ^3J = 7.0 Hz, 4H), 2.88 (t, ^3J = 7.0 Hz, 4H). ^{13}C-NMR (101 MHz, $CDCl_3$): δ ppm = 14.16 (CH_3), 14.23 (CH_3), 14.25 × 2 (CH_3), 14.43 (CH_3), 22.75 × 3 (CH_2), 22.79 (CH_2), 22.85 (CH_2), 23.23 (CH_2), 23.26 (CH_2), 23.31 (CH_2), 23.63 (CH_2), 33.12 (CH_2), 80.17 (C), 80.30 (C), 80.57 (C), 81.65 (C), 100.48 (C), 103.74 (C), 103.78 (C), 104.11 (C), 104.25 (C), 107.49 (C), 120.25 (C), 123.92 (C), 125.80

(C), 126.03 (C), 126.32 (C), 126.97 (C), 127.09 (C), 131.07 (C), 132.16 (C), 133.29 (C), 135.96 (C). IR (KBr): ν cm^{-1} = 3433, 3085, 2959, 1679, 1471, 1131, 922. MS (MALDI): *m*/*z* (%): 910.5 (M^+).

4.2.3.3. UV and Fluorescent spectra

All spectra were recorded in spectroscopic grade solvents and are uncorrected. Absorption spectra were recorded on a Perkin Elmer Lamda 19 UV/Vis/NIR Spectrometer and emission spectra were recorded on an Edinburgh Instruments FLS920 Combined Steady State and Lifetime Spectrometer.

Decapentynylcorannulene (D12)

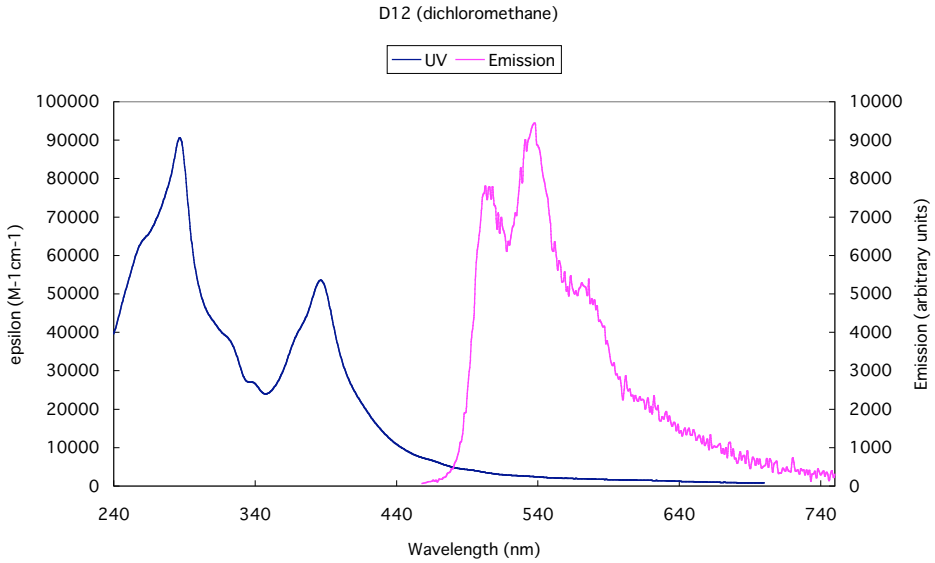

Biscumulenyl[10]annulene (D13)

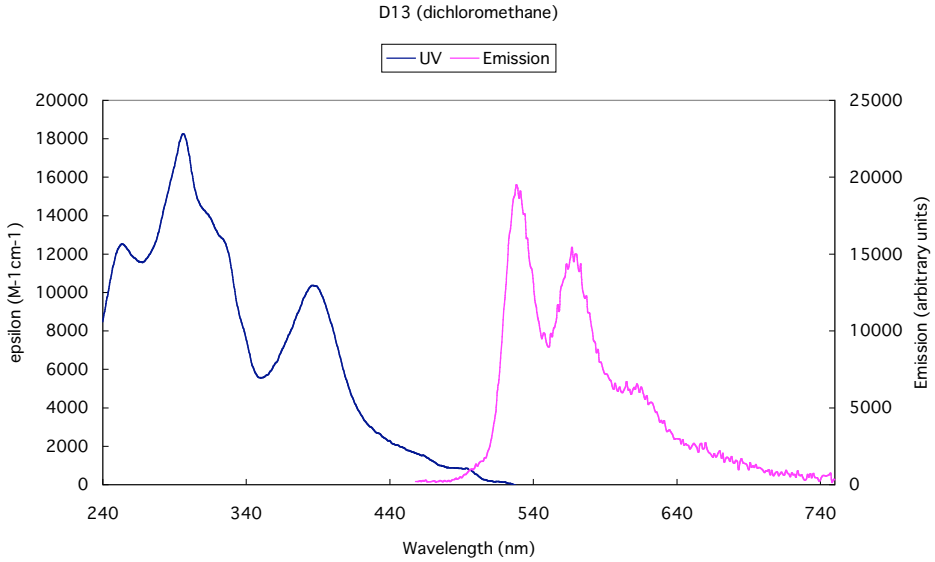

4.3. Appendix

4.3.1. Crystallographic Data of D12

Crystallised from		*n*-PrOH / CH_2Cl_2
Empirical formula		$C_{70}H_{70}$
Formula weight [g mol^{-1}]		911.32
Crystal colour, habit		brown, tablet
Crystal dimensions [mm]		0.10 × 0.30 × 0.30
Temperature [K]		160(1)
Crystal system		monoclinic
Space group		*Pn* (#7)
Z		2
Reflections for cell determination		4885
2θ range for cell determination [°]		5 – 50
Unit cell parameters	*a* [Å]	11.8218(6)
	b [Å]	19.234(1)
	c [Å]	12.5458(8)
	α [°]	90
	β [°]	107.123(4)
	γ [°]	90
	V [Å^3]	2726.2(3)
F(000)		980
D_x [g cm^{-3}]		1.110
μ(Mo *K*α) [mm^{-1}]		0.0622
Scan type		ω
$2\theta_{(max)}$ [°]		50
Total reflections measured		31018
Symmetry independent reflections		4804
R_{int}		0.085
Reflections with $I > 2\sigma(I)$		3775
Reflections used in refinement		4804
Parameters refined; restraints		813; 264
Final	$R(F)$ [$I > 2\sigma(I)$ reflections]	0.0592
	$wR(F^2)$ (all data)	0.1569
Weights:	$w = [\sigma^2(F_o^2) + (0.1021P)^2 + 0.1764P]^{-1}$ where $P = (F_o^2 + 2F_c^2)/3$	

Goodness of fit	1.044
Secondary extinction coefficient	0.031(5)
Final Δ_{max}/σ	0.002
$\Delta\rho$ (max; min) [e Å^{-3}]	0.31; -0.17
$\sigma(d_{(C-C)})$ [Å]	0.005 – 0.01

4.3.2. Crystallographic Data of D13

Crystallised from		CH_2Cl_2 / n-PrOH
Empirical formula		$C_{70}H_{70}$
Formula weight [g mol^{-1}]		911.32
Crystal colour, habit		red, block
Crystal dimensions [mm]		0.25 × 0.25 × 0.25
Temperature [K]		100(1)
Crystal system		monoclinic
Space group		$P2_1/c$ (#14)
Z		12
Reflections for cell determination		177867
2θ range for cell determination [°]		2.5–55
Unit cell parameters	a [Å]	35.385(1)
	b [Å]	19.860(1)
	c [Å]	22.686(1)
	α [°]	90
	β [°]	96.436(1)
	γ [°]	90
	V [Å^3]	15842(1)
$F(000)$		5880
D_x [g cm^{-3}]		1.146
μ(Mo $K\alpha$) [mm^{-1}]		0.0642
Scan type		ϕ
$2\theta_{(max)}$ [°]		55
Total reflections measured		177867
Symmetry independent reflections		26090
R_{int}		0.067
Reflections with $I > 2\sigma(I)$		18177
Reflections used in refinement		26090

Parameters refined; restraints	5049; 28418
Final $R(F)$ [$I > 2\sigma(I)$ re107lections]	0.1242
$wR(F^2)$ (all data)	0.3785
Weights:	$w = [\sigma^2(F_o^2) + (0.16P)^2]^{-1}$ where $P = (F_o^2 + 2F_c^2)/3$
Goodness of fit	2.031
Secondary extinction coefficient	0.011(1)
Final Δ_{max}/σ	0.51
$\Delta\rho$ (max; min) [e Å^{-3}]	0.63; -0.51

4.4. References

[1] Iijima, S. *Nature* **1991**, *354*, 56.

[2] Reich, S.; Thomsen, C.; Maultzsch, J. *Carbon Nanotubes: Basic Concepts and Physical Properties*, Wiley-VCH, Weinheim, 2004.

[3] (a) Journet, C.; Bernier, P. *Appl. Phys. A: Mater. Sci. Process.* **1998**, *67*, 1. (b) Bronikowski, M. J.; Willis, P. A.; Colbert, D. T.; Smith, K. A.; Smalley, R. E. *J. Vac. Sci. Technol. A* **2001**, *19*, 1800. (c) Dai, H. *Topics in Applied Physics, Vol. 80, Carbon Nanotubes*; Dresselhaus, M. S.; Dresselhaus, G.; Avouris, P. (eds), Springer, Berlin, 2001, 29. (d) Charlier, J.-C.; Iijima, S. *Topics in Applied Physics, Vol. 80, Carbon Nanotubes*; Dresselhaus, M. S.; Dresselhaus, G.; Avouris, P. (eds), Springer, Berlin, 2001, 55.

[4] (a) Varadan, V. K.; Xie, J. *Smart Mater. Struct.* **2002**, *11*, 728. (b) Lee, C. J.; Lyu, S. C.; Kim, H.-W.; Park, C.-Y.; Yang, C.-W. *Chem. Phys. Lett.* **2002**, *359*, 109. (c) Seo, J. W.; Couteau, E.; Umek, P.; Hernadi, K.; Marcoux, P.; Lukic, B.; Mikó, Cs.; Milas, M.; Gaál, R.; Forró, L. *New J. Phys.* **2003**, *5*, 120.1.

[5] Banerjee, S.; Hemraj-Benny, T.; Wong, S. S. *Adv. Mater.* **2005**, *1*, 17.

[6] Baldridge, K. K.; Siegel, J. S. *Theoret. Chem. Acc.* **1997**, *97*, 67.

[7] Dale, J. *Chemistry of Acetylenes*; Viehe, H. G. (ed), Marcel Dekker, Inc, New York, 1969, Chapter 1.

[8] (a) Diederich, F. *Nature* **1994**, *369*, 199. (b) Diederich, F. *Chem. Comm.* **2001**, 219.

[9] Rubin, Y.; Knobler, C. B.; Diederich, F. *Angew. Chem. Int. Ed. Engl.* **1991**, *30*, 698.

[10] Diercks, R.; Armstrong, J. C.; Boese, R.; Vollhardt, K. P. C. *Angew. Chem. Int. Ed. Engl.* **1986**, *25*, 268.

[11] (a) Hopf, H. *Classics in Hydrocarbon Chemistry: Syntheses, Concepts, Perspectives*. Wiley-VCH, Weinheim, c. 2000, 558. (b) *Acetylene Chemistry: Chemistry, Biology and Material Science*. Diederich, F.; Stang, P. J.; Tykwinski, R. R.; Eds, Wiley-VCH, Weinheim, c. 2005, 508.

[12] Benson, Sidney W., *Thermochemical Kinetics: Methods for the Estimation of Thermochemical Data and Rate Parameters*, 2nd Ed. Wiley, New York, NY, c. 1976, 336.

[13] Samdal, S.; Hedberg, L.; Hedberg, K.; Richardson, A. D.; Bancu, M.; Scott, L. T. *J. Phys. Chem.* **2003**, *107*, 411.

[14] Computational Methods: Structure and properties of molecules described in this study, were carried out using GAMESS[a] software. Structures were obtained using both MP2[b] and

HDFT (Becke's 3 parameter functional[c] with nonlocal correlation provided by Lee-Yang-Parr [d,e] with both local and nonlocal terms, B3LYP). The cc-pVDZ,[f], DZ(2d,p) and DZ+(2d,p),[g] basis sets were employed. Full geometry optimizations were performed and characterized via Hessian analysis, and ZPE corrections extracted for energetic predictions. From the fully optimized structures, single point MP2 energies enable accurate energy barriers, and single point time-dependent absorption computations[g] for evaluation of spectral properties, using the DZ+(2d,p) basis set. These levels of theory have been previously shown to be reliable for predicted structure and properties.[h] Molecular orbital contour plots, were generated and depicted using QMView.[i] (a) Schmidt, M. W.; Baldridge, K. K.; Boatz, J. A.; Elbert, S. T.; Gordon, M. S.; Jensen, J. H.; Koseki, S.; Matsunaga, N.; Nguyen, K. A.; Su, S.; Windus, T. L.; Elbert, S. T. *J. Comp. Chem.* **1993**, *14*, 1347. (b) Moller, C.; Plesset, M. S. Phys. Rev. **1934**, 46, 618-622. (c) Becke, A. D. *J. Chem. Phys.* **1993**, *98*, 5648-5652. (d) Lee, C.; Yang, W.; Parr, R. G. *Phys. Rev. B* **1988**, *37*, 785. (e) Miehlich, B.; Savin, A.; Stoll, H.; Preuss, H. *Chem. Phys. Lett* **1989**, *157*, 200. (f) Dunning, T. H. *J. Chem. Phys.* **1989**, *90*, 1007. (g) Dunning, T.H.; Hay, P.J. In *Modern theoretical Chemistry*, Ed., H.f. Schaefer, III, Plenum, New York, **1976**, *3*, 1. (g) Casida, M.E.; Jamorski, C.; Casida, K.C.; Salahub, D.R. *J. Chem. Phys.,* **1998***, 108*, 4439. (h) Seiders, T.J.; Baldridge, K.K.; Grube, G.H.; Siegel, J.S. *J. Am. Chem. Soc.,* **2001***, 123,* 517-525. (i) Baldridge, K. K.; Greenberg, J. P. *J. Mol. Graphics* **1995**, *13*, 63.

[15] Petrukhina, M. A.; Andreini, K. W.; Mack, J.; Scott, L. T.; *J. Org. Chem.* **2005**, *70*, 5713.

[16] Jones, G. B.; Warner, P. M. *J. Am. Chem. Soc.* **2001**, *123*, 2134.

[17] Diederich, F. N. et al. *Science* **1989**, *245*, 1088; b) Hutter, J.; Lüthi, H.-P.; Diederich, F. N. *J. Am. Chem. Soc.* **1994**, *116*, 750. c) Martin, J.; Taylor, P. *J. Phys. Chem.* **1996**, *100*, 6047.

[18] (a) Bergman, R. G. *Acc. Chem. Res.* **1973**, *6*, 25. (b) Klein, M.; Walenzyk, T.; König, B. *Collect. Czech. Chem. Commun.* **2004**, *69*, 945.

[19] Wilcox, C. F. J; Weber, K. A. *J. Org. Chem.* **1986**, *51*, 1088.

[20] Schottelius, M. J.; Chen, P. *J. Am. Chem. Soc.* **1996**, *118*, 4896.

[21] (a) Kötting, C.; Sander, W.; Kammermeier, S.; Herges, R. *Eur. J. Org. Chem.* **1998**, 799. (b) Marquardt, R.; Balster, A.; Sander, W.; Kraka, E.; Cremer, D.; Radziszewski, J. G. *Angew. Chem. Int. Ed. Engl.* **1998**, *37*, 955. (c) Wenk, H. H.; W. Sander *Eur. J. Org. Chem.* **1999**, 57.

[22] Darby, N; Kim, C. U.; Salaun, J. A.; Shelton, K. W.; Takada, S.; Masamune, S. *J. Chem. Soc. (D)* **1971**, 1516.

[23] The synthesis of IPr-HCl: (a) Arduengo, A. J. III; Krafczyk, R.; Schmutzler, R. *Tetrahedron* **1999**, *55*, 14523. (b) Jafarpour, L.; Stevens, E. D.; Nolan, S. P. *J. Organomet. Chem.* **2000**, *606*, 49.

[24] Stille, J. K.; Simpson, J. H. *J. Am. Chem. Soc.* **1987**, *109*, 2138.

Chapter 5. Synthetic Receptor

5.1. Introduction

Today, the accumulation of structural data for various toxins allows for a structure-based approach to drug design. The structures and functions of cholera or heat-labile enterotoxin have already been investigated in detail and thus, much information is available.[1] In this chapter, the synthesis of a corannulene-based synthetic receptor for cholera toxin will be discussed.

5.1.1. Cholera Toxin and Heat-Labile Enterotoxin

Cholera toxin (CT) from *Vibrio cholerae* and heat-labile enterotoxin (LT) from enterotoxigenic *Escherichia coli* (ETEC) have a similar structure and belong to the AB_5 bacterial toxins.[2] CT causes a fatal disease known as cholera, while LT causes serious diarrhea. Although they are extremely notorious diseases, no effective drug exists and allopathy is general, for example oral rehydration. Therefore, the development of useful therapeutics for CT or LT poisonings is desired all over the world.

Generally, AB_5 bacterial toxins are represented as the combination of a single catalytically active component A and the nontoxic receptor-binding component B pentamer. Thus, the pentamer B plays a crucial role in molecular recognition. CT and LT share 80% homology in both the A and B subunits.

The crystal structure of LT was first reported in 1991.[3] The toxin has a symmetrical pentamer of B subunits surrounding a central pore and each of them opens the receptor-binding site (Figure E1). The subunit A consists of two functional domains: wedge-shaped A1 moiety and elongated A2 moiety. The former has the enzyme active site and the latter connects to the B pentamer. Since this initial structure has no agonist in the receptor binding sites, it is inactive. When the receptor-binding happens, cleavage of the peptide chain and reduction of a disulfide bond between A1 and A2 break their connection, followed by the appearance of an enzymatic effect.[4] The study of LT-lactose complex shows that the receptor-binding sites of the toxin are located at the bottom of the B pentamer.[5] From the structural point of view, there are three potential target areas for drug design: blocking the enzyme-active site on A1, the interruption of A2-B pentamer interactions, and preventing receptor binding on the B pentamer.

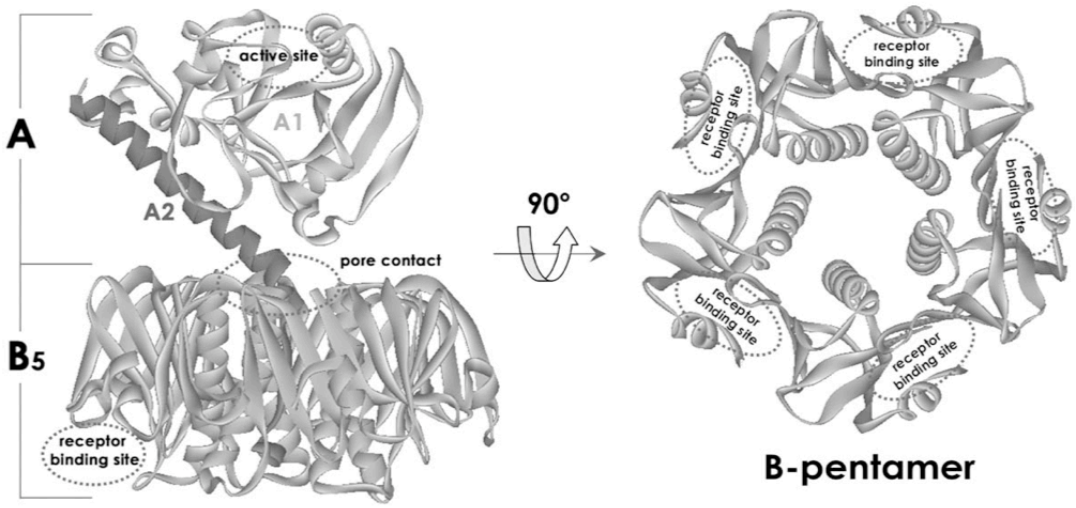

Figure E1. Crystal structure of LT with the sites for molecular recognition.

The mechanism of the toxin reaction cascade has already been elucidated at the molecular level. First of all, B subunits bind to ganglioside GM1 on intestinal epithelial cell membranes, followed by cleavage of the A chain and disulfide bond reduction to yield two fragments A1 and A2. Then after A1 is translocated across the cell membrane, it modifies the alpha subunit of the stimulatory G protein through an NAD-dependent ADP-ribosylation reaction. It locks the G protein in its GTP-bound form, which continually stimulates adenylate cyclase to produce the second messenger cAMP. The increased cAMP level causes dramatic leaking of ions and water from the host to result in severe diarrhea.[6]

The inhibition of receptor binding has received the most attention because of the relative ease of making antagonists that led to the structural studies of the receptor-binding sites on the B pentamer. After the structural elucidation of LT and the LT-lactose complex, the very high resolution structure of CT B pentamer-oligosaccharide head group of its native receptor GM1 complex (GM1-OS) was reported in 1994.[7] This structure revealed that galactose, which is the terminal sugar of GM1-OS, binds specifically at the buried pocket of the receptor-binding site.

To improve the affinity for the toxin pentamer, other modified galactose derivatives were explored. This led to the discovery of *m*-nitrophenyl-α-D-galactopyranoside (MNPG), which has a 100-fold increase in affinity relative to D-galactose (Figure E2).[8] Based on this result, the inhibitor design using MNPG was reported.[9] So far, many different kinds of galactose or MNPG derivatives have been investigated and utilized as a monovalent inhibitor for CT or LT with the analysis of their crystal structures. One of the important points for the modification is the improvement of aqueous solubility. The morpholine ring-containing compound (3-nitro-5-(3-morpholin-4-yl-propylaminocarbonyl)phenyl)-α-D-galactopyranoside (MP-MNPG) has 14-fold affinity gain over MNPG, and its derivative N-[3-[4-(3-aminopropyl)-piperazin-1-yl]propyl]-3-nitro-5-(3,4,5-trihydroxy-6-hydroxymethyltetrahydro-pyran-2-yloxy)-benzamide (APP-MNPG) is still a better monovalent inhibitor.[10] The IC_{50} of APP-MNPG is around 350 μM making it one of the most potent monovalent compounds with good aqueous solubility.

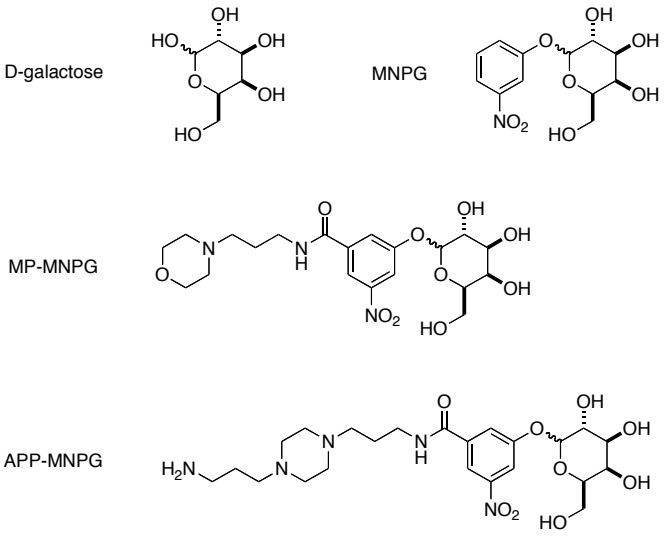

Figure E2. Monovalent ligands to CT and LT.

5.1.2. Symmetrical Pentavalent Recognition

The symmetrical character of the B pentamer enables multivalent recognition. Various kinds of multivalent CT or LT binders were developed starting from weak ligands, such as lactose or galactose.[11,12] Generally, multivalent binders showed better efficiency than monovalent binders. Such a multivalent recognition could bring their affinity closer to that required for practical application against CT or LT toxins.

The most dramatic improvement in receptor-binding antagonist design was achieved with a symmetrical pentavalent molecule by Fan and co-workers.[12] Their basic concept to improve the affinity was a modular approach of "Finger-Linker-Core" (Figure E3). The pentavalent "Core" is extended by five long flexible "Linkers" with each "Linker" ending in a "Finger" which includes the receptor-binding sugar.

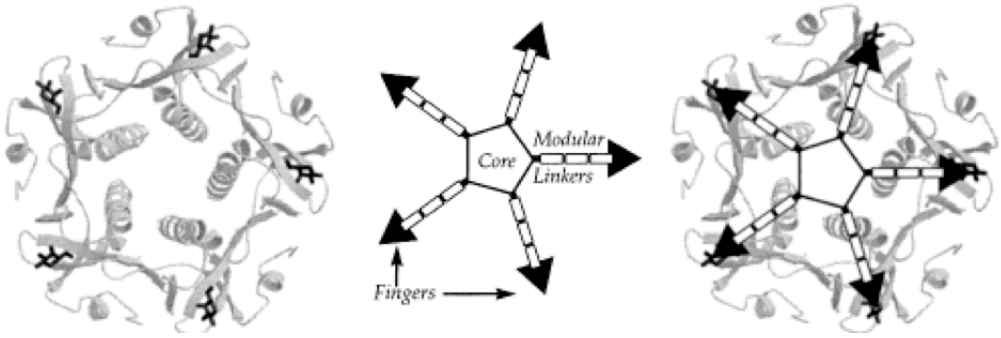

Figure E3. B-pentamer (left), pentavalent inhibitor (middle), and their complex (right).

Based on this strategy, the IC_{50} of pentavalent inhibitors against the CT or LT B pentamer was studied. Acylated pentacyclen (**E1**) was used as a core with flexible linkers synthesized from 4,7,10-trioxa-1,13-tridecanediamine (**E2**), and the binding ability against LT was investigated (Figure E4).[12a]

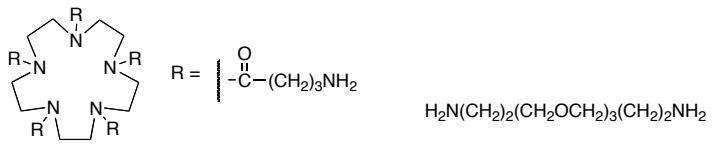

Figure E4. Acylated pentacyclen (finger) and 4,7,10-trioxa-1,13-tridecanediamine (linker).

The results clearly show that the structure-based design of pentavalent ligands leads to very significant affinity gains compared to the monovalent ligand (Table E1). The binding ability of the best pentavalent ligand (**E7**) is 10^5-fold better than that of galactose. In addition, the report demonstrated that the effective length of the "Linkers" is a critical factor in governing the affinity of multivalent ligands for the B pentamer. The modification of individual "Fingers" (from galactose to MNPG) also leads to the better affinity.[12b]

Table E1. The inhibition ability of pentavalent ligands against the LT B pentamer.

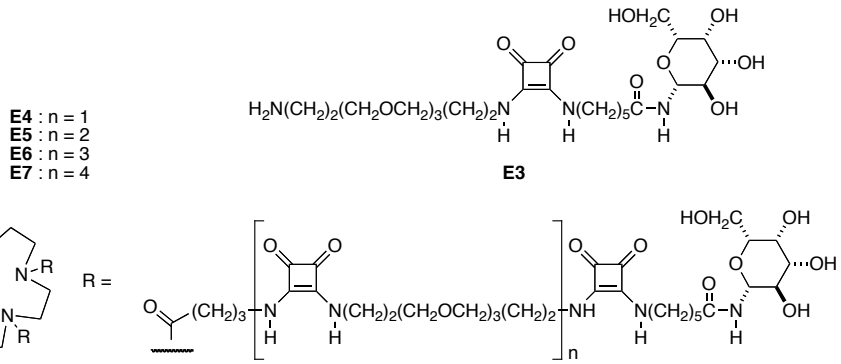

ligand	IC_{50}[a] (μM)	gain over galactose
galactose	58000 ± 8000	1
E3	5000 ± 200	11
E4	242 ± 91	240
E5	16 ± 8	3600
E6	6 ± 4	10000
E7	0.56 ± 0.06	104000
GM1-OS	0.01 ± 0.01	5800000

[a] IC_{50} was obtained from ELISA experiment.

Also reported were the "Core" units using different sizes of large cyclic peptides (Figure E5).[12e] In this report, the easy synthetic access to the peptide "Core," was demonstrated based on solid phase techniques and that a larger core unit with shorter linkers leads to effective inhibition.

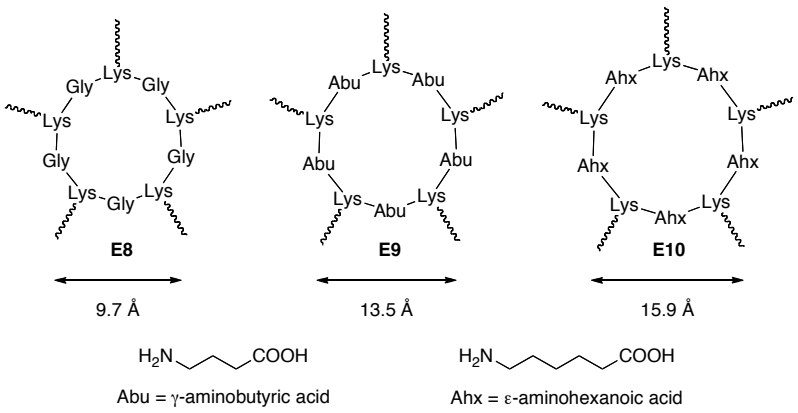

Figure E5. Core units using large cyclic peptides.

5.2. Present Work

5.2.1. Experimental Design

The five-fold symmetry of *sym*-pentachlorocorannulene (**E11**) can be utilized for the synthesis of corannulene-based AB_5 toxin antagonists using the "Finger-Linker-Core" approach (Scheme E1). One of the advantages of using a corannulene "Core" is the adjustable recognition circle (Figure E6). The bowl inversion of corannulene is very fast at room temperature and therefore, the receptor could bind to the toxin B pentamer by adjusting the bowl depth. When the "Linker" length is 30 Å, r_1 and r_2 are approximately 35 Å and 47 Å, respectively. On the other hand, the biggest disadvantage of the corannulene is its low solubility in water, which is desired in drug design.

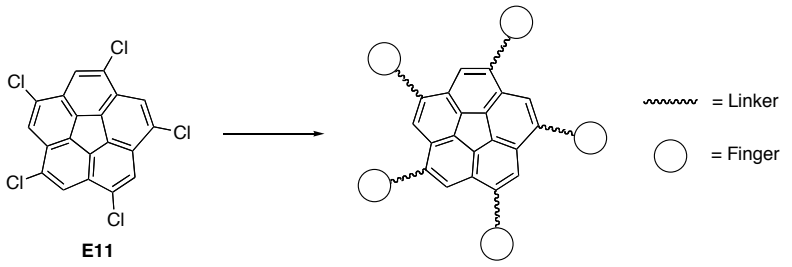

Scheme E1. Corannulene-based synthetic receptor from E11.

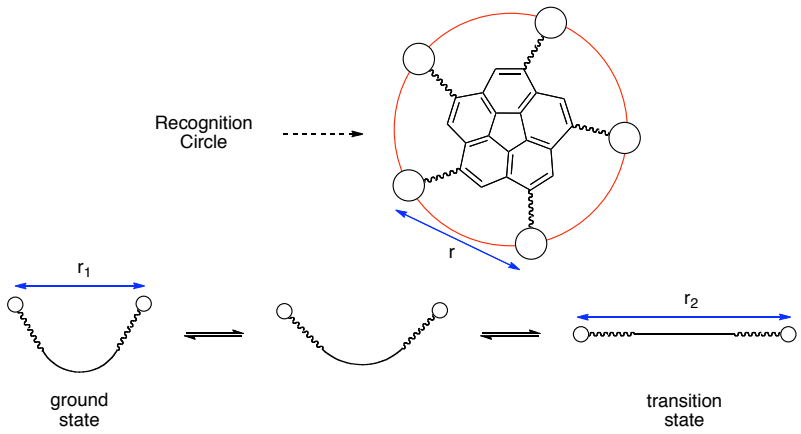

Figure E6. Adjustable recognition circle.

Of the three described units, the crucial point is the "Linker" structures. The distance between two consecutive binding sites is about 35 Å (Figure E7).[12d] Therefore, this number will give the appropriate criterion for the linker length, although the corannulene "Core" can adjust to some extent. In addition, the "Linkers" need to improve the water solubility, and moderate robustness is desired to avoid the tangle with other "Linkers." Synthetic ease is also important. For the "Finger" moiety the simplest sugar, galactose is enough to evaluate the efficiency of corannulene-based synthetic receptors.

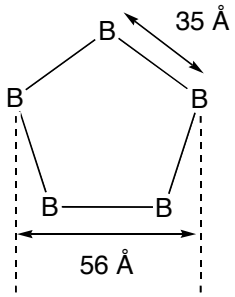

Figure E7. Distance between the binding sites of CT B pentamer.

The proposed structure is separated into smaller components (Figure E8). First, the component A is selected because of its robustness. It has almost no flexibility and thus would lead to the enlargement of the corannulene "Core" (Figure E9). Next, the shorter linker straightens the moving range. The extremely large moving range from the highly flexible "Linkers" could cause the decrease of affinity to the toxin B pentamer. From the synthetic point of view, the aryl-corannulene bond can be produced by a coupling reaction.

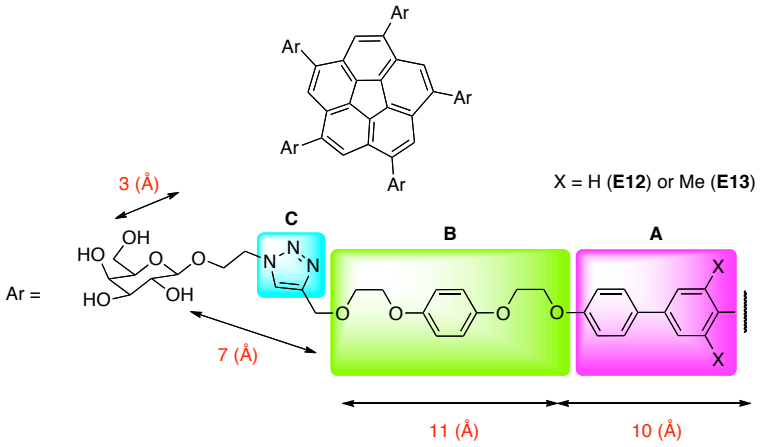

Figure E8. Proposed structure of the corannulene-based synthetic receptor.

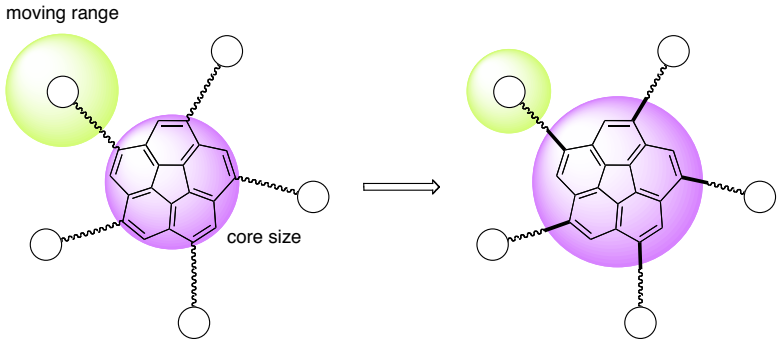

Figure E9. Larger "Core" with shorter "Linker" fixes the movement of the "Finger" parts.

Second, the component B was selected for its moderate robustness and the presence of four oxygens. The oxygens would increase the solubility in water and the structure would be more robust than a normal ethylene glycol because of the central phenyl ring. Another advantage is that the starting dialcohol is commercially available.

Thirdly, from the synthetic point of view, the most important part is the 1,2,3-triazol component C. This component can be synthesized in very high efficiency by the Cu-catalyzed azide-alkyne 1,3-dipolar cycloaddition (CuAAC).[13] Therefore, the introduction of the highly polar sugar moiety is possible at any point.

The total length of the "Linker" is approximately 30 Å and designed using the following considerations. The crystal structure of *sym*-pentamanisylcorannulene (**E14**) was already reported and the average distance between the neighboring manisyl oxygens is about 10 Å (Figure E10).[14] On the other hand, the distances from the center of the corannulene ring to the root of the "Linker" and from the root to the manisyl oxygen are 4 and 5.67 Å, respectively. Therefore, when 35 Å is desired for the distance between the neighboring sugars, the "Linker" length should be about 30 Å. Although this distance depends on the ground state structure and the "Linker" or "Core" are flexible, it will be a reasonable value for the design of the "Linkers" for **E13**. The compound **E12** has no dimethyl groups and must have a different bowl depth. However, 30 Å will still be a reasonable starting length of the "Linker," because there is currently no information available about this system to calculate more reliable values.

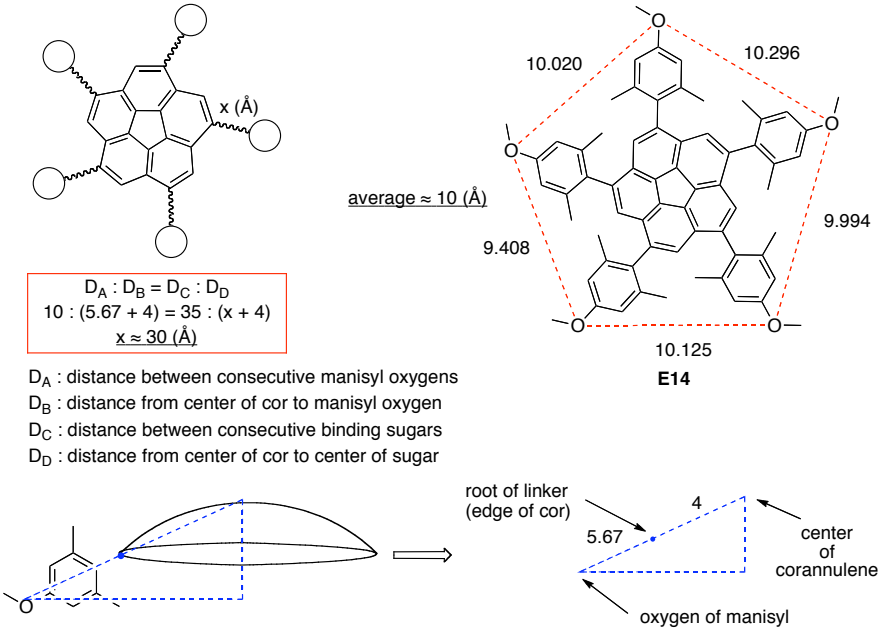

Figure E10. Calculation of "Linker" length.

A simple retrosynthetic analysis is presented in Scheme E2. The key point is the introduction of the sugar moieties. The high polarity of the sugar moieties may be problematic for the purification steps, and thus they will be introduced at the end of the synthesis.

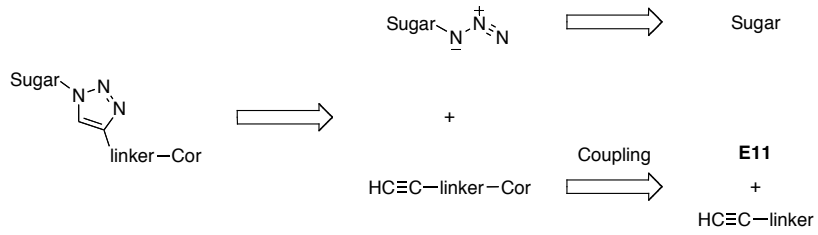

Scheme E2. Retrosynthetic analysis of the synthetic receptor.

5.2.2. Synthesis

The synthesis of sugar azide (**E20**) starts from the acetylation of the simplest sugar D-(+)-galactose (**E15**) (Scheme E3). After the bromination of **E16**, a Koenigs-Knorr displacement reaction with 2-bromoethanol produces **E18**. The azide (**E19**) can be prepared in excellent yield by treatment of **E18** with sodium azide in DMF, followed by the removal of the acetyl groups with sodium methoxide to afford the sugar azide (**E20**).

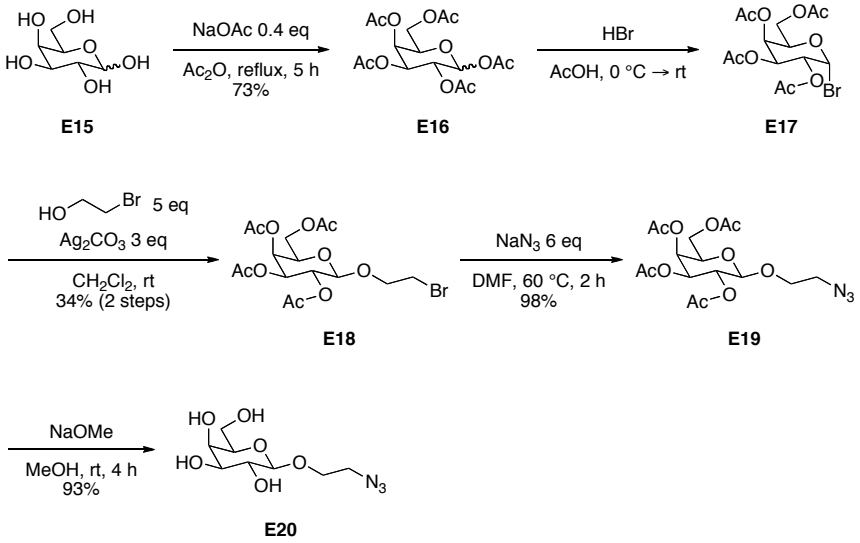

Scheme E3. Synthesis of sugar component.

The "Linker" component is prepared from two moieties. The synthesis of 4-bromo-4'-hydroxy-3,5-dimethylbiphenyl (**E26**) starts from the bromination of 3,5-dimethylanisole (**E21**) with *N*-bromosuccimide (NBS) (Scheme E4). Next, the methoxy group of the bromide (**E22**) is deprotected with boron tribromide followed by a triflation to yield **E24**. After the Negishi coupling of **E24** with 4-bromoanisole, the similar removal of the methoxy group gives **E26**.

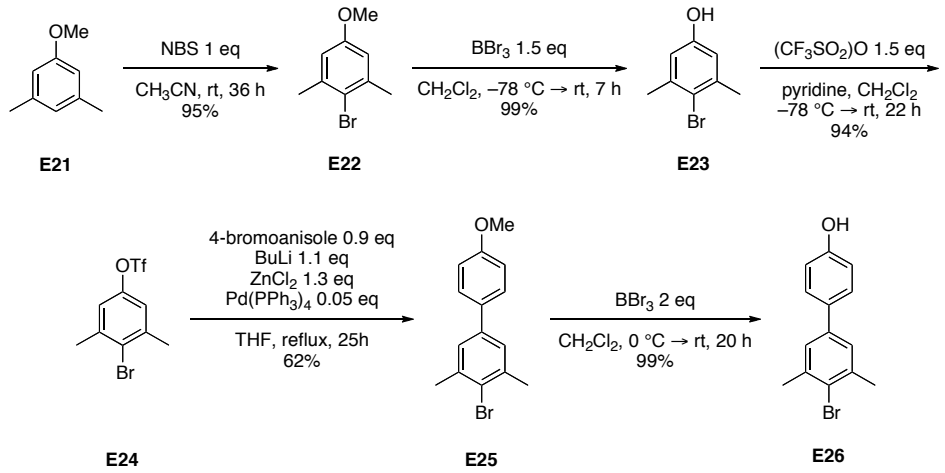

Scheme E4. Synthesis of bromophenol (E26).

Another moiety of the "Linker" component is the silyl-protected alkynyl chloride (**E30**) (Scheme E5). In this compound, the triisopropylsilyl (TIPS) group is introduced to suppress the reactivity of the alkynyl hydrogen during the coupling process with **E11** and to increase the solubility for the purification steps. The starting compound is commercially available hydroquinone bishydroxyethylether (**E27**) and is coupled with propargyl bromide under a basic conditions. The next step is the protection of the alkynyl group. In this step, two sequential reactions are used; double protection of alkyne and alcohol, and selective deprotection of silyl alcohol (Scheme E6). Usually, for the selective silyl protection of alkynyl alcohols, ethyl-magnesium halide is used. However, in the case of **E28**, this method did not work and only the starting material was recovered. The hydroxyl group of TIPS-protected alcohol **E29** was converted to the corresponding chloride (**E30**) with thionyl chloride and pyridine. Finally, the Williamson ether synthesis of **E30** and **E26** affords TIPS-protected alkynyl bromide **E31**.

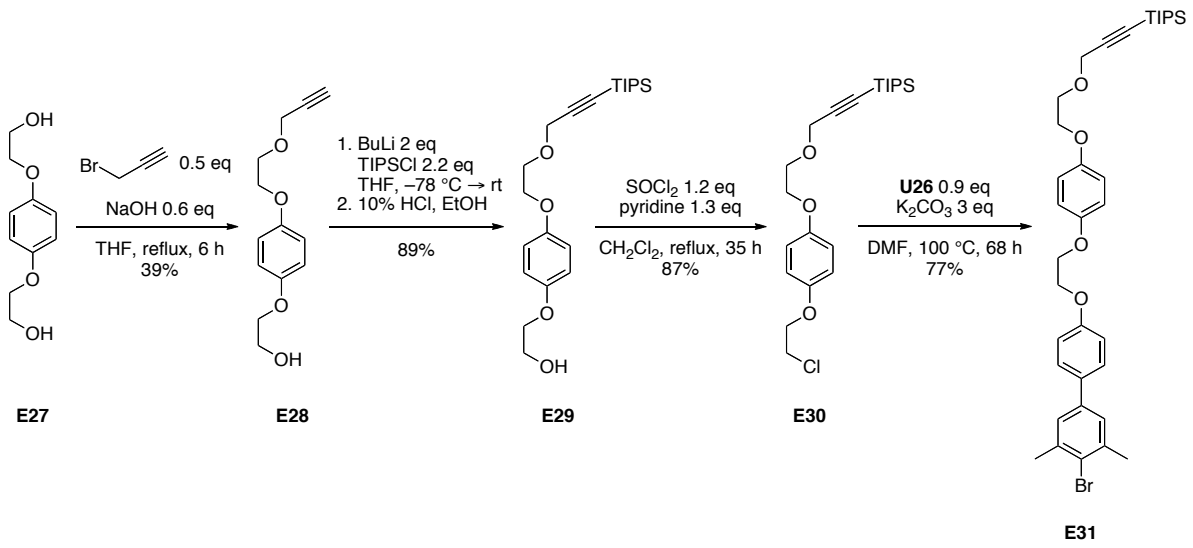

Scheme E5. Synthesis of arylbromide (E31).

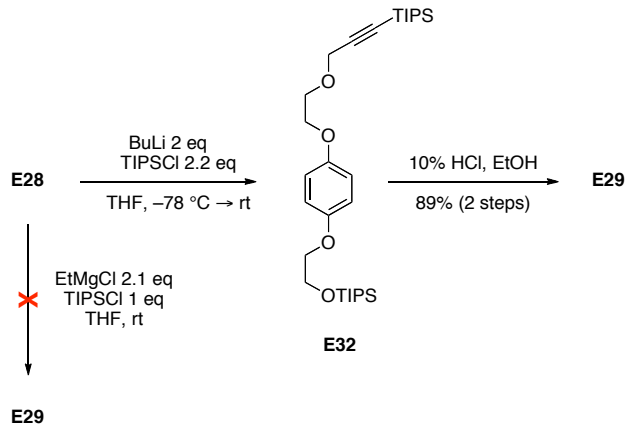

Scheme E6. Selective protection with TIPS group.

The next step is the key coupling reaction with **E11**. First, the Negishi coupling using the bromide (**E31**) was attempted (Scheme E7, entry 1 and 2). The combination of the carbene ligand (IPr-HCl)[15] and palladium (II) acetate, or the carbene complex of palladium ((IPr)Pd(allyl)Cl)[16] were used, because of the low reactivity of the chlorides. However, the MS (MALDI) did not show the peak of the target compound. When the reaction was quenched with water to check the lithiation step of the bromide (**E31**), the expected compound (**E33**) was not confirmed and thin layer chromatography (TLC) analysis showed many UV-absorbing spots (entry 3). Therefore, in the Negishi coupling, the lithiation step with butyl lithium (BuLi) did not appear to work. Meanwhile, the stannane preparation, without the lithiation reaction, was attempted using a palladium-catalyzed coupling reaction,[17] but this also did not give the target stannane (**E34**) (entry 4). Fortunately, the use of *tert*-BuLi and trimethyltin chloride yielded **E34**, although this product contained some impurities (entry 5). The Stille coupling of **E34** with the model compound, 1-chloronaphthalene (**E35**), was attempted, but the expected compound (**E36**) was not detected (entry 6 and 7). The Negishi coupling after the lithiation with *tert*-BuLi also did not work at all (entry 8).

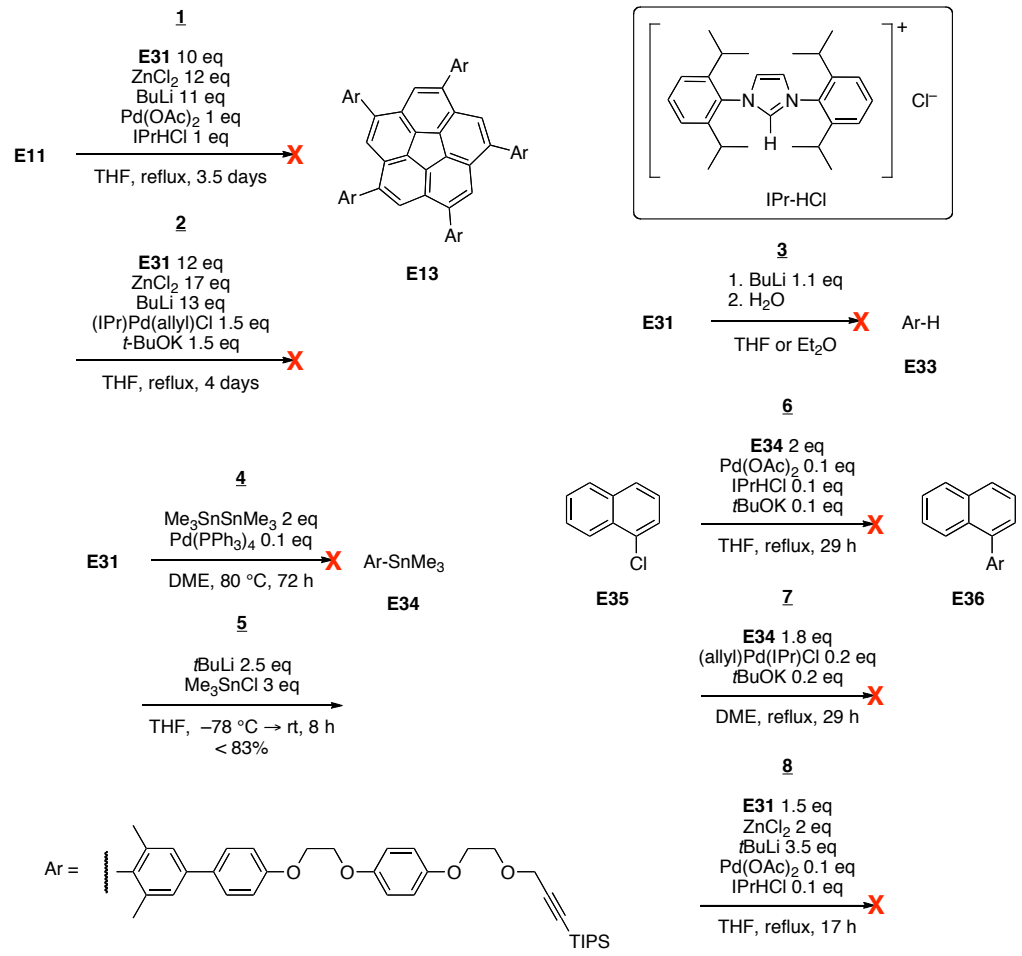

entry	result
1	no TM (MS(MALDI))
2	no TM (MS(MALDI))
3	many spots including SM (TLC, UV)
4	only the spot of SM (TLC, UV)
5	the peak of TM (MS(EI)), isolated as a mixture (^{1}HNMR)
6	no TM (MS(EI)), large amount of **E34** was recovered
7	no TM (MS(MALDI))
8	no TM (MS(EI)), small amount of SM remained (TLC)

Scheme E7. Negishi coupling with E11 (entry 1-2), lithiation with butyllithium (entry 3), stannane (E34) preparation (entry 4-5), and Negishi or Stille coupling with E35 (entry 6-8).

Based on these results, the bromide (**E40**) was prepared (Scheme E8). When compared with **E31** and **E40**, **E40** loses two potentially problematic methyl groups. This at least means that the coupling reaction with **E40** should be more efficient than with **E31**. **E40** was prepared from 1-bromo-4-dodobenzene (**E37**). After the first Negishi coupling, removal of the methoxy group followed by a similar ether synthesis, affords **E40**.

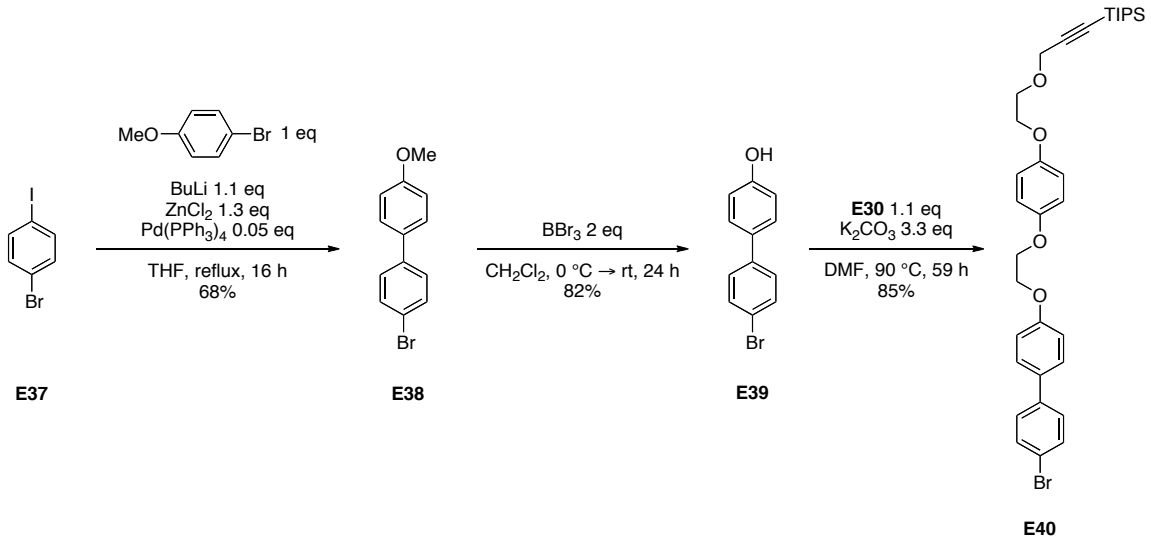

Scheme E8. Synthesis of arylbromide (E40).

Surprisingly, the preparation of stannane **E41** by the coupling reaction was also unsuccessful in spite of its very simple structure (Scheme E9). The reason is not clear, but the ethylene glycol linkages may be one cause. On the other hand, the boronic ester (**E42**) is accessible using a normal coupling method with the pinacol ester. Fortunately, when **E42** was used for the Suzuki coupling with the model compound **E35**, the expected compound (**E43**) was found as a major product in MS (EI), although it was not isolated.

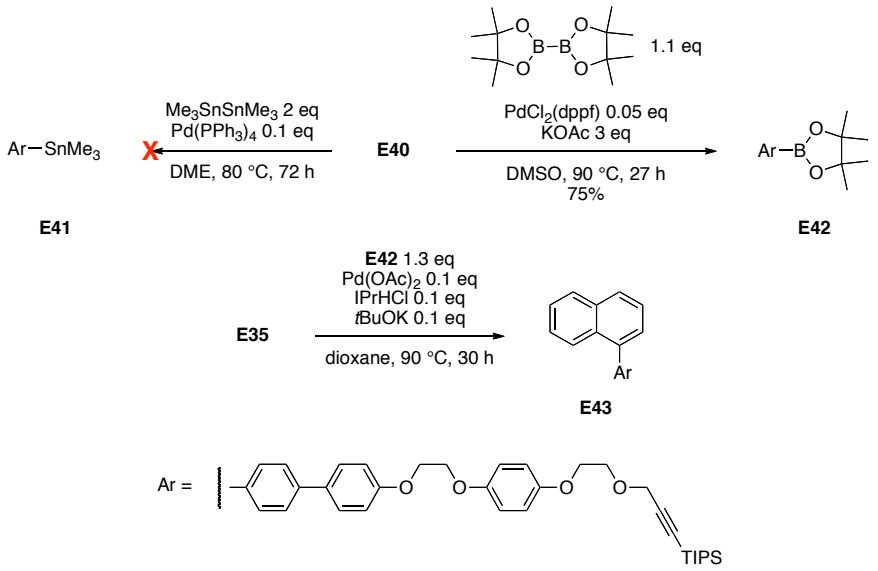

Scheme E9. Successful Suzuki coupling with boronic ester (E42).

Based on this successful result, the similar conditions were applied for **E11** and the moderately good chemical yield of 32% was obtained (Scheme E10). The removal of five TIPS protecting groups with excess tetrabutyl ammonium fluoride gave the corannulene derivative **E45**, which has five free alkynyl moieties.

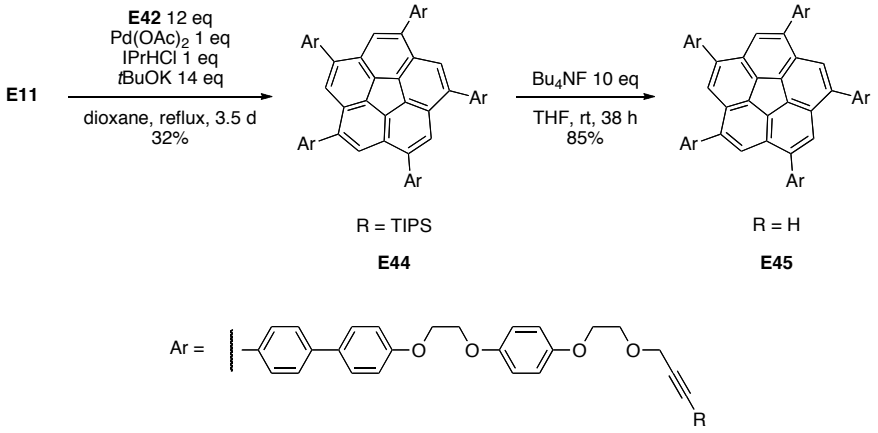

Scheme E10. Coupling reaction with E11 followed by removal of TIPS group.

The same strategy was attempted to prepare **E46**. However, although the boronic ester **E46** could be prepared, the crude mixture did not show the peak of the target compound (**E13**) (MS(MALDI)) in the coupling reaction with **E11**.

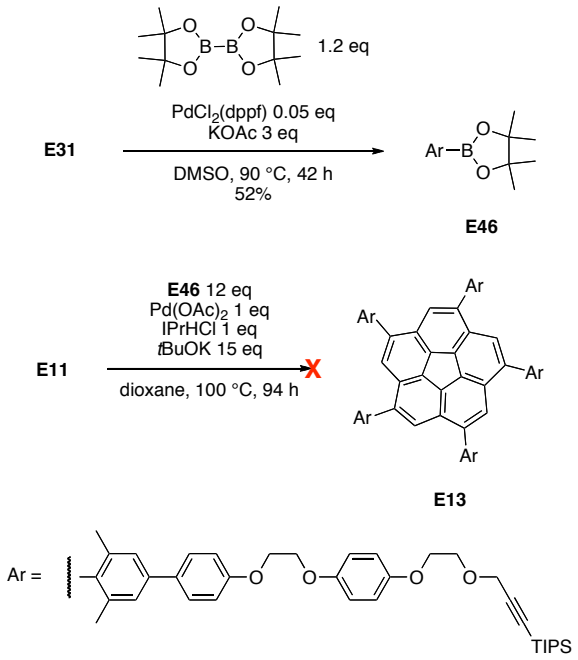

Scheme E11. Unsuccessful Suzuki coupling with boronic ester (E46).

As already explained, CuAAC, sometimes called the "Click reaction," should be used to make the connection between the "Linker" and the sugar components. In the CuAAC, copper (I) sources are necessary to overcome the relatively high energy barrier (ca. 26 kcal/mol for methyl azide and propyne[18]) (Scheme E12).[19] The copper (I) salts are used for aqueous solvents and coordination complexes are particularly effective in organic solvents.[19c]

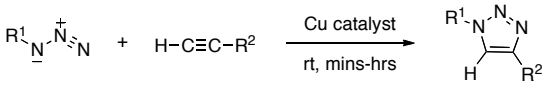

1) aqueous solvent + Copper (I) salts (CuI, CuBr)

2) organic solvent + coordination complexes (ex. $[Cu(CH_3CN)_4]PF_6$, $(EtO)_3P{\cdot}CuI$, $[Cu(PPh_3)_3]Br$)

Scheme E12. General reaction scheme of the CuAAC.

Before applying this reaction to the complicated corannulene system, the CuAAC was attempted using the single linker component (Scheme E13). First, the linker having a free alkyne (**E47**) was prepared from **E40** with the usual TIPS-deprotection reaction. Because of the low solubility of **E47** in water, THF was used as a solvent with the coordination complex, bromotris-(triphenylphosphine)copper (I) ($Cu(PPh_3)_3Br$).[20,21] When the free hydroxyl sugar component (**E20**) was used, the target compound (**E48**) was found by MS (ESI). However, **E48** did not dissolve well in any solvent except DMF, DMSO, or the mixture of those two solvents with another solvent (for example, methanol). Therefore, the impurities could not be removed. In the meantime, the use of acetyl protected sugar **E19** afforded **E49**, which is soluble in many organic solvents and could be purified by chromatography. In this reaction, the chemical yield was almost quantitative and showed the excellence of the CuAAC. The removal of acetyl groups with sodium methoxide in the mixture of methanol and dichloromethane produced **E48**, which was purified from the crude mixture by washing with methanol, water, and hexane.

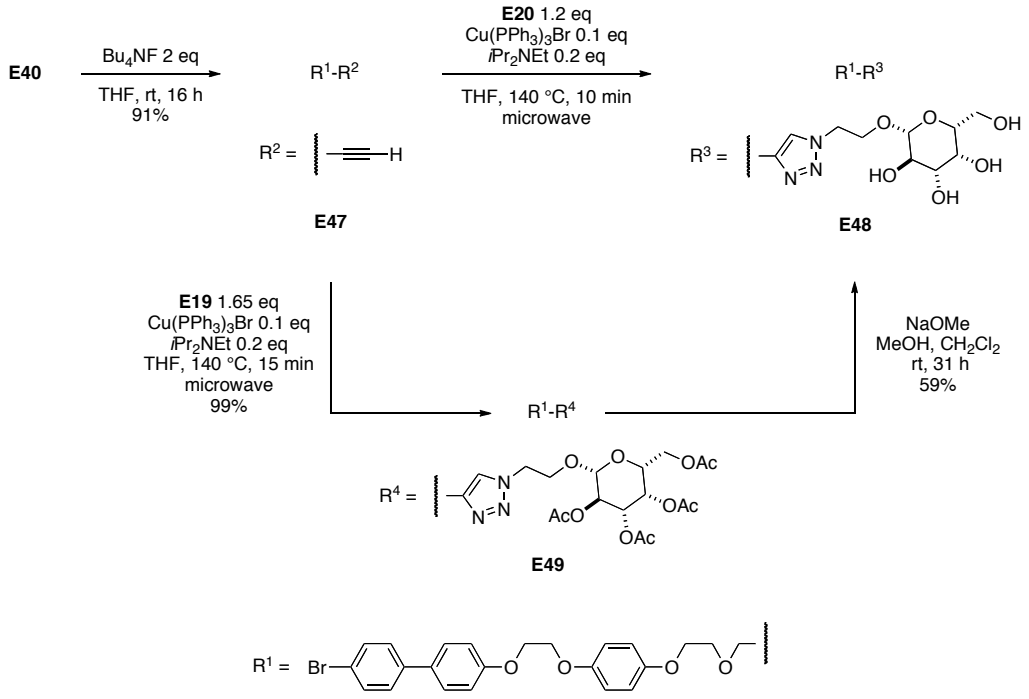

Scheme E13. CuAAC of U40 with deprotected sugar E20.

This successful reaction sequence was then applied to the corannulene system (Scheme E14). The pentaalkynylcorannulene (**E45**) was coupled with **E19** to afford the polyacetylated corannulene (**E50**) in very good yield (93%). After removal of acetyl groups with sodium methoxide in a mixture of methanol and dichloromethane, a yellow mixture was obtained. The MS(MALDI) showed the final compound **E12** as a major product along with some impurities (Figure E 11). The major side product seems to be **E51**, which has four linkers with sugar moieties and one linker without a sugar moiety. The reaction and workup conditions are not so harsh, so such a dissociation reaction should not happen readily. These peaks of side products may result from a fragmentation of the mass process due to the acidic matrix (in this measurement, a-cyano-4-hydroxycinnamic acid (HCCA)). In the meanwhile, ^{1}H-NMR and ^{13}C-NMR spectra suggest the pure **E12**.

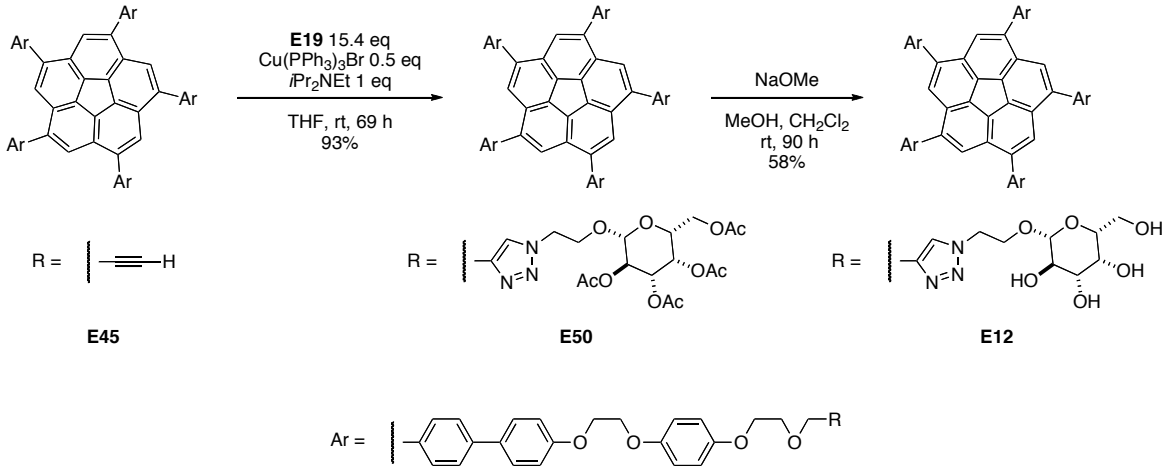

Scheme E14. Synthesis of target compound (E12) with using the CuAAC.

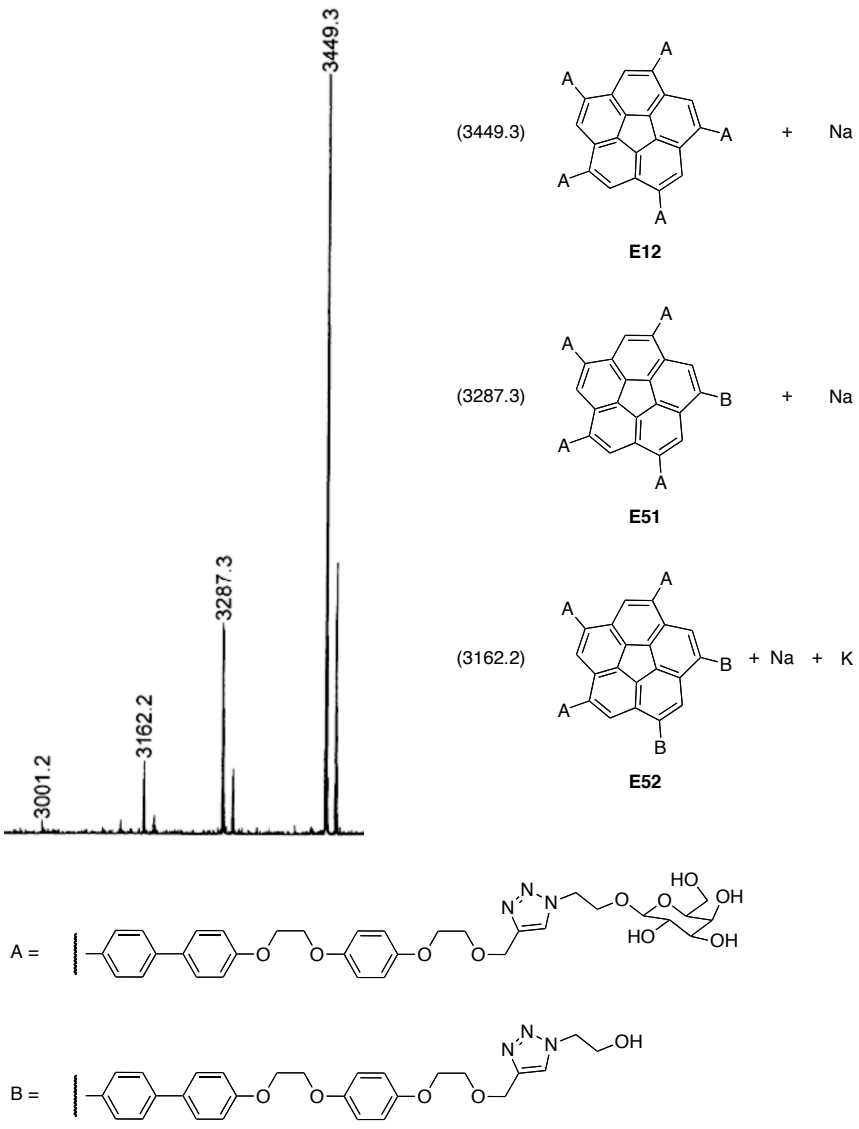

Figure E 11. MS(MALDI) shows the peaks of final product E12 and side products E51 and E52.

Naturally, a pure compound for the affinity measurement would be best, however, even if the sample is not the pure **E12**, the structure of the major impurity (**E51**) has been identified. An affinity measurement using this sample should be worthwhile. The affinity of **E51** for CT is presumably lower than that of **E12** because of one lost sugar residue.

5.2.3. Affinity Measurement

The unexpected low water solubility of **E12** is a confusing result, because **E12** has many free hydroxyl groups and ether linkages. To investigate the affinity of **E12** for CT, a pure water or water-based solvent would be desirable. Therefore, the solubility of **E12** in H_2O/DMSO was investigated.

First, when a mixture of H_2O/DMSO = 80/20 v/v% was added to a small amount of **E12**, particles of solid material remained after shaking and no UV absorption was detected in the solution. On the other hand, when only DMSO was added, all the compound dissolved. Fortunately, even when the solution was diluted with water, no precipitate was observed and UV and fluorescent spectra of this solution could be measured (Figure E12). This fact implies that the structural change of **E12** in solvent has a very strong influence on the solubility.

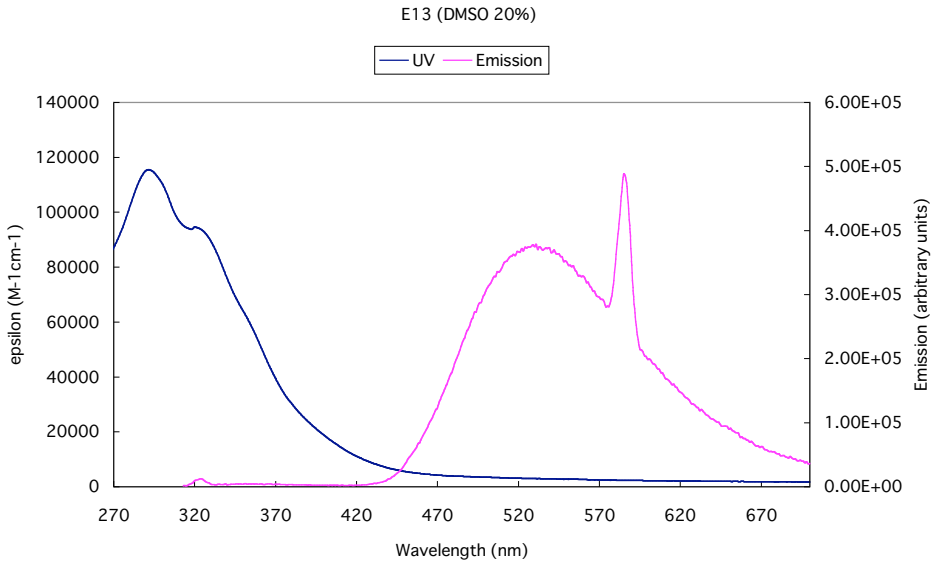

Figure E12. UV and fluorescent spectra of E12 in H_2O/DMSO = 80/20 v/v%.

As a next step, the affinity of **E12** for CT toxin should be investigated. Although many techniques could be used, one prospective method is by fluorescence analysis. Studies of the affinity measurement of CT with simple sugars (galactose, lactose, and fucose) have already been reported.[22] In these studies, the bathochromic shift in the fluorescence (near 350 nm) of a single tryptophan (W88) in CT was used (Figure E13). Since no emmision was confirmed in this region in the fluorescent spectrum of **E12**, the same technique could be used. Some other

biological methods like enzyme-linked immunosorbent assay (ELISA) may also be useful.

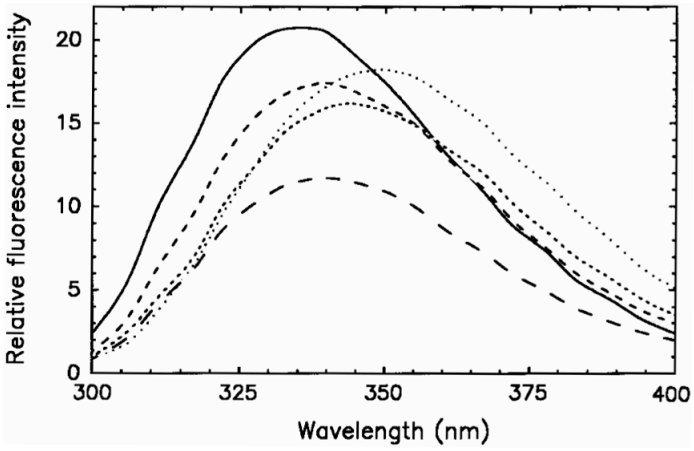

Figure E13. Binding effect of ganglioside GM1 and sugar on the fluorescence emission spectrum of CT. The spectra are without any addition (dotted line), with GM1 (solid line), galactose (long dashed line), lactose (medium dashed line), or fucose (short dashed line).

For a longer-term modification, when the size of the synthetic receptor will be changed, the length of the "Linkers" can be easily adjusted. In the above synthesis, 2-bromoethanol was used in the Koenigs-Knorr displacement reaction, and thus the use of a different α,ω-bromoalcohol will also give an azide (**E53**) with a different spacer length (Scheme E3, Scheme E15). The similar coupling reaction of **E45** with **E54** followed the acetyl deprotection will give a different size of the synthetic receptor **E56**. Because all these reaction sequences will be done under very mild conditions, even some kinds of functional groups could be introduced near the sugar moiety in the linker part. Such functional groups could also improve the affinity for CT. In summary, the effectiveness of our synthetic method was demonstrated.

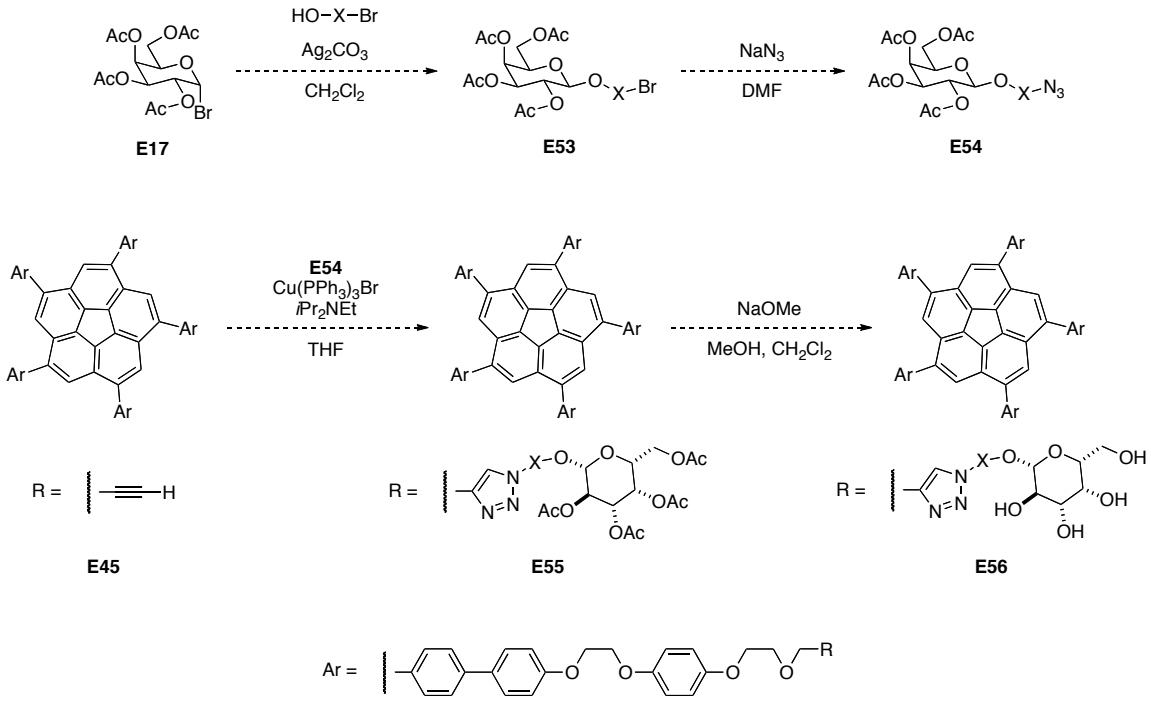

Scheme E15. Adjustment of the "Linker" length is possible from intermediate E17.

5.2.4. Experimental Section

5.2.4.1. Materials and Methods

General: ^{1}H and ^{13}C NMR: Bruker AV-300 (300 and 75.5 MHz), AV2-400 (400 and 101 MHz), DRX-500 (126 MHz). – IR: Perkin Elmer Spectrum One (FT-IR). – EI-MS: Finnigan MAT95 MS, ESI-MS: Bruker EsquireLC MS, MALDI-MS: Bruker Autoflex I MALDI-TOF spectrometer. – Chromatography: Merck silica gel 60 (230–400 mesh) or Fluka neutral alumina (Brockmann I, Activity II). – Melting points were measured to a maximum temperature of 350 °C. All experiments were carried out under nitrogen in freshly distilled anhydrous solvents unless otherwise noted. Solvents for chromatography were technical grade and freshly distilled before use. *sym*-Pentachlorocorannulene (**E11**)[23] and *N*,*N*'-bis(2,6-diisopropylphenyl)imidazol-2-ylidene hydrogen chloride (IPr-HCl)[15] were prepared according to the literature procedures. Other compounds, which are not mentioned, are commercially available.

5.2.4.2. Synthetic Procedures

1,2,3,4,6-Penta-*O*-acetyl-D-galactopilanoside (E16)

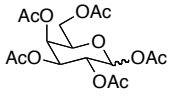

$C_{16}H_{22}O_{11}$
Mol. Wt.: 390.3393

Sodium acetate trihydrate (2.40 g, 17.6 mmol) was dissolved in hot acetic anhydride (40 mL) at 130 °C and D-(+)-galactose (**E15**) (8.00 g, 44.4 mmol) was added very slowly to the mixture. The mixture was stirred at 150 °C for 5 h. After cooling to room temperature, the mixture was put into ice water (100 mL). The organic layer was separated, washed with saturated sodium hydrogen carbonate (100 mL), dried with magnesium sulfate, and evaporated. The product was passed through a plug of silica gel eluted with dichloromethane to yield **E16** as a white solid (12.7 g, 73%). The spectroscopic data were identical with those reported.[24] Mp 113-114 °C (lit. 113 °C).[24]

2,3,4,6-Tetra-*O*-acetyl-α-D-galactopyranosyl bromide (E17)

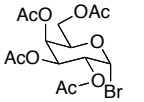

$C_{14}H_{19}BrO_9$
Mol. Wt.: 411.1993

Hydrobromic acid (45% in acetic acid, 20 mL) was added dropwise to 1,2,3,4,6-penta-*O*-acetyl-

D-galactopilanoside (**E16**) (6.47 g, 16.6 mmol) in acetic acid (25 mL) at 0 °C in an ice bath. The mixture was warmed to room temperature for 10 h and put into ice water (150 mL). After extraction with dichloromethane (100 mL × 2), the organic layer was washed with saturated sodium hydrogen carbonate (100 mL × 2) and saturated sodium chloride (100 mL), dried with magnesium sulfate, and evaporated at 25 °C to yield a white solid (6.19 g). The crude mixture was used for the next reaction without any purification. The spectroscopic data of the purified sample were identical with those reported.[25] Mp 85-86 °C (lit. 84-85 °C).[25]

2-Bromoethyl-2,3,4,6-tetra-*O*-acetyl-β-D-galactopyranoside (E18)

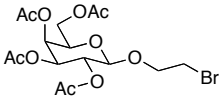

$C_{16}H_{23}BrO_{10}$
Mol. Wt.: 455.2518

The mixture of 2-bromoethanol (9.44 g, 75.5 mmol), silver (II) carbonate (12.5 g, 45.2 mmol), and a crystal of iodine in dichloromethane (30 mL) with molecular sieve 4 Å was stirred for 15 min. The crude mixture of the previous step in dichloromethane (20 mL) with molecular sieve 4 Å were stirred for 15 min and added dropwise to the mixture (bubbles generated). The flask was covered in an aluminium foil and stirred for 18 h. The mixture was diluted with ethyl acetate (100 mL), filtered over celite, and evaporated. The product was purified by column chromatography on silica gel eluted with hexane/ethyl acetate = 3/1, 2/1, and 1/1 to yield **E18** as yellow syrup (2.41 g, 34%, two steps) [R_f = 0.52 (SiO_2, hexane/ethyl acetate = 1:1)]. The spectroscopic data were identical with those reported.[26] ^{1}H-NMR (300 MHz, $CDCl_3$): δ ppm = 1.99 (s, 3H), 2.06 (s, 3H), 2.09 (s, 3H), 2.16 (s, 3H), 3.45-3.49 (m, 2H), 3.78-3.87 (m, 1H), 3.89-3.94 (m, 1H), 4.09-4.22 (m, 3H), 4.54 (d, ^3J = 7.8 Hz, 1H), 5.03 (dd, ^3J = 3.6, 10.5 Hz, 1H), 5.23 (dd, ^3J = 7.8, 10.5 Hz, 1H), 5.40 (dd, ^3J = 1.2, 3.6 Hz, 1H).

2-Azidoethyl-2,3,4,6-tetra-*O*-acetyl-β-D-galactopyranoside (E19)

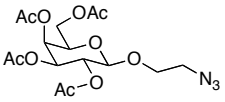

$C_{16}H_{23}N_3O_{10}$
Mol. Wt.: 417.3679

To a solution of 2-bromoethyl-2,3,4,6-tetra-*O*-acetyl-β-D-galactopyranoside (**E18**) (2.41 g, 5.29 mmol) in DMF (150 mL), sodium azide (2.07 g, 31.8 mmol) was added. The mixture was

stirred at 60 °C for 2 h. After evaporation of the solvent, dichloromethane (100 mL) and water (100 mL) were added. The organic layer was washed with water (100 mL), dried with magnesium sulfate, and evaporated. The product was purified by column chromatography on silica gel eluted with hexane/ethyl acetate = 2/1, and 1/1 to yield **E19** as yellow syrup (2.17 g, 98%) [R_f = 0.45 (SiO_2, hexane/ethyl acetate = 1:1)]. The spectroscopic data were identical with those reported.[27] ^{1}H-NMR (400 MHz, $CDCl_3$): δ ppm = 1.99 (s, 3H), 2.05 (s, 3H), 2.07 (s, 3H), 2.16 (s, 3H), 3.31 (ddd, ^3J = 3.4, 4.7, 13.4 Hz, 1H), 3.48-3.54 (m, 1H), 3.67-3.73 (m, 1H), 3.93 (dt, ^3J = 1.2, 6.6 Hz, 1H), 4.05 (ddd, ^3J = 3.4, 4.7, 10.7 Hz, 1H), 4.11-4.21 (m, 2H), 4.56 (d, ^3J = 8.0 Hz, 1H), 4.03 (dd, ^3J = 3.4, 10.5 Hz, 1H), 5.25 (dd, ^3J = 8.0, 10.5 Hz, 1H), 5.40 (dd, ^3J = 1.2, 3.4 Hz, 1H).

2-Azidoethyl-β-D-galactopyranoside (E20)

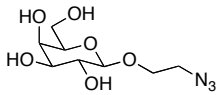

$C_8H_{15}N_3O_6$
Mol. Wt.: 249.2212

To a solution of 2-azidoethyl-2,3,4,6-tetra-*O*-acetyl-β-D-galactopyranoside (**E19**) (2.17 g, 5 mmol) in methanol (50 mL), sodium methoxide (5.4 M in methanol) was added until pH became 10. The mixture was stirred at room temperature for 4 h. Dowex 50 was added until pH became 6-7. The mixture was filtered and the filtrate was evaporated to yield **E20** as pale yellow syrup (1.21 g, 93%). The spectroscopic data were identical with those reported.[27] ^{1}H-NMR (300 MHz, D_2O): δ ppm = 3.52-3.59 (m, 3H), 3.64-3.73 (m, 2H), 3.77-3.89 (m, 3H), 3.94 (dd, ^3J = 0.87, 3.4 Hz, 1H), 4.04-4.11 (m, 1H), 4.45 (d, ^3J = 7.8 Hz, 1H).

2-(4-(2-(Prop-2-ynyloxy)ethoxy)phenoxy)ethanol (E28)

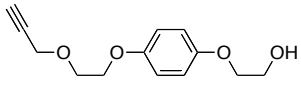

$C_{13}H_{16}O_4$
Mol. Wt.: 236.2637

To a mixture of propargyl bromide (80 wt% in toluene, 12.6 g, 85 mmol) and hydroquinone bishydroxyethylether (**E27**) (33.7 g, 170 mmol) in THF (220 mL), fine powder of sodium hydroxide (4.08 g, 102 mmol) was added at 0 °C. The mixture was refluxed for 6 h. After cooling to room temperature, dichloromethane (300 mL) and water (300 mL) were added. The water layer was separated and extracted with dichloromethane (150 mL). The combined organic

layer was washed with water (200 mL), dried with sodium sulfate, and evaporated. The product was purified by column chromatography on silica gel eluted with hexane/ethyl acetate = 1/1 and 1/1.5 to yield **E28** as a white solid (7.68 g, 39%) [R_f = 0.48 (SiO_2, hexane/ethyl acetate = 1:1)]. Mp 64-67 °C. ^{1}H-NMR (300 MHz, $CDCl_3$): δ ppm = 2.02 (t, ^3J = 6.0 Hz, 1H), 2.46 (t, ^4J = 2.4 Hz, 1H), 3.87-3.97 (m, 4H), 4.01-4.05 (m, 2H), 4.09-4.13 (m, 2H), 4.27 (d, ^4J = 2.4 Hz, 2H), 6.857 (s, 2H), 6.860 (s, 2H). ^{13}C-NMR (75.5 MHz, $CDCl_3$): δ ppm = 58.4 (CH_2), 61.5 (CH_2), 67.8 (CH_2), 68.2 (CH_2), 69.8 (CH_2), 74.6 (C), 79.4 (CH), 115.5 (CH), 115.6 (CH), 152.9 (C), 153.1 (C). IR (KBr): ν cm^{-1} = 3273, 2925, 2866, 1509, 1454, 1237, 1106, 923, 830, 748, 673. MS (ESI): *m*/*z* (%): 259.1 (M^+ + Na). HRMS (EI): calcd for $C_{13}H_{16}O_4$: 236.1049; found: 236.1048.

2-(4-(2-(3-(Triisopropylsilyl)prop-2-ynyloxy)ethoxy)phenoxy)ethanol (E29)

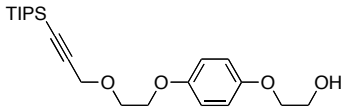

$C_{22}H_{36}O_4Si$
Mol. Wt.: 392.6043

To 2-(4-(2-(prop-2-ynyloxy)ethoxy)phenoxy)ethanol (**E28**) (4.00 g, 16.9 mmol) in THF (350 mL), butyllithium (1.5 M in hex, 22.6 mL, 33.9 mmol) was added dropwise at –78 °C. After stirring for one hour, triisopropylsilyl chloride (7.17 g, 37.2 mmol) was added and the mixture was slowly warmed to room temperature for 14 h. Water (200 mL) was added and the mixture was extracted with dichloromethane (300 mL). The organic layer was washed with saturated sodium hydrogen carbonate (300 mL) and saturated sodium chloride (300 mL), dried with magnesium sulfate, and evaporated. The product was roughly purified by column chromatography on silica gel eluted with hexane/ethyl acetate = 40/1 and 30/1 to yield the 8.21 g colorless oil [R_f = 0.39 (SiO_2, hexane/ethyl acetate = 20:1)]. The crude mixture was dissolved in ethanol (260 mL) and 10% hydrochloric acid (50 mL). The mixture was stirred at room temperature for 3.5 h. Water (300 mL) and dichloromethane (300 mL) were added and the water layer was extracted with dichloromethane (200 mL × 2). The combined organic layer was dried with magnesium sulfate, and evaporated. The product was purified by column chromatography on silica gel eluted with hexane/ethyl acetate = 3/1, 2/1, and 1/1 to yield **E29** as colorless oil (5.94 g, 89%) [R_f = 0.18 (SiO_2, hexane/ethyl acetate = 4:1)]. ^{1}H-NMR (300 MHz, $CDCl_3$): δ ppm = 1.08 (s, 21H), 2.67 (br s, 1H), 3.88-3.91 (m, 4H), 3.98-4.01 (m, 2H), 4.08-4.11

(m, 2H), 4.30 (s, 2H), 6.832 (s, 2H), 6.836 (s, 2H). ^{13}C-NMR (75.5 MHz, $CDCl_3$): δ ppm = 12.3 (CH), 19.7 (CH_3), 60.4 (CH_2), 62.6 (CH_2), 69.0 (CH_2), 69.1 (CH_2), 71.1 (CH_2), 89.1 (C), 104.2 (C), 116.7 (CH), 116.8 (CH), 154.2 (C), 154.4 (C). IR (KBr): ν cm^{-1} = 3408, 2942, 2865, 2171, 1508, 1462, 1232, 1107, 1037, 883, 679. HRMS (EI): calcd for $C_{22}H_{36}O_4Si$: 392.2387; found: 392.2378.

(3-(2-(4-(2-Chloroethoxy)phenoxy)ethoxy)prop-1-ynyl)triisopropylsilane (E30)

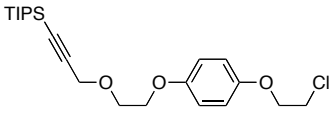

$C_{22}H_{35}ClO_3Si$
Mol. Wt.: 411.05

To a mixture of 2-(4-(2-(3-(triisopropylsilyl)prop-2-ynyloxy)ethoxy)phenoxy)ethanol (**E29**) (5.16 g, 13.1 mmol) and pyridine (1.35 g, 17.1 mmol) in dichloromethane (130 mL), thionyl chloride (1.88 g, 15.8 mmol) was added dropwise. The mixture was refluxed for 35 h. After cooling to room temperature, the mixture was poured into saturated sodium hydrogen carbonate (200 mL) and stirred for 5 min Water (100 mL) and dichloromethane (100 mL) were added and the organic layer was extracted with dichloromethane (100 mL × 2). The combined organic layer was dried with magnesium sulfate, and evaporated. The product was purified by column chromatography on silica gel eluted with hexane/dichloromethane = 2/1 and 1/1 to yield **E30** as pale yellow oil (4.67 g, 87%) [R_f = 0.31 (SiO_2, hexane/dichloromethane = 1:1)]. ^{1}H-NMR (400 MHz, $CDCl_3$): δ ppm = 1.08 (s, 21H), 3.77 (t, ^3J = 6.0 Hz, 2H), 3.88-3.91 (m, 2H), 4.10-4.12 (m, 2H), 4.17 (t, ^3J = 6.0 Hz, 2H), 4.30 (s, 2H), 6.848 (s, 2H), 6.854 (s, 2H). ^{13}C-NMR (75.5 MHz, $CDCl_3$): δ ppm = 11.0 (CH), 18.5 (CH_3), 41.9 (CH_2), 59.2 (CH_2), 67.7 (CH_2), 67.8 (CH_2), 68.7 (CH_2), 87.9 (C), 102.9 (C), 115.6 (CH), 115.8 (CH), 152.4 (C), 153.4 (C). IR (KBr): ν cm^{-1} = 2943, 2866, 2171, 1508, 1459, 1230, 1108, 1037, 883, 825, 678. MS (EI): *m/z* (%): 410.2 (M^+). HRMS (EI): calcd for $C_{22}H_{35}O_3SiCl$: 410.2044; found: 410.2052.

4-Bromo-4'-methoxybiphenyl (E38)

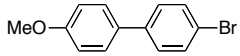

$C_{13}H_{11}BrO$
Mol. Wt.: 263.1298

4-Bromoanisole (5.00 g, 26.7 mmol) in THF (45 mL) was cooled to –78 °C in a dry ice/ acetone bath and butyllithium (1.5 M in hex, 19.6 mL, 29.4 mmol) was added dropwise. After 30 min,

zinc chloride (4.73 g, 34.7 mmol) in THF (20 mL) was added to the solution and the bath was removed. After 30 min, the resulting solution was transferred to the flask containing 1-bromo-4-iodobenzene (**E37**) (7.55g, 26.7 mmol) and tetrakistriphenylphosphine palladium (1.55g, 1.34 mmol) in THF (45 mL). The mixture was refluxed for 16 h. After cooling to room temperature, dichloromethane (100 mL) was added. The organic layer was washed with saturated ethylenediaminetetraacetic acid (200 mL) and water (200 mL × 2), dried with magnesium sulfate, and evaporated. The product was purified by column chromatography on silica gel eluted with hex, hexane/dichloromethane = 10/1 and 5/1 to yield **E38** as a white solid (4.75 g, 68%) [R_f = 0.11 (SiO_2, hexane)]. The spectroscopic data were identical with those reported.[28] ^{1}H-NMR: (300 MHz, $CDCl_3$) δ ppm = 3.85 (s, 3H), 6.97 (d, ^3J = 9.6 Hz, 2H), 7.41 (d, ^3J = 9.3 Hz, 2H), 7.49 (d, ^3J = 8.7 Hz, 2H), 7.53 (d, ^3J = 8.4 Hz, 2H).

4-Bromo-4'-hydroxybiphenyl (E39)

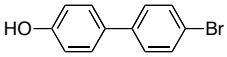

$C_{12}H_9BrO$
Mol. Wt.: 249.1033

4-Bromo-4'-methoxybiphenyl (**E38**) (2.08 g, 7.90 mmol) was dissolved in dichloromethane (40 mL) and boron tribromide (1M in dichloromethane, 15.8 mL, 15.8 mmol) was added dropwise at –78 °C. The mixture was warmed to room temperature for 24 h. Water was added dropwise to the mixture in an ice bath until the bubble stopped. After the addition of ethyl acetate (100 mL), the mixture was washed with water (100 mL × 2), dried with magnesium sulfate, and evaporated. The product was purified by column chromatography on silica gel eluted with hexane/ethyl acetate = 4/1, 3/1, and 2/1 to yield **E39** as a white solid (1.62 g, 82%) [R_f = 0.33 (SiO_2, hexane/ethyl acetate = 4:1)]. The spectroscopic data were identical with those reported.[29] ^{1}H-NMR (300 MHz, $CDCl_3$): δ ppm = 4.86 (s, 1H), 6.90 (d, ^3J = 9.0 Hz, 2H), 7.40 (d, ^3J = 9.3 Hz, 2H), 7.44 (d, ^3J = 9.3 Hz, 2H), 7.53 (d, ^3J = 8.4 Hz, 2H).

4-Bromo-4'-(2-(4-(2-(3-(triisopropylsilyl)prop-2-ynyloxy)ethoxy)phenoxy)ethoxy)-biphenyl (E40)

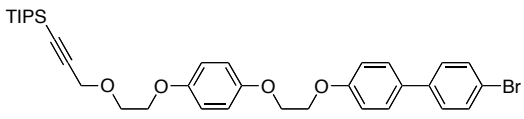

$C_{34}H_{43}BrO_4Si$
Mol. Wt.: 623.6923

The mixture of (3-(2-(4-(2-chloroethoxy)phenoxy)ethoxy)prop-1-ynyl)triisopropylsilane (**E30**) (1.65 g, 4.01 mmol), 4-bromo-4'-hydroxybiphenyl (**E39**) (900 mg, 3.61 mmol), and potassium carbonate (1.66 g, 12.0 mmol) in DMF (50 mL) was stirred with molecular sieve (4Å, 644 mg) at 90 °C for 59 h. After cooling to room temperature, dichloromethane (200 mL) and 1N hydrochloric acid (150 mL) were added. The organic layer was dried with sodium sulfate, and evaporated. The product was purified by column chromatography on silica gel eluted with hexane/dichloromethane = 1/1, 1/1.5, and 1/2 to yield **E40** as a white solid (1.92 g, 85%) [R_f = 0.39 (SiO_2, hexane/dichloromethane = 1:2)]. Mp 146-147 °C. ^{1}H-NMR (300 MHz, $CDCl_3$): δ ppm = 1.08 (s, 21H), 3.89-3.92 (m, 2H), 4.10-4.14 (m, 2H), 4.27-4.36 (m, 4H), 4.31 (s, 2H), 6.88 (s, 4H), 7.02 (d, ^3J = 8.4 Hz, 2H), 7.42 (d, ^3J = 9.0 Hz, 2H), 7.49 (d, ^3J = 9.0 Hz, 2H), 7.54 (d, ^3J = 8.4 Hz, 2H). ^{13}C-NMR (101 MHz, $CDCl_3$): δ ppm = 11.2 (CH), 18.6 (CH_3), 59.3 (CH_2), 66.8 (CH_2), 67.2 (CH_2), 67.9 (CH_2), 68.0 (CH_2), 88.0 (C), 103.0 (C), 115.1 (CH), 115.7 (CH), 115.8 (CH), 120.9 (C), 128.0 (CH), 128.3 (CH), 131.8 (CH), 132.9 (C), 139.7 (C), 153.0 (C), 153.3 (C), 158.5 (C). IR (KBr): ν cm^{-1} = 3450, 2941, 2865, 2175, 1607, 1483, 1455, 1256, 1070, 947, 825, 679. HRMS (EI): calcd for $C_{34}H_{43}O_4SiBr$: 622.2114; found: 622.2123.

4-(4,4,5,5-Terramethyl-1,3,2-dioxaborolan-2-yl)-4'-(2-(4-(2-(3-(triisopropylsilyl)prop-2-ynyloxy)ethoxy)phenoxy)ethoxy)biphenyl (E42)

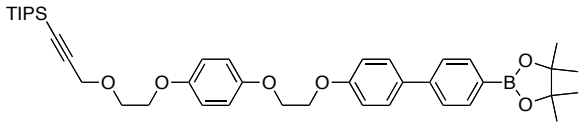

$C_{40}H_{55}BO_6Si$
Mol. Wt.: 670.7576

To the mixture of 4-bromo-4'-(2-(4-(2-(3-(triisopropylsilyl)prop-2-ynyloxy)ethoxy)phenoxy)-ethoxy)biphenyl (**E40**) (600 mg, 0.962 mmol), bis(pinacolato)diborane (269 mg, 1.06 mmol), dichloro[1,1'-bis(diphenylphosphino)fellocene]palladium (II) (35 mg, 0.0481 mmol), and potassium acetate (283 mg, 2.89 mmol), DMSO (18 mL) was added. The mixture was stirred at 90 °C for 27 h. After cooling to room temperature, ethyl acetate (100 mL) was added and washed with water (100 mL × 3). The organic layer was dried with sodium sulfate, and evaporated. The product was purified by column chromatography on silica gel eluted with hexane/ethyl acetate = 4/1 to yield **E42** as a pale green solid (483 mg, 75%) [R_f = 0.45 (SiO_2, hexane/ethyl acetate = 4:1)]. Mp 107-109 °C. ^{1}H-NMR (400 MHz, $CDCl_3$): δ ppm = 1.08 (s, 21H), 1.36 (s, 12H), 3.89-3.92 (m, 2H), 4.10-4.14 (m, 2H), 4.30-4.35 (m, 4H), 4.31 (s, 2H), 6.880

(s, 2H), 6.882 (s, 2H), 7.02 (d, ^3J = 8.8 Hz, 2H), 7.56 (dd, ^3J and ^4J = 8.4, 3.2 Hz, 4H), 7.86 (d, ^3J = 8.8 Hz, 2H). ^{13}C-NMR (101 MHz, $CDCl_3$): δ ppm = 11.2 (CH), 18.6 (CH_3), 24.9 (CH_3), 59.3 (CH_2), 66.8 (CH_2), 67.3 (CH_2), 67.9 × 2 (CH_2), 83.5 (C), 83.8 (C), 88.0 (C), 103.0 (C), 115.0 (CH), 115.7 (CH), 115.8 (CH), 126.0 (CH), 128.3 (CH), 133.9 (C), 135.3 (CH), 143.4 (C), 153.0 (C), 153.3 (C), 158.5 (C). IR (KBr): ν cm^{-1} = 3417, 2941, 2866, 2174, 1604, 1508, 1362, 1229, 1143, 822, 671. MS (EI): *m/z* (%): 670.3 (M^+). HRMS (EI): calcd for $C_{40}H_{55}O_6BSi$: 670.3888; found: 670.3869.

4-Bromo-4'-(2-(4-(2-(prop-2-ynyloxy)ethoxy)phenoxy)ethoxy)biphenyl (E47)

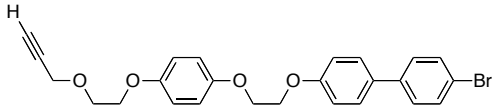

$C_{25}H_{23}BrO_4$
Mol. Wt.: 467.3517

To 4-bromo-4'-(2-(4-(2-(3-(triisopropylsilyl)prop-2-ynyloxy)ethoxy)phenoxy)ethoxy)-biphenyl (**E40**) (150 mg, 0.241 mmol) in THF (10 mL), tetrabutylammonium fluoride (1.0 M in THF, 0.481 mL, 0.481 mmol) was added. After 16 h, ethyl acetate (100 mL) and 10% ammonium chloride (100 mL) were added. The organic layer was washed with water (100 mL), dried with sodium sulfate, and evaporated. The product was purified by washing with hexane to yield **E47** as a white solid (102 mg, 91%). Mp 171-172 °C. ^{1}H-NMR (400 MHz, $CDCl_3$): δ ppm = 2.45 (t, ^4J = 2.4 Hz, 1H), 3.87-3.90 (m, 2H), 4.10-4.13 (m, 2H), 4.27 (d, ^4J = 2.4 Hz, 2H), 4.28-4.35 (m, 4H), 6.88 (s, 2H), 6.89 (s, 2H), 7.02 (d, ^3J = 8.4 Hz, 2H), 7.41 (d, ^3J = 9.2 Hz, 2H), 7.49 (d, ^3J = 8.4 Hz, 2H), 7.53 (d, ^3J = 9.2 Hz, 2H). ^{13}C-NMR (101 MHz, $CDCl_3$): δ ppm = 58.6 (CH_2), 66.8 (CH_2), 67.3 (CH_2), 67.9 (CH_2), 68.4 (CH_2), 77.2 (CH), 79.5 (C), 115.1 (CH), 115.7 (CH), 115.8 (CH), 120.9 (C), 128.0 (CH), 128.3 (CH), 131.8 (CH), 132.9 (C), 139.7 (C), 153.0 (C), 153.3 (C), 158.5 (C). IR (KBr): ν cm^{-1} = 3436, 3294, 2928, 1606, 1512, 1483, 1236, 1069, 943, 822, 633. MS (EI): *m/z* (%): 466.0 (M^+). HRMS (EI): calcd for $C_{25}H_{23}O_4Br$: 466.0780; found: 466.0782.

2-(1,2,3-Triazole-4-(2-(4-(2-(4-(4-bromophenyl)phenoxy)ethoxy)phenoxy)ethoxymethyl))-ethyl-2,3,4,6-tetra-*O*-acetyl-β-D-galactopyranoside (E49)

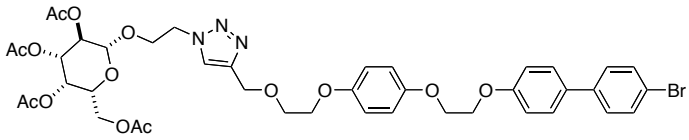

$C_{41}H_{46}BrN_3O_{14}$
Mol. Wt.: 884.7196

The mixture of 4-bromo-4'-(2-(4-(2-(prop-2-ynyloxy)ethoxy)phenoxy)ethoxy)biphenyl (**E47**) (50 mg, 0.107 mmol), 2-azidoethyl-2,3,4,6-tetra-*O*-acetyl-β-D-galactopyranoside (**E19**) (73.6 mg, 0.176 mmol), bromotris(triphenylphosphine)copper (I) (9.95 mg, 0.0107 mmol), and diisopropylethylamine (2.77 mg, 0.0214 mmol) in THF (2 mL) was stirred in a microwave reactor at 140 °C (300 W) for 15 min. The solvent was evaporated. The product was purified by column chromatography on silica gel eluted with dichloromethane, dichloromethane/ethyl acetate = 3/1 and 1/1 to yield **E49** as a white solid (103 mg, 99%) [R_f = 0.43 (SiO_2, dichloromethane/ethyl acetate = 1:1)]. Mp > 350 °C (dec.). ^{1}H-NMR (300 MHz, CD_2Cl_2): δ ppm = 1.95 (s, 3H), 1.96 (s, 3H), 2.02 (s, 3H), 2.13 (s, 3H), 3.87-3.94 (m, 4H), 4.06-4.16 (m, 4H), 4.18-4.35 (m, 5H), 4.47 (d, ^3J = 7.9 Hz, 1H), 4.52-4.64 (m, 2H), 4.69 (s, 2H), 4.84 (dd, ^3J = 10.5, 3.4 Hz, 1H), 5.14 (dd, ^3J = 10.5, 7.9 Hz, 1H), 5.37 (dd, ^3J = 3.4, 1.0 Hz, 1H), 6.87 (d, ^3J = 2.9 Hz, 4H), 7.02 (d, ^3J = 8.7 Hz, 2H), 7.45 (d, ^3J = 8.6 Hz, 2H), 7.54 (dd, ^3J = 8.7, 6.5 Hz, 4H), 7.65 (br s, 1H). ^{13}C-NMR (101 MHz, CD_2Cl_2): δ ppm = 20.90 (CH_3), 20.96 (CH_3), 21.00 (CH_3), 21.03 (CH_3), 50.6 (CH_2), 61.9 (CH_2), 65.1 (CH_2), 67.4 (CH_2), 67.6 (CH), 67.8 (CH_2), 68.3 (CH_2), 68.5 (CH_2), 69.0 (CH), 69.6 (CH_2), 71.2 (CH), 71.5 (CH), 101.6 (CH), 115.5 (CH), 116.0 (CH), 116.1 (CH), 121.2 (C), 124.4 (CH), 128.5 (CH), 128.8 (CH), 132.3 (CH), 133.2 (C), 140.2 (C), 145.3 (C), 153.5 (C), 153.8 (C), 159.2 (C). IR (KBr): ν cm^{-1} = 3458, 2929, 1750, 1607, 1510, 1370, 1227, 1069, 821, 722, 542. MS (ESI): *m/z* (%): 908.5 (M^+ + Na). HRMS (ESI): calcd for $C_{41}H_{46}N_3O_{14}NaBr$: 906.2061; found: 906.2052.

2-(1,2,3-Triazole-4-(2-(4-(2-(4-(4-bromophenyl)phenoxy)ethoxy)phenoxy)ethoxymethyl))-ethyl -β-D-galactopyranoside (E48)

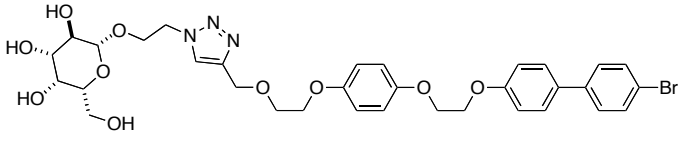

$C_{33}H_{38}BrN_3O_{10}$
Mol. Wt.: 716.5729

To a solution of 2-(1,2,3-triazole-4-(2-(4-(2-(4-(4-bromophenyl)phenoxy)ethoxy)phenoxy)-ethoxymethyl))ethyl-2,3,4,6-tetra-*O*-acetyl-β-D-galactopyranoside (**E49**) (58 mg, 0.0693 mmol) in methanol (5 mL) and dichloromethane (5 mL), sodium methoxide (5.4 M in methaol, 1 mL) was added. The mixture was stirred at room temperature for 31 h. Methanol was added to dilute and Dowex 50 was added until pH became 5-6. DMF was added until the white suspension dissapeared. The mixture was filtered and washed with the mixture of methanol and DMF. The filtrate was evaporated. Methanol was added and filtered. The solid was washed with water, methanol, and hexane to yield **E48** a white solid (29 mg, 59%). Mp 166-168 °C. ^{1}H-NMR: (400 MHz, $(CD_3)_2SO$) δ ppm = 3.24-3.37 (m, 3H), 3.46-3.56 (m, 2H), 3.62-3.64 (m, 1H), 3.75-3.77 (m, 2H), 3.85-3.91 (m, 1H), 4.03-4.10 (m, 3H), 4.17 (d, ^{3}J = 7.2 Hz, 1H), 4.25-4.34 (m, 4H), 4.37 (d, ^{3}J = 4.6 Hz, 1H), 4.51-4.58 (m, 5H), 4.71 (d, ^{3}J = 5.2 Hz, 1H), 4.93 (d, ^{3}J = 4.5 Hz, 1H), 6.87-6.93 (m, 4H), 7.08 (d, ^{3}J = 8.8 Hz, 2H), 7.57-7.64 (m, 6H), 8.17 (s, 1H). ^{13}C-NMR: (101 MHz, $(CD_3)_2SO$) δ ppm = 49.5 (CH_2), 60.4 (CH_2), 63.5 (CH_2), 66.5 (CH_2), 66.6 (CH_2), 67.1 (CH_2), 67.3 (CH_2), 68.1 (CH), 68.1 (CH_2), 70.3 (CH), 73.2 (CH), 75.3 (CH), 103.4 (CH), 115.0 (CH), 115.28 (CH), 115.34 (CH), 120.0 (C), 124.6 (CH), 127.7 (CH), 128.2 (CH), 131.3 (C), 131.6 (CH), 138.8 (C), 143.5 (C), 152.3 (C), 152.6 (C), 158.2 (C). IR (KBr): ν cm^{-1} = 3425, 2927, 1640, 1514, 1236, 1069, 822. MS (ESI): *m*/*z* (%): 740.4 (M^+ + Na). HRMS (ESI): calcd for $C_{33}H_{38}N_3O_{10}NaBr$: 738.1638; found: 738.1633.

***sym*-Penta(4-(4-(2-(4-(2-(3-triisopropylsilylprop-2-ynyloxy)ethoxy)phenoxy)ethoxy)phenyl)-phenyl)corannulene (E44)**

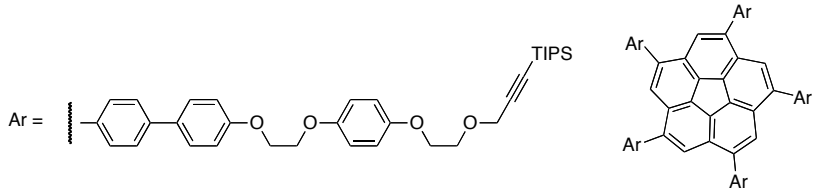

$C_{190}H_{220}O_{20}Si_5$
Mol. Wt.: 2964.1953

To a mixture of *sym*-pentachlorocorannulene (**E11**) (35 mg, 0.0834 mmol), 4-(4,4,5,5-terramethyl-1,3,2-dioxaborolan-2-yl)-4'-(2-(4-(2-(3-(triisopropylsilyl)prop-2-ynyloxy)ethoxy)-phenoxy)ethoxy)biphenyl (**E42**) (671 mg, 1.00 mmol), palladium (II) acetate (19 mg, 0.0834 mmol), IPr-HCl (35 mg, 0.0834 mmol), and potassium *tert*-butoxide (131 mg, 1.17 mmol), anhydrous dioxane (15 mL) was added. The mixture was refluxed for 3.5 d. After cooling to room temperature, dichloromethane (100 mL) and water (100 mL) were added. The organic

layer was dried with sodium sulfate, and evaporated. The product was purified by column chromatography on aluminum oxide (5% deactivated with water) eluted with hexane/dichloromethane = 1/3, 1/4, 1/5, dichloromethane, and dichloromethane/ethyl acetate = 5/1, followed by column chromatography on silica gel eluted with dichloromethane, dichloromethane/ethyl acetate = 100/1, 50/1, 30/1, and 20/1. The solvent was evaporated to yield **E44** as a yellow solid (79 mg, 32%) [R_f = 0.17 (Al_2O_3, hexane/dichloromethane = 1:5)]. Mp 210-213 °C. ^{1}H-NMR (400 MHz, CD_2Cl_2): δ ppm = 1.11-1.12 (m, 105H), 3.86-3.88 (m, 10H), 4.02-4.04 (m, 10H), 4.20 (br s, 10H), 4.30 (s, 10H), 4.31 (br s, 10H), 6.77-6.87 (m, 30H), 6.92-6.94 (m, 10H), 7.21-7.43 (m, 25H). ^{13}C-NMR (101 MHz, CD_2Cl_2): δ ppm = 11.6 (CH), 18.8 (CH_3), 59.5 (CH_2), 67.3 (CH_2), 67.7 (CH_2), 68.2 (CH_2), 68.6 (CH_2), 88.0 (C), 103.9 (C), 115.4 (CH), 115.9 × 2 (CH), 116.0 × 2 (CH), 125.1 (C), 126.4 (CH), 128.2 (CH), 130.8 × 2 (C), 133.0 (C), 137.8 (C), 138.5 (C), 153.4 (C), 153.7 (C), 158.8 (C). IR (KBr): ν cm^{-1} = 3445, 2939, 2864, 1610, 1508, 1231, 1109, 1071, 825, 672. MS (MALDI): *m*/*z* (%): 2962.7 (M^+).

***sym*-Penta(4-(4-(2-(4-(2-(prop-2-ynyloxy)ethoxy)phenoxy)ethoxy)phenyl)phenyl)-corannulene (E45)**

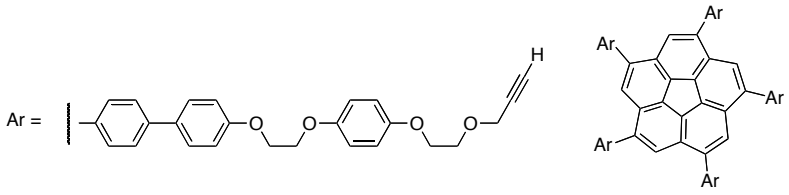

$C_{145}H_{120}O_{20}$
Mol. Wt.: 2182.4923

To *sym*-penta(4-(4-(2-(4-(2-(3-triisopropylsilylprop-2-ynyloxy)ethoxy)phenoxy)ethoxy)phenyl)-phenyl)corannulene (**E44**) (52.7 mg, 0.0178 mmol) in THF (10 mL), tetrabutylammonium fluoride (1.0 M in THF, 0.178 mL, 0.178 mmol) was added. After 38 h, ethyl acetate (100 mL) and 10% ammonium chloride (100 mL) were added. The organic layer was washed with water (100 mL), dried with sodium sulfate, and evaporated. The product was purified by washing with hexane to yield **E45** as a yellow solid (33.1 mg, 85%). Mp > 350 °C (dec.). ^{1}H-NMR (400 MHz, $CDCl_3$): δ ppm = 2.45-2.48 (m, 5H), 3.87-3.90 (m, 10H), 4.10-4.11 (m, 10H), 4.27-4.35 (m, 30H), 6.86-6.89 (m, 25H), 7.03 (br s, 10H), 7.52-7.69 (m, 30H). IR (KBr): ν cm^{-1} = 3444, 2927, 2872, 1607, 1507, 1454, 1230, 1108, 1071, 931, 826, 524 MS (MALDI): *m*/*z* (%): 2180.9 (M^+).

***sym*-Penta(4-(4-(2-(4-(2-(2,3,4-triazole-4-(2-(2,3,4,6-tetra-*O*-acetyl-β-D-galacto-pyranoside)ethyl)methoxy)ethoxy)phenoxy)ethoxy)phenyl)phenyl)corannulene (E50)**

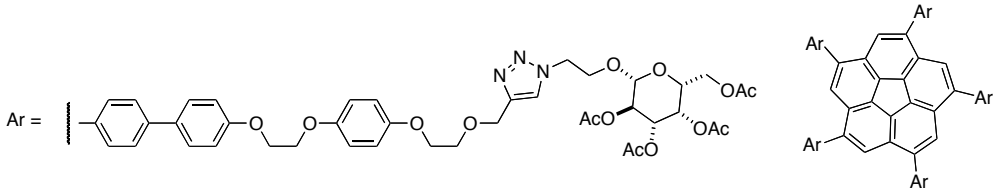

$C_{225}H_{235}N_{15}O_{70}$
Mol. Wt.: 4269.3319

The mixture of *sym*-penta(4-(4-(2-(4-(2-(prop-2-ynyloxy)ethoxy)phenoxy)ethoxy)phenyl)-phenyl)corannulene (**E45**) (7.6 mg, 0.00348 mmol), 2-azidoethyl-2,3,4,6-tetra-*O*-acetyl-β-D-galactopyranoside (**E19**) (22.4 mg, 0.0537 mmol), bromotris(triphenylphosphine)copper (I) (1.62 mg, 0.00174 mmol), and diisopropylethylamine (0.450 mg, 0.00348 mmol) in THF (2 mL) was stirred at room temperature for 69 h. The solvent was evaporated. The product was purified by column chromatography on silica gel eluted with dichloromethane, dichloromethane/ethyl acetate = 1/1, dichloromethane/methanol = 20/1 and 10/1 to yield **E50** as a yellow solid (13.8 mg, 93%) [R_f = 0.55 (SiO_2, dichloromethane/methanol = 20:1)]. Mp 273-276 °C. ^{1}H-NMR (400 MHz, CD_2Cl_2): δ ppm = 1.95 (s, 15H), 1.97 (s, 15H), 2.02 (s, 15H), 2.13 (s, 15H), 3.85-3.87 (m, 10H), 3.91-3.96 (m, 10H), 4.05-4.18 (m, 20H), 4.23-4.35 (m, 25H), 4.49-4.63 (m, 15H), 4.70 (s, 10H), 4.98-5.17 (m, 10H), 5.38-5.39 (m, 5H), 6.83-6.85 (m, 25H), 7.01 (br s, 10H), 7.71-7.74 (m, 35H). ^{13}C-NMR (101 MHz, CD_2Cl_2): δ ppm = 20.9 (CH_3), 21.00 (CH_3), 21.04 (CH_3), 21.1 (CH_3), 50.6 (CH_2), 61.9 (CH_2), 65.1 (CH_2), 67.5 (CH_2), 67.6 (CH), 67.8 (CH_2), 68.4 (CH_2), 68.5 (CH_2), 69.0 (CH), 69.6 (CH_2), 71.3 (CH), 71.6 (CH), 101.6 (CH), 115.6 (CH), 116.0 (CH) × 2, 116.1 (CH) × 2, 124.5 (CH), 125.6 (C), 126.8 (CH), 128.4 (CH), 131.0 (C) × 2, 133.2 (C), 138.1 (C), 139.6 (C), 145.2 (C), 153.6 (C), 153.8 (C), 159.1 (C), 170.0 (C), 170.5 (C), 170.7 (C), 170.8 (C). IR (KBr): ν cm^{-1} = 3441, 2928, 1750, 1608, 1508, 1370, 1226, 1053, 826, 588. MS (MALDI): *m*/*z* (%): 4289.5 (M^+ + Na).

sym-Penta(4-(4-(2-(4-(2-(2,3,4-triazole-4-(2-(β-D-galactopyranosyloxy)ethyl)methoxy)-ethoxy)phenoxy)ethoxy)phenyl)phenyl)corannulene (E12)

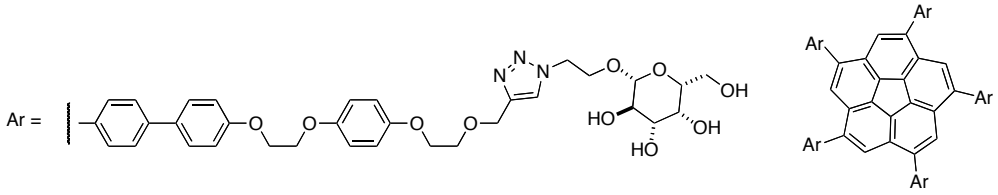

$C_{185}H_{195}N_{15}O_{50}$
Mol. Wt.: 3428.5983

To a solution of *sym*-penta(4-(4-(2-(4-(2-(2,3,4-triazole-4-(2-(2,3,4,6-tetra-*O*-acetyl-β-D-galacto-pyranoside)ethyl)methoxy)ethoxy)phenoxy)ethoxy)phenyl)phenyl)corannulene (**E50**) (13.8 mg, 0.00323 mmol) in methanol (5 mL) and dichloromethane (5 mL), sodium methoxide (5.4 M in methaol, 0.2 mL) was added. The mixture was stirred at room temperature for 90 h. Methanol was added to dilute and Dowex 50 was added until pH became 5. DMF was added until the suspension dissapeared. The mixture was filtered and washed with the mixture of methanol and DMF. The filtrate was evaporated. The solid was washed with methanol and hexane to yield **E12** as a yellow solid (6.4 mg, 58%). Mp > 350 °C (dec.). ^{1}H-NMR (400 MHz, DMF-d_7): δ ppm = 3.47-3.54 (m, 10H), 3.73 (s, 15H), 3.86 (s, 15H), 4.02-4.08 (m, 15H), 4.22-4.50 (m, 35H), 4.69-4.80 (m, 30H), 5.09 (s, 5H), 6.89-7.79 (m, 65H), 8.26 (s, 5H). ^{13}C-NMR (126 MHz, DMF-d_7, 350 K): δ ppm = 50.8, 62.2, 65.0, 68.2 × 2, 68.5, 69.1, 69.5, 69.8, 72.1, 75.0, 76.7, 104.8, 116.3, 116.68 × 2, 116.74 × 2, 125.1, 125.8, 127.0, 128.5, 131.1 × 2, 133.1, 138.3, 140.0, 145.2, 154.0, 154.3, 159.8. IR (KBr): ν cm^{-1} = 3416, 2923, 1633, 1508, 1229, 1064, 826. MS (MALDI): *m*/*z* (%): 3465.3 (M^+ + K), 3449.3 (M^+ + Na).

5.2.4.3. UV and Fluorescent Spectra

All spectra were recorded in spectroscopic grade solvents and are uncorrected. Absorption spectra were recorded on a Perkin Elmer Lamda 19 UV/Vis/NIR Spectrometer and emission spectra were recorded on an Edinburgh Instruments FLS920 Combined Steady State and Lifetime Spectrometer.

***sym*-Penta(4-(4-(2-(4-(2-(2,3,4-triazole-4-(2-(β-D-galactopyranosyloxy)ethyl)methoxy)-ethoxy)phenoxy)ethoxy)phenyl)phenyl)corannulene (E12)**

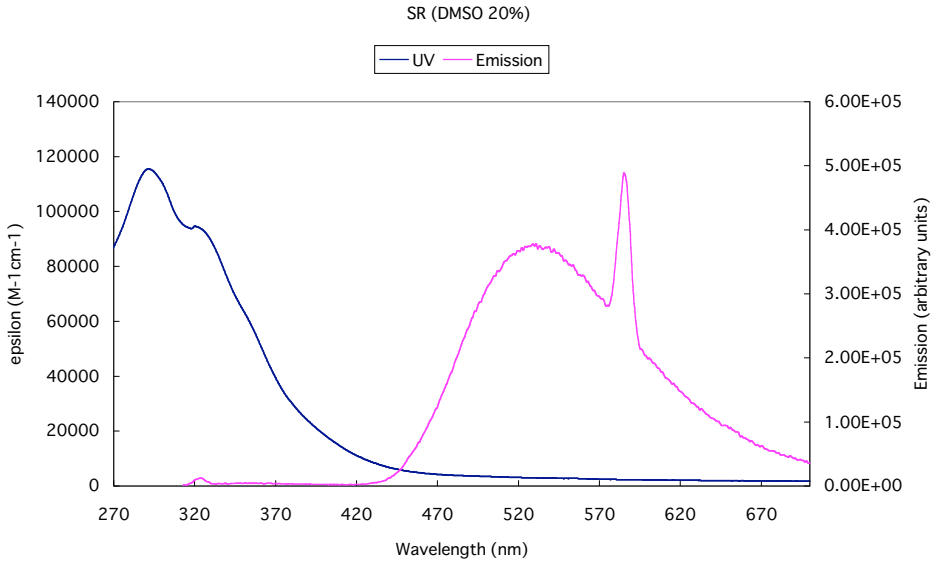

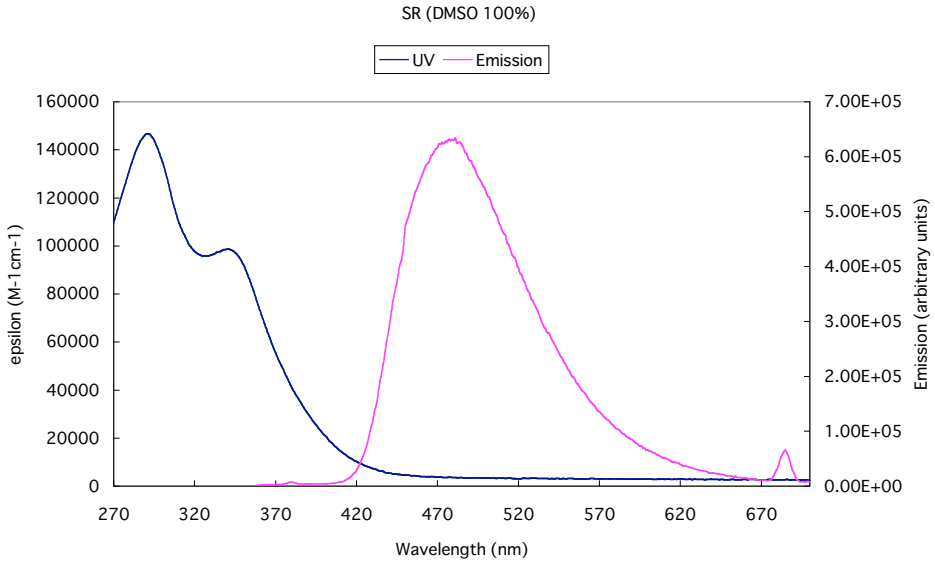

The spectra were measured in H_2O/DMSO = 80/20 v/v% and in DMSO.

5.3. References

[1] For latest review, see: Fan, E.; O'Neal, C. J.; Mitchell, D. D.; Robien, M. A.; Zhang, Z.; Pickens, J. C.; Tan, X.-J.; Korotkov, K.; Roach, C.; Krumm, B.; Verlinde, C. L. M. J.; Merritt, E. A.; Hol, W. G. J. *Int. J. Med. Microbiol.* **2004**, *294*, 217.

[2] (a) Spangler, B. D. *Microbiol. Rev.* **1992**, *56*, 622. (b) Merritt, E. A.; Hol, W. G. J. *Struct. Biol.* **1995**, *5*, 165.

[3] Sixma, T. K.; Pronk, S. E.; Kalk, K. H.; Wartna, E. S.; van Zanten, B. A.; Witholt, B.; Hol, W. G. *Nature* **1991**, *351*, 371.

[4] Mekalanos, J. J.; Collier, R. J.; Romig, W. R. *J. Biol. Chem.* **1979**, *254*, 5855.

[5] Sixma, T. K.; Pronk, S. E.; Kalk, K. H.; van Zanten, B. A.; Berghuis, A. M.; Hol, W. G. *Nature* **1992**, *355*, 561.

[6] (a) Fishman, P. H. *ADP-Ribosylating Toxins and G Proteins: Insights into Signal Transduction*; Moss, J.; Vaughan, M. (eds), American Society of Microbiology, Wahington, DC, 1990, 127. (b) Moss, J.; Vaughan, M. *Annu. Rev. Biochem.* **1979**, *48*, 581.

[7] Merritt, E. A.; Sarfaty, S.; van den Akker, F.; L'Hoir, C.; Martial, J. A.; Hol, W. G. *Protein Sci.* **1994**, *3*, 166.

[8] Minke, W. E.; Roach, C.; Hol, W. G. J.; Verlinde, C. L. *Biochemistry* **1999**, *38*, 5684.

[9] Pickens, J.; Merritt, E. A.; Ahn, M.; Verlinde, C. L. *Chem. Biol.* **2002**, *9*, 215.

[10] Mitchell, D.; Pickens, J.; Korotkov, K.; Fan, E.; Hol, W. G. J. *Bioorg. Med. Chem.* **2004**, *12*, 907.

[11] (a) Vrasidas, I.; de Mol, N. J.; Liskamp, R. M. J.; Pieters, R. J. *Euro. J. Org. Chem.* **2001**, 4685. (b) Arosio, D.; Vrasidas, I.; Valentini, P.; Liskamp, R. M. J.; Pieters, R. J.; Bernardi, A. *Org. Biomol. Chem.* **2004**, *2*, 2113.

[12] (a) Fan, E.; Zhang, Z. S.; Minke, W. E.; Hou, Z.; Verlinde, C. L. M. J.; Hol, W. G. J. *J. Am. Chem. Soc.* **2000**, *122*, 2663. (b) Merritt, E. A.; Zhang, Z. S.; Pickens, J. C.; Ahn, M.; Hol, W. G. J.; Fan, E. *J. Am. Chem. Soc.* **2002**, *124*, 8818. (c) Zhang, Z. S.; Merritt, E. A.; Ahn, M.; Roach, C.; Hou, Z.; Verlinde, C. L. M. J.; Hol, W. G. J.; Fan, E. *J. Am. Chem. Soc.* **2002**, *124*, 12991. (d) Pickens, J. C.; Mitchell, D. D.; Liu, J.; Tan, X.; Zhang, Z.; Verlinde, C. L. M. J.; Hol, W. G. J.; Fan, E. *Chem. Biol.* **2004**, *11*, 1205. (e) Zhang, Z.; Liu, J.; Verlinde, C. L. M. J.; Hol, W. G. J.; Fan, E. *J. Org. Chem.* **2004**, *69*, 7737.

[13] (a) Rostovtsev, V. V.; Green, L. G.; Fokin, V. V.; Sharpless, K. B. *Angew. Chem. Int. Ed.* **2002**,

41, 2596. (b) Tornøe, C. W.; Christensen, C.; Meldal, M. *J. Org. Chem.* **2002**, *67*, 3057.

[14] (a) Hayama, T.; Siegel, J. S; et al. Manuscript in preparation. (b) Hayama, T. Diplomarbeit, University of Zurich, Zurich, 2005.

[15] (a) Arduengo, A. J. III; Krafczyk, R.; Schmutzler, R. *Tetrahedron* **1999**, *55*, 14523. (b) Jafarpour, L.; Stevens, E. D.; Nolan, S. P. *J. Organomet. Chem.* **2000**, *606*, 49.

[16] (a) Viciu, M. S.; Germaneau, R. F.; Navarro-Fernandez, O.; Stevens, E. D.; Nolan, S. P. *Organometallics* **2002**, *21*, 5470. (b) Viciu, M. S.; Germaneau, R. F.; Nolan, S. P. *Org. Lett.* **2002**, *4*, 4053. (c) Navarro, O.; Kaur, H.; Mahjoor, P.; Nolan, S. P. *J. Org. Chem.* **2004**, *69*, 3173.

[17] Benaglia, M.; Toyota, S.; Woods, C. R.; Siegel, J. S. *Tetrahedron Lett.* **1997**, *38*, 4737.

[18] Himo, F; Lovell, T.; Hilgraf, R.; Rostovtsev, V. V.; Noodleman, L.; Sharpless, K. B.; Fokin, V. V. *J. Am. Chem. Soc.* **2005**, *127*, 210.

[19] For review on the CuAAC, see: (a) Bock, V. D.; Hiemstra, H.; van Maarseveen, J. H. *Eur. J. Org. Chem.* **2006**, 51. (b) Kolb, H. C.; Sharpless, K. B. *Drug Discovery Today* **2003**, *8*, 1128. (c) Wu, P.; Fokin, V. V. *Aldrichimica Acta* **2007**, 40, 7.

[20] For synthesis of $Cu(PPh_3)_3Br$, see: Gujadhur, R.; Venkataraman, D.; Kintigh, J. T. *Tetrahedron Lett.* **2001**, *42*, 4791.

[21] (a) Malkoch, M.; Schleicher, K.; Drockenmuller, E.; Hawker, C. J.; Russell, T. P.; Wu, P.; Fokin, V. V. *Macromolecules* **2005**, *38*, 3663. (b) Wu, P.; Feldman, A. K.; Nugent, A. K.; Hawker, C. J.; Scheel, A.; Voit, B.; Pyun, J.; Fréchet, J. M. J.; Sharpless, K. B.; Fokin, V. V. *Angew. Chem. Int. Ed.* **2004**, *43*, 3928.

[22] Mertz, J. A.; McCann, J. A.; Picking, W. D. *Biochem. Biophys. Res. Commun.* **1996**, *226*, 140.

[23] Scott. L. T.; *Pure Appl. Chem.* **1996**, *68*, 291.

[24] Tiwari, P.; Misra, A. K. *J. Org. Chem.* **2006**, *71*, 2911.

[25] Mitchell, S. A.; Pratt, M. R.; Hruby, V. J.; Polt, R. *J. Org. Chem.* **2001**, *66*, 2327.

[26] Jung, M. E.; Yang, E. C.; Vu, B. T.; Kiankarimi, M.; Spyrou, E.; Kaunitz, J. *J. Med. Chem.* **1999**, *42*, 3899.

[27] Fazio, F.; Bryan, M. C.; Blixt, O.; Paulson, J. C.; Wong, C.-H. *J. Am. Chem. Soc.* **2002**, *124*, 14397.

[28] Saeki, T.; Son, E.-C.; Tamao, K. *Bull. Chem. Soc. Jpn.* **2005**, *78*, 1654.

[29] Frankovskii, Ch. S.; Startseva, N. V.; Ionin, B. I.; El'kis, E. Sh.; Zaplatina, V. A. *Russian. J. Org. Chem.* **1970**, *6*, 1898.